VOLUME 33 – NO. 2 FEBRUARY 1993 BIMONTHLY ISSN: 0304-3894

JOURNAL OF HAZARDOUS MATERIALS

ELSEVIER

JOURNAL OF HAZARDOUS MATERIALS

Management — Handling — Disposal — Risk Assessment

Review papers, normal papers, project reports and short communications are published dealing with all aspects of hazardous materials arising from their inherent chemical or physical properties. The scope of the journal is wide, ranging from basic aspects of preparation and handling to risk assessment and the presentation of case histories of incidents involving real hazards to employees or the public.

The following list, though not exhaustive, gives a general outline of the scope:

Properties: toxicity, corrosiveness, flammability, explosiveness, radioactivity, information data banks, dose–response relationships

Safety and health hazards: manufacturing, processing, transport, storage, disposal, major hazards and hazardous installations

Legislation: international, national and local codes of practice, threshold values, standards

Incidents: prevention, control, clean-up, communication, labelling, sources of information and assistance, case histories

Assessment: economic and general risk assessment, insurance, test methods, technical aspects of risk assessment of industrial hazards, reliability and consequence modelling, decision-making in risk management

Special Issue

Process Safety Assessment and Management

Guest Editor

John L. Woodward

DNV Technica Inc., 355 E. Campus View Boulevard, Suite 170, Columbus, OH 43235

Guest Editorial

Safety technology advances should not depend on major disasters

Historically, major disasters have provided the driving force for sponsoring research into improving the technology of safely processing, storing, and transporting hazardous materials. Learning by experience is a costly mode. Fortunately, there are farsighted organizations and individuals willing to sponsor research in the technology of safety on a preemptive rather than a reactive basis.

Industrial consortia dedicated to safety issues are to be commended and encouraged. The Emergency Response Planning Guideline Committee of the American Industrial Hygiene Association is one such organization, and their work is highlighted in this issue. The Center for Chemical Process Safety (CCPS) of the American Institute of Chemical Engineers (AIChE) is another, along with AIChE's Design Institute of Emergency Relief Systems (DIERS) and the Joint Research Center at Ispra sponsored by the European Economic Community (EEC). Recently my own company, DNV Technica Inc., has been able to assemble a confederation of industrial sponsors to develop an Offshore Hazard and Risk Analysis toolkit (OHRA) as well as the confederation of sponsors for SAFETI-92 (Software for Assessment of Flammable, Explosive, and Toxic Impact). These organizations provide more than economic support. They provide encouragement and intellectual stimulation as well as "real world input" to the entire community of safety professionals, researchers, and practicing engineers.

A related development is also to be commended, the application of quality control methodology to assess and improve the management in the processing industry. Recently, with sponsorship by the European Economic Community, TNO in The Netherlands and SRD in the UK have begun developing the SMART mode and associated tools. SMART is based on the ISO 9004 guideline for quality control, thereby emphasizing that safety and quality are achieved concomitantly. The DNV ISRS auditing system is a similar methodology, just coming into application.

This special issue focuses on process and transportation safety. The issue is, in fact, a product of research sponsored by a variety of industrial consortia, governmental bodies, and academic institutions. Among these sponsors are the Canadian Department of National Defence, the UK Health and Safety

Executive, and the U.S. National Institute of Standards Technology. Other papers come from interactions within the DIERS program.

Some of the issues addressed in this special edition are: Why are detonations a sometime occurrence? How are ERPG values established? What is the best way to calculate a "toxic load" representing a specified level of toxicity for risk analyses? Does rail or road transportation of hazardous materials pose the greater risk in the UK? Should a particular reactor vessel be insulated or not?

In addition, important new models are discussed for the phenomena of a descending smoke plume from a large fire, for discharge from a spherical vessel, and for the "expansion zone" portion of a discharging jet. I wish to thank and commend the contributing authors for the quality of their work.

John L. Woodward
DNV Technica Inc.
Columbus, Ohio

Announcement from the Publisher

Journal of Hazardous Materials prefers the submission of electronic manuscripts on computer disk.

The preferred storage medium is a 5¼ or 3½ inch disk in MS-DOS format, although other systems are welcome, e.g. Macintosh.

After **final acceptance**, your disk plus one final, printed and exactly matching version (as a printout) should be submitted together to the editor. **It is important that the file on disk and the printout are identical**. Both will then be forwarded by the editor to Elsevier.

Illustrations should be provided in the usual manner.

Please follow the general instructions on style/arrangement and, in particular, the reference style of this journal as given in 'Instructions to Authors'.

Please label the disk with your name, the software & hardware used and the name of the file to be processed.

Contact the Publisher for further information:

Desk Editorial Office
Journal of Hazardous Materials
P.O. Box 330
1000 AH Amsterdam, The Netherlands
Phone: (+31-20) 5862 758 Fax: (+31-20) 5862 459

ELSEVIER SCIENCE PUBLISHERS

711\414\140\079\03

Journal of Hazardous Materials, 33 (1993) 159–192
Elsevier Science Publishers B.V., Amsterdam

Transition to detonation in fuel–air explosive clouds

I.O. Moen

Research and Development Branch, Department of National Defence, Ottawa, Ontario K1A 0K2 (Canada)

Abstract

Several experimental observations of transition to detonation in fuel–air mixtures have clearly demonstrated that transition phenomena, similar to those identified in more sensitive fuel–oxygen mixtures, can also occur in fuel–air mixtures. This means that the worst case detonation scenario cannot be excluded *a priori* in assessing the hazards from vapour cloud explosions. The present paper describes the considerable progress that has been made towards quantifying the potential for transition to detonation in a fuel–air cloud.

1. Introduction

The accidental release of combustible gases or evaporating liquids can lead to devastating explosions. The most dangerous situation occurs when a combustible fuel–air cloud is formed prior to ignition. Such a cloud is most likely to burn as a deflagration, but the most severe explosion is a detonation that propagates through the detonable parts of the vapour cloud at velocities of more than 1.5 km/s producing over-pressures in excess of 1.5 MPa. Because of the large energies required to directly initiate detonations in common fuel–air mixtures, this worst case scenario is typically excluded in hazard assessments. However, during the past decade several experiments have shown that transition to detonation can occur, even in relatively insensitive fuel–air mixtures [1–7].

A sequence of photographs from an experiment which illustrates the worst case scenario is shown in Fig. 1. In this experiment, a lane 1.8 m × 1.8 m in cross-section and 15.5 m long, with an array of obstacles simulating pipes in a chemical plant, was filled with acetylene–air and then ignited by four weak sparks at one end. As the flame encounters the turbulent flow around the obstacles it accelerates, reaching a speed of about 250 m/s at Frame a in Fig. 1. Several bright spots, indicating localized explosions, can be seen within the

Correspondence to: I.O. Moen, Research and Development Branch, Department of National Defence, Ottawa, Ontario K1A 0K2 (Canada).

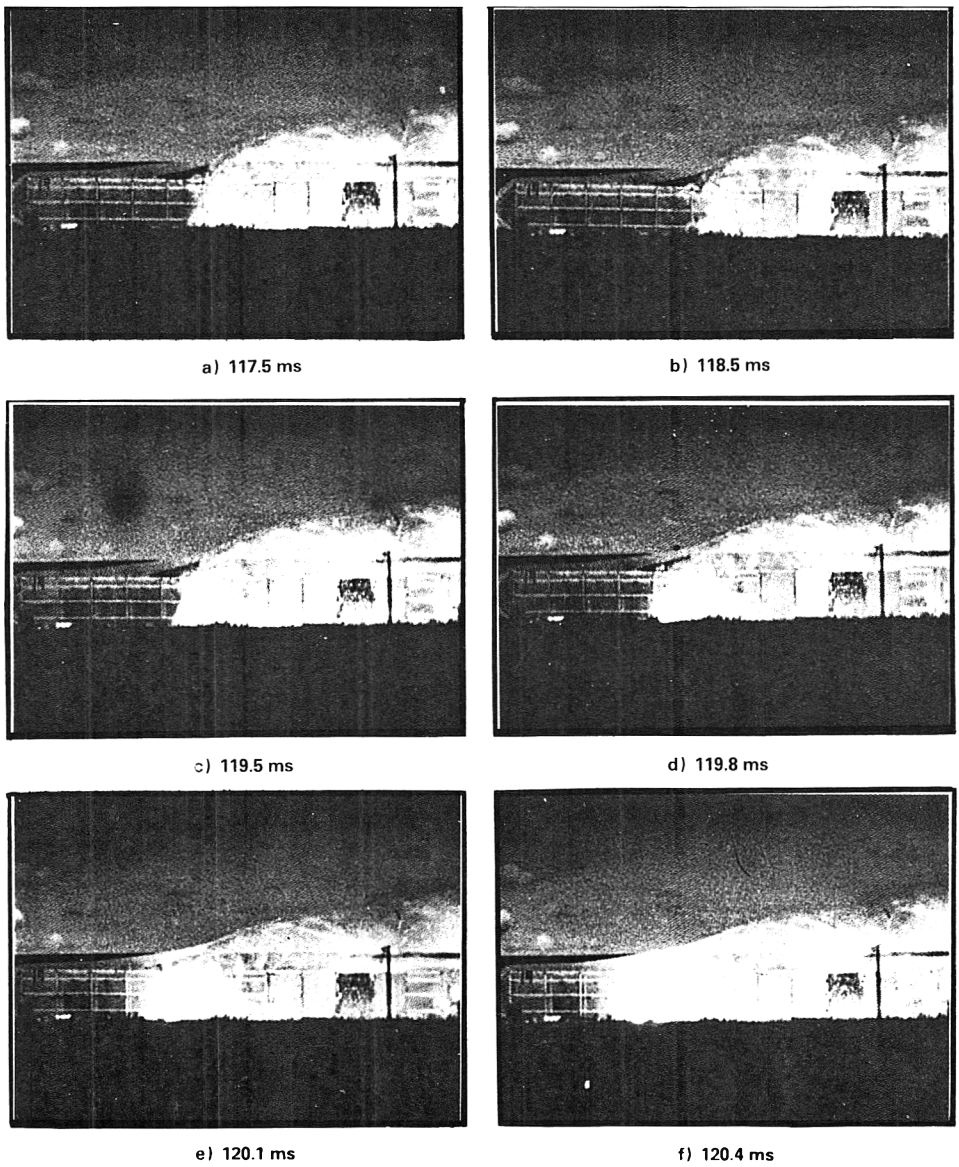

Fig. 1. Ignition, flame acceleration and transition to detonation with acetylene–air in a 1.8 m × 1.8 m lane, 15.5 m long [4].

flame brush in both Frames a and b, but it is the local explosion near the flame front in Frame c, which grows into the detonation wave seen in Frame f.

A similar transition process is revealed with good clarity in the sequence of schlieren photographs from a laboratory experiment shown in Fig. 2 [8]. The first two frames in Fig. 2 (0 and 5 μs) clearly show a fast deflagration with

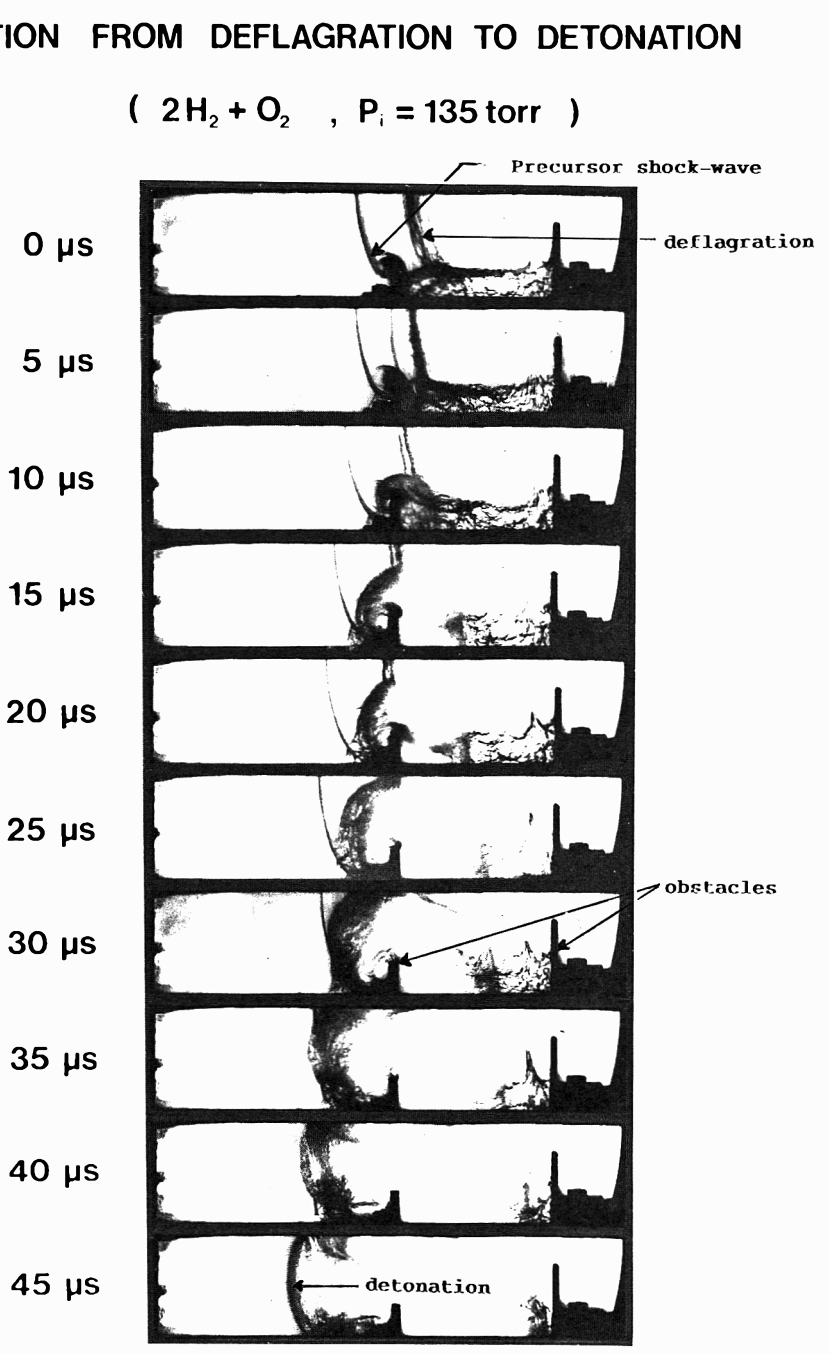

Fig. 2. Sequence of schlieren photographs illustrating the transition from deflagration to detonation phenomenon [8].

a precursor shock wave diffracting over an obstacle. A local explosion occurs at about 15 μs when the flame rolls up into the turbulent vortex ahead of the obstacle. The growth of the explosion bubble and its merger with the precursor shock wave to form a detonation wave can be seen in the subsequent frames.

These two examples show that the key feature associated with the onset of detonation is the formation of localized explosions somewhere in the turbulent frame-shock wave region. For direct initiation of detonation the initiating explosion is provided by an external high-energy source (e.g., a high explosive charge). The strong shock waves produced by such explosions directly initiate a self-sustained detonation without going through a deflagration phase.

Deflagration to Detonation Transition (DDT) refers to the phenomena where the critical conditions for the onset of detonation are established by the combustion process itself without an external high-energy source. There are several ways by which the conditions necessary for transition to detonation can be achieved. These include: (i) flame acceleration to some critical speed, (ii) ignition of a turbulent pocket, and (iii) jet ignition.

One of the proposed transition mechanisms is Shock Wave Amplification by Coherent Energy Release (SWACER) [9, 10], where the chemical energy is released in such a manner that the resulting shock waves are amplified to strengths sufficient to initiate detonation. The SWACER mechanism and other mechanisms for transition from deflagration to detonation were reviewed by Lee and Moen [11] in 1980, and more recently by Shepherd and Lee [12]. The qualitative 'picture' of the transition phenomena presented in the 1980 review paper remains essentially unchanged. However, considerable progress has been made in quantifying the flame acceleration phenomena, and in quantifying the requirements for initiation and propagation of detonations.

The aim of the present contribution is to describe some of the new developments which impact on the DDT problem. In particular, theoretical and experimental results on the nature, behaviour and initiation of gaseous detonations are reviewed. Observations of transition to detonation in fuel–air mixtures are also summarized, and the influence of mixture composition, experimental configuration and scale on flame acceleration and transition phenomena are discussed. Some of the proposed models for transition to detonation are also discussed, and proposals are made for future research to obtain a better understanding of the DDT phenomena.

2. General considerations

All of the complex phenomena involved in the accidental release of fuels with subsequent ignition cannot be quantified. However, a general description of the events leading to explosions can be given. The sequence of events begins with a spill of combustible fuel. If ignition occurs immediately, the result will be a diffusion flame whose rate of burning is controlled by the mixing of fuel with air. In this case, the hazards due to thermal effects from the burning

fireball are more important than the blast effects. These hazards will not be discussed here, rather we shall assume that ignition is delayed so that a potentially explosive fuel–air cloud has been formed through the mixing of the spilled fuel with air. Depending on the nature of the ignition source and the reactivity of the fuel, such a cloud can either burn as a deflagration or detonate. For a deflagration, the explosion pressure depends on the rate of combustion and the degree of confinement. Laminar flames are typically associated with low flame velocities (≤ 10 m/s) and small pressure changes (~ 1 kPa). Completely confined explosions can produce damaging overpressures (~ 0.8 MPa), and detonations produce overpressures in excess of 1.5 MPa.

Weak ignition of an explosive cloud in an unobstructed, unconfined environment is unlikely to lead to a damaging explosion. There is no mechanism for flame acceleration to high flame speeds or for producing pockets with rapid enough energy release to cause transition to detonation within such clouds. However, the influence of obstacles in the cloud can be quite dramatic, particularly repeated obstacles. Confined and partially confined regions within the cloud are also hazardous, and jet ignition from explosions in such regions can dramatically increase the severity of the explosion in an external unconfined cloud.

It is not necessary to have a detonation for severe damage to occur. In many cases, industrial structures will fail under loadings that result from fast flames. However, the damage from detonations will be much more severe and extensive; the detonation pressure is higher and the detonation will propagate through the detonable parts of the cloud at the detonation velocity, whereas the speed of a flame adjusts to the environment and will decrease to non-damaging levels in unconfined areas without obstacles.

In the present paper we are concerned with the onset of detonation from localized explosions (or regions of violent combustion) within the cloud. As will be discussed later, localized explosions can occur in the turbulent flame brush of fast flames, in the flame jet from confined explosions, and in highly turbulent burning vortices. In order for such explosions to cause the onset of detonation, a high rate of energy release in a sufficiently large volume is required. The rate of energy release and the minimum explosion volume depend on the susceptibility of the explosive mixture to detonation. The nature of detonations and methods for characterizing this susceptibility are described in the next section.

3. Detonation waves

3.1 Equilibrium detonation properties

A detonation wave can be described as a coupled reaction zone-shock wave complex which propagates through a uniform combustible mixture at a constant supersonic velocity. The shock wave heats up the mixture to a temperature above the ignition temperature, thus providing the ignition source for

the combustion to begin, and the chemical energy released in the reaction zone provides the energy required to maintain the shock wave.

The velocity of a detonation can be calculated from the total chemical energy released. The corresponding thermodynamic conditions (i.e., pressure, temperature, etc.) at the end of the reaction zone, or the so-called Chapman–Jouguet (CJ) point, can also be calculated from equilibrium chemistry alone. Standard numerical codes which combine chemical equilibrium calculations with the gasdynamic CJ conditions are available for this purpose (e.g., the NASA [13] and TIGER [14] codes). Detonation pressure ratios and velocities for some common fuel–air mixtures at stoichiometric composition are given in Table 1. Also included in this table is the chemical energy released in the detonation wave.

The equilibrium detonation parameters determine the pressure and flow field inside and outside the detonating cloud. Fairly straightforward

TABLE 1

Equilibrium detonation parameters for fuel air mixtures (stoichiometric composition; atmospheric initial pressure, 101.3 kPa; initial temperature 298.15 K)

Fuel	% Fuel by volume	Detonation pressure ratio	Velocity (m/s)	Energy release (MJ/kg Mixture)
Acetylene (C_2H_2)	7.75	19.1	1864	2.44
Hydrogen (H_2)	29.6	15.6	1968	2.82
Ethylene (C_2H_4)	6.54	18.4	1822	2.35
Ethane (C_2H_6)	5.66	18.0	1825	2.31
Propylene (C_3H_6)	4.46	18.5	1809	2.31
Propane (C_3H_8)	4.03	18.3	1798	2.29
n-Butane (C_3H_{10})	3.13	18.4	1796	2.28
Methane (CH_4)	9.48	17.2	1801	2.31
Hydrogen sulphide (H_2S)	12.3	15.3	1647	1.96
n-Hexane	Aerosol	18.6	1795	2.28

finite-difference numerical codes are available for calculating the blast field associated with ideal clouds of uniform composition. Inside such a cloud, the peak pressure is the detonation pressure, whereas the duration of the pressure pulse depends on the size of the cloud and the distance from the cloud boundaries. The far-field blast waves beyond about two cloud diameters from a detonating cloud are for all practical purposes the same as that from a TNT charge with the same energy release, located at the centre of the cloud [15].

The equilibrium detonation parameters provide no information on the detonation initiation and propagation requirements. These are determined by the structure and transient behaviour of the detonation wave.

3.2 Structure of detonation waves

A one-dimensional model of the detonation wave, called the Zeldovich–Von Neumann–Döring (ZND) model, includes an induction zone separating the leading shock wave and the onset of chemical reaction [16]. Although it is known that the structure of detonations is three-dimensional with waves moving transverse to the direction of propagation, the ZND model provides a useful first approximation to the detonation structure. This model has been used, together with detailed chemical kinetic models, to calculate a ZND induction zone length, Δ, which is then assumed to be directly proportional to the cell size, S, characteristic of the cellular structure of the detonation [17–20].

The cellular structure of gaseous detonations can be attributed to instabilities in the reacting flow behind the leading shock wave. When the level of instability is relatively mild, the detonation wave consists of two families of shock waves moving in opposite directions transverse to the leading shock wave. As illustrated in Fig. 3a, the triple-point shock trajectories trace out a "fish scale" pattern, which can be recorded by placing a lightly-sooted polished metal (or mylar) foil, commonly referred to as a smoked foil, parallel to the direction of propagation. In most fuel–air systems, a large number of instability modes interact in a non-linear manner to produce a complex irregular pattern such as that shown in Fig. 3b [21]. Although the identification of a characteristic cell size is subject to some interpretation, it has been possible to identify cell sizes for many fuel–air systems from smoked foil records. Detonation cell sizes for several fuel–air mixtures at stoichiometric composition are given in Table 2. Cell size data for other compositions can be found in Refs. [22] and [23].

3.3 Geometric propagation and transition limits

The detonation cell size is a characteristic length scale that can be used to assess the geometric propagation and transition limits of detonations. Knystautas and co-workers [23–25] found that DDT in a round tube is possible only if the tube diameter is larger than the detonation cell size. The cell size therefore represents the minimum geometric dimension below which transition does not occur even in a completely confined tube. Similarly, a

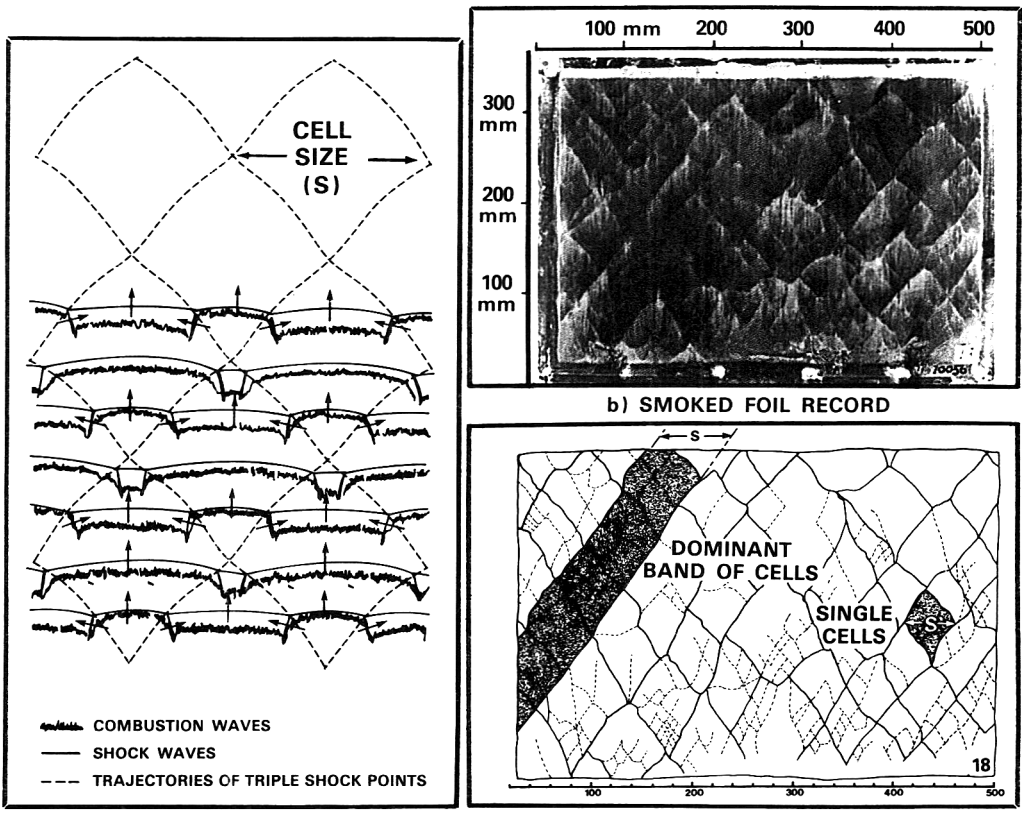

Fig. 3. Typical cellular structure of detonations in fuel–air mixtures [21].

detonation will fail if the tube is sufficiently small so that the transverse waves are suppressed. For systems with regular cellular structure (e.g., acetylene–oxygen highly diluted with argon), failure occurs when the tube diameter is approximately equal to the cell size. However in irregular systems, typical of fuel–air, the detonation wave merely adjusts its structure and continues to propagate in round tubes with diameters much smaller than the dominant cell size [26]. In square tubes, however, failure is observed near the cell size limit even in fuel–air mixtures [27].

A detonation wave also fails when its transverse waves are attenuated by acoustic absorbing tube walls [28]. This indicates that transverse waves are necessary for detonations to propagate. In confined tubes, the tube walls act as reflective surfaces that help to maintain the transverse waves. Once these reflective surfaces are removed, by using an absorbing material or by removing the tube walls, the detonation will fail unless the transverse wave structure can be self-supporting.

TABLE 2

Detonability parameters for fuel–air mixtures at stoichiometric composition (atmospheric initial pressure, 101.3 kPa; initial temperature 298 K)

Fuel	Cell size (mm)	Critical tube diameter (m)	Detonation initiation energy (g Tetryl)	Critical explosion diameter (m)
Acetylene	9.8	0.15	1.25	0.15
Hydrogen	15	0.2	1.1	0.16
Ethylene	28	0.43	10–15	0.36
Ethane	54–62	0.9	30–40	0.48
Proplyene	52	—	45–52	0.54
Propane	69	0.9	50–55	0.54
n-Butane	50–62	0.9	50–80	0.62
Hydrogen sulphide	90–130	—	—	—
Methane	250–310	—	22000	4.0

The first observation that a minimum tube diameter is required for a detonation wave to emerge from a tube and become a detonation in an unconfined cloud was made by Zeldovich et al. [29]. This minimum or critical tube diameter, d_c, is a measure of the minimum dimension of an unconfined detonable cloud. Experimentally, this dimension is between 10–30 detonation cell widths, depending on the explosive mixture. For most fuel–air mixtures, $d_c \simeq 13S$ [22, 26].

The critical tube diameter is determined from "Go–No Go" experiments, in which the fate of the detonation is monitored as it emerges from a tube into an unconfined explosive cloud. Selected frames from high-speed photographic records illustrating successful transmission and failure to transmit from 0.9 m diameter tube are shown in Fig. 4. The first frames of both sequences show the planar detonation wave just as it emerges from the tube. The initial planar detonation core shrinks (Frames 2 and 3) as the expansion waves sweep in towards the centre. For successful transmission, re-ignition is seen to occur at nuclei near the center in Frame 3. The subsequent formation of a detonation wave which sweeps through the pre-shocked region just outside the central core of burned gas can be seen in Frame 4. This detonation wave engulfs the whole region in Frame 5. In the case of detonation failure, no ignition nuclei are formed and the detonation is quenched when the head of the expansion wave reaches the centre at about one tube diameter from the tube exit.

The critical tube diameters for several fuel–air mixtures at stoichiometric composition are given in Table 2. The values range from 0.1–0.2 m for acetylene– and hydrogen–air mixtures to almost 1 m for propane–, ethane– and butane–air mixtures. Critical tube diameters for other compositions can be found in Refs. [22] and [23].

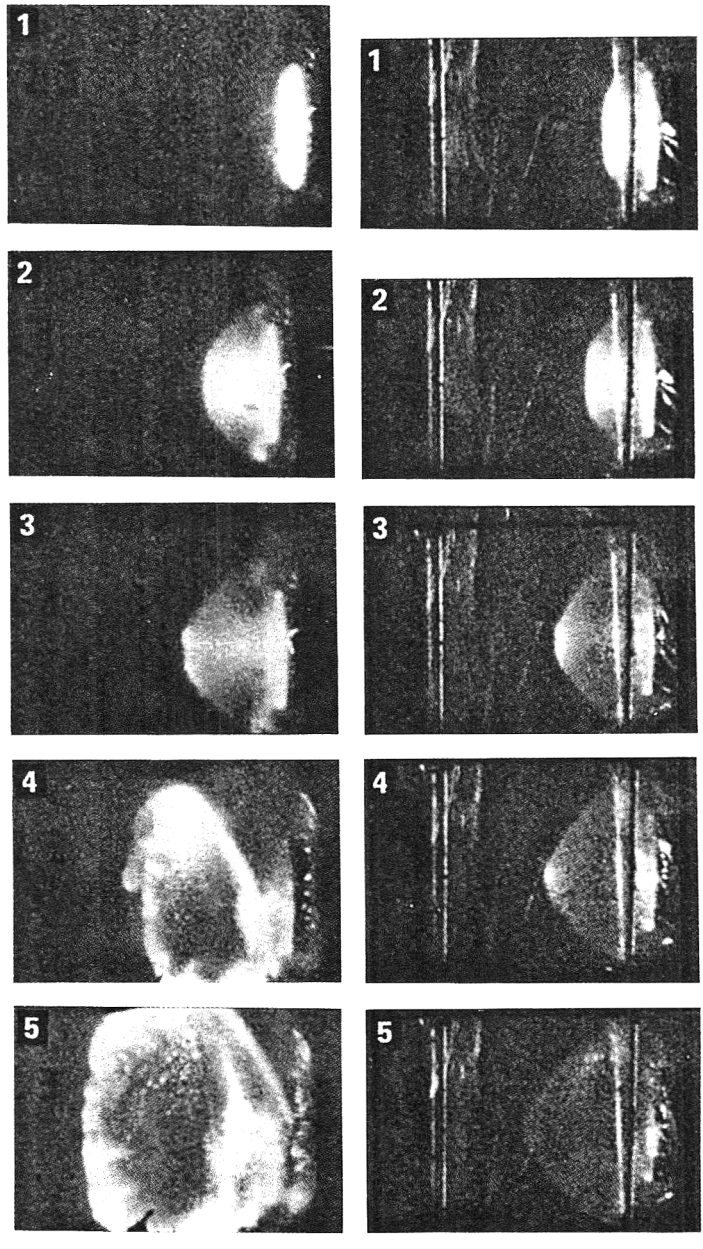

Fig. 4. Selected frames from high-speed photographic records illustrating successful transmission and failure when a detonation emerges from a 0.9 m diameter tube.

3.4 Direct initiation of detonation

The detonation length scales S and d_c provide a measure of how large an explosive cloud must be in order to support a detonation. A minimum quantity of energy is required to establish a detonation wave in this explosive cloud. For unconfined fuel–air clouds, the critical initiation energy is usually characterized by the minimum mass of high-explosive required to initiate a spherical detonation wave. Bull [30] proposed that tetryl be used as the high-explosive standard. The equivalent energy of tetryl is approximately 4.3 MJ/kg. Unless otherwise specified we shall adopt this standard and use this energy equivalency.

Experimental values of the critical initiation energy for several fuel–air mixtures at stoichiometric composition are given in Table 2. The initiation requirements vary from 1 g of tetryl for hydrogen and acetylene fuels to several kilograms for methane. For common fuels such as propane and butane, the detonation initiation requirements are about 50 g of tetryl.

For most fuel–air mixtures, the variation in critical initiation energy with composition takes the form of a U-shaped curve with a minimum near stoichiometric composition. This is illustrated in Fig. 5, where the critical initiation energies for selected fuel–air systems are plotted vs. the equivalence ratio ϕ, where ϕ is the volume ratio of fuel to air relative to that at stoichiometric composition.

The earliest theoretical concept of critical initiation energy is due to Zeldovich and co-workers [29]. Their concept still remains the simplest and most direct. The rapid release of energy results in a decaying blast wave. The heuristic limiting condition proposed for successful initiation is that at least one chemical induction time must have elapsed before the blast wave Mach number has decayed to the CJ value. For spherical geometry, this assumption leads to the relationship $E_c \propto \Delta^3$, between the critical energy, E_c, and the ZND chemical induction zone length, Δ. Numerous refinements and re-interpretations of the theory of initiation have been developed, but the fundamental concept remains unchanged. All the models predict that $E_c \propto L_c^3$ where L_c is one of the chemical length scales (i.e., Δ, S or d_c). If it is also assumed that the chemical length scales are linearly related, it is then possible to determine the variation of detonability with composition through chemical kinetic calculations [17–19]. Some indication of the reliability of such estimates can be obtained by referring to Fig. 6, where E_c is plotted vs d_c. The general $E_c \propto d_c^3$ trend is valid for a given fuel. However, the proportionality factor for acetylene–air is almost 20 times larger than that for ethane–air.

In summary, a fairly good qualitative understanding of detonations and detonability properties has emerged during the past decade. This understanding, together with the empirical relationships that have been derived from a large pool of new data, has provided a good background against which the DDT problem can be addressed.

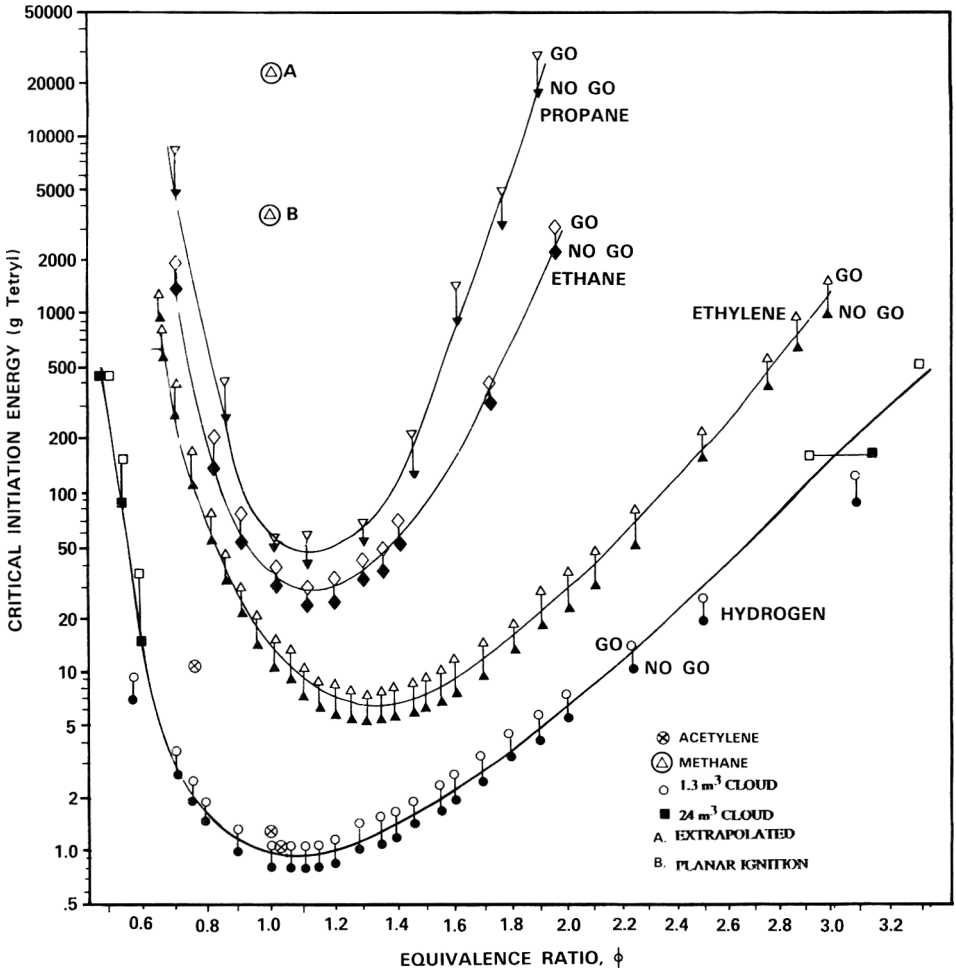

Fig. 5. Critical initiation energy vs. equivalence ratio, ϕ, for selected fuel–air mixtures [30, 31].

5. Transition to detonation

5.1 Mechanisms and criteria

Transition to detonation is the onset of detonation in a combustible mixture without an external high energy source. In this case, the energy required to initiate detonation is provided by combustion of the mixture. This "self-initiation" requires a rapid release of combustion energy to produce a blast wave of sufficient strength to cause detonation. As described by Lee and Moen [11], such shock waves can be produced by prescribing a spatial and temperal coherence of the energy release. Theoretically, the required coherence can be achieved by pre-conditioning the explosive mixture so that the induction time

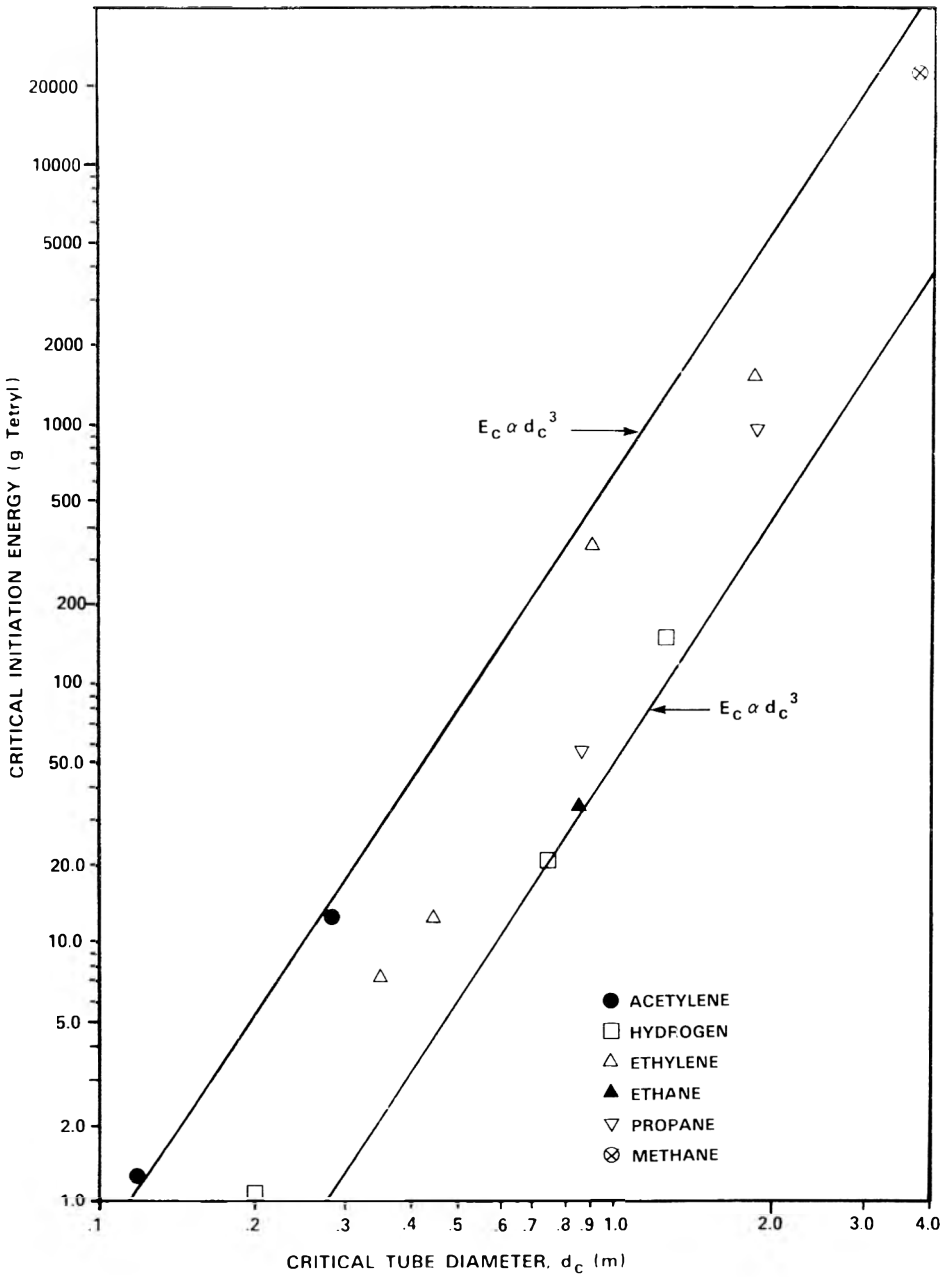

Fig. 6. Critical initiation energy vs. critical tube diameter.

τ (i.e., time to ignition) increases in a prescribed manner away from an initial ignition point to produce an energy source which propagates at a velocity $V_0 = (\partial\tau/\partial x)^{-1}$. Numerical calculations indicate that a source velocity close to the Chapman–Jouguet detonation velocity produces the best shock wave amplification [11].

Spatial gradients in induction time are due to gradients in temperature and/or free radical concentrations. The so-called SWACER mechanism was first proposed to account for photochemical initiation in $H_2 + Cl_2$ mixtures [9]. In these experiments, the induction time gradient was produced by irradiating the explosive mixture with a strong short-duration flash. Photo-dissociation thus produces a gradient in free radical concentration (Cl) which decreases exponentially in the direction of the incident light.

Gradients in temperature and free-radicals are also produced by turbulent mixing of hot combustion products with unburned gas in turbulent eddies associated with flame propagation around obstacles or in turbulent flame jets. It was Knystautas et al. [10] who first demonstrated that initiation of detonation could be achieved by injecting a hot turbulent jet into a quiescent explosive fuel–oxygen mixture.

Coherent energy release by itself is not enough for transition or detonation, the volume of coherent energy release must also be large enough to produce a strong enough shock wave with long enough duration to initiate detonation in the surrounding unburned mixture. A lower bound on the volume required for transition to occur in an unconfined cloud can be obtained by equating the chemical energy in a spherical volume to the critical initiation energy by an external source:

$$E_c = \pi \rho_0 Q D_c^3 / 6, \tag{5.1}$$

where Q is the chemical energy release per unit volume, ρ_0 is the density of the unburned mixture, and D_c is the critical explosion diameter. This diameter is of the same order of magnitude as the critical tube diameter (see Table 2). Critical diameters for fuel–air mixtures are at least an order of magnitude larger than for fuel–oxygen, so that field experiments are required to clarify the potential for DDT in unconfined fuel–air clouds.

There are several ways by which the conditions necessary for transition to detonation can be achieved. These include: (i) flame acceleration to some critical speed, (ii) ignition of a turbulent pocket, and (iii) jet ignition. In the remainder of this section we will discuss these, but first let us make some general observations.

A wide variety of experiments, both large and small scale, have been performed so that there is now a considerable data base on flame acceleration and transition to detonation in fuel–air mixtures. The results prior to 1986 have been summarized and compiled in a report by Moen and Saber [32]. Particularly hazardous configurations were identified as those which are heavily confined. In tubes, pipes and confined channels, for example, high flame speeds and pressures are reached within less than four diameters, even in insensitive

mixtures of methane and air. Similar flame acceleration is also observed in clouds confined on top and bottom. Such clouds could be produced by a release into an area which is covered by a roof. Explosions in confined spaces can also serve as strong ignition sources for external clouds, greatly enhancing the potential for DDT. Weak spark ignition of unconfined clouds in a relatively unobstructed environment is unlikely to result in transition to detonation or damaging explosions, even for sensitive fuel–air mixtures such as acetylene– and hydrogen–air. However, transition can be expected to occur in long channels or tubes for most fuel–air mixtures, provided the channel or tube is large enough and long enough.

5.2 Flame acceleration

One method of creating the conditions necessary for transition to detonation is flame acceleration to some critical speed. Flame acceleration is particularly dramatic in repeated obstacle environments. In such environments, the flame is repeatedly perturbed, so that a positive feed-back mechanism is established, resulting in high flame speeds after only a short distance of flame travel.

The mechanisms of transition in fast turbulent flames were revealed with unsurpassed clarity by the stroboscopic laser–schlieren photographs of Urtiew and Oppenheim [33]. Their photographs clearly show that localized explosions somewhere between the precursor shock wave and the end of the turbulent flame brush lead to the onset of detonation. An example of onset of detonation due to a localized explosion immediately behind the precursor shock wave is shown in Fig. 7.

In order for transition to occur, sufficiently high flame speeds must be reached. The flame speeds observed prior to the rapid acceleration phase, characteristic of the transition phase, are between 500 and 800 m/s [24, 25, 34]. Since most flame acceleration mechanisms are very effective in confined tubes, acceleration of the flame to speeds sufficient to cause onset of detonation can be expected, provided the tube is long enough. Transition to detonation will then occur if the detonation cell size is not larger than the tube diameter. The run-up or transition distance depends on many factors, including: fuel–air mixture, tube diameter, ignition source, obstacles, etc. In stoichiometric hydrogen–air, for example, the transition distances observed by Bartknecht [35] in smooth tubes are 7.5–12.5 m, whereas Knystautas et al. [25] observe transition just after a 3 m long obstacle section. The transition distance observed in pipes was reviewed by Steen and Schampel in 1983 [36]. In pipes with no obstacles, the transition distance increases with increasing tube diameter. In propane–air mixtures, for example, the transition distance was found to be about 8 m in a 50 mm diameter pipe and more than 30 m in a 400 mm diameter pipe.

Flame propagation in tubes has been studied experimentally by several authors [24, 25, 34–39], and Hjertager and co-workers [39–42] have developed numerical methods for describing the flame acceleration phenomena in tubes, with and without obstacles. The actual mechanisms responsible for DDT in tubes are not understood so that transition cannot be predicted *a priori*, but

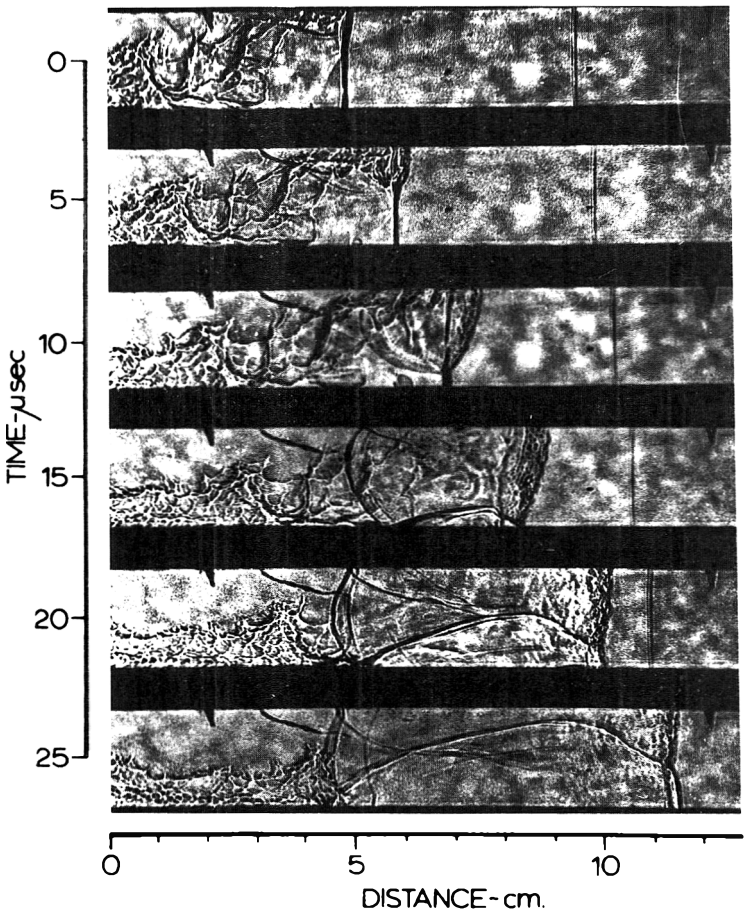

Fig. 7. Stroboscobic schlieren record of the onset of detonation in a low pressure hydrogen/oxygen mixture, with localized auto-explosion immediately behind the precursor shock-wave at about 5 μs [33].

tube configurations which produce flame speeds in excess of 500 m/s can be expected to lead to the onset of detonation in mixtures whose detonation cell size is less than the tube diameter. Long tubes or channels therefore represent the most hazardous configurations for DDT. The consequences of such transitions will be particularly devastating if the detonation is transmitted into a large external cloud. As discussed in Section 3.3, this will occur if the tube diameter is greater than the critical tube diameter.

Flame acceleration and transition phenomena were studied on a relatively large scale at SANDIA in their FLAME apparatus (a channel 30.5 m long, 2.4 m high and 1.8 m wide) designed to investigate hydrogen combustion relevant to nuclear reactor safety [3, 43]. Transition to detonation was observed in

near-stoichiometric hydrogen–air mixtures with no obstacles for a closed-top channel and with 13% top venting. However, with 50% of the top of the channel open, continuous flame acceleration leading to transition to detonation was not observed.

The results from the FLAME experiments confirm that the flame acceleration and transition phenomena observed on a smaller scale also occur on a large scale. They also show that the degree of confinement plays an important role in controlling the flame acceleration. This is consistent with the laboratory results obtained by Chan et al. [44] in an investigation on the influence of top venting on flame acceleration in a channel with repeated obstacles. They found that the maximum flame speed of 350 m/s with a closed top decreased to 5 m/s when 50% of the top was open. A similar influence of top venting on flame acceleration was also observed by Van Wingerden and Zeeuwen [45] in their pipe-rack obstacle arrays. These results show that the flame acceleration and thus the possibility of transition to detonation is reduced significantly by removing confinement.

The first observations of transition to detonation in large partially confined clouds were made by Pförtner et al. [1, 46], who used a fan to generate tubulence in a hydrogen–air cloud contained in an open-top lane, 3 m × 3 m in cross-section and 10 m long. With no obstacles or turbulence generators, the maximum flame speed was 200 m/s, with an associated maximum pressure of 20 kPa. However, when a fan (1.25 m in diameter at 225 rpm) was placed 1 m from the ignition end to generate turbulence, transition to detonation occurred about 2 m downstream of the fan.

Transition to detonation following flame acceleration in a lane with repeated obstacles was observed by Moen et al. [4, 47]. This phenomena was described in the Introduction. The test section was a channel 1.8 m × 1.8 m in cross-section, 15.5 m long, confined on three sides with a plastic envelope covering the top. The obstacle arrays consisted of 500 mm or 220 mm diameter pipes mounted across the channel at regular intervals as illustrated in Fig. 8. Experiments were performed with acetylene, propane and hydrogen sulphide fuels.

The potential for flame acceleration and transition to detonation is clearly illustrated by the results obtained in near stoichiometric acetylene–air mixtures. For these mixtures, the flame accelerates down the channel and reaches speeds between 250 and 400 m/s prior to the occurrence of localized explosions which trigger the onset of detonation. The flame velocity and peak overpressure observed as the flame propagates down the channel are shown in Fig. 9. With the larger (500 mm) obstacles, the leading flame front reaches the end of the channel with a velocity of about 400 m/s, at which time an explosion near the bottom of the channel triggers detonation of the remaining unburned mixture. Also shown in Fig. 9 are the results of numerical calculations (for the larger obstacles) using a k–ε turbulence model, which incorporates turbulent combustion through a mixing model limited by a single-step induction time [40–42].

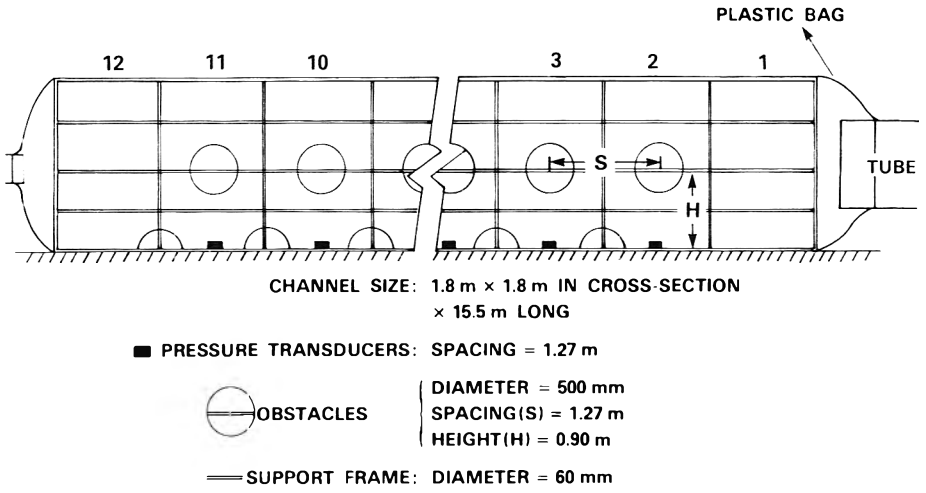

SIDE VIEW OF FLAME ACCELERATION CHANNEL

WITH 500 mm DIAMETER OBSTACLES

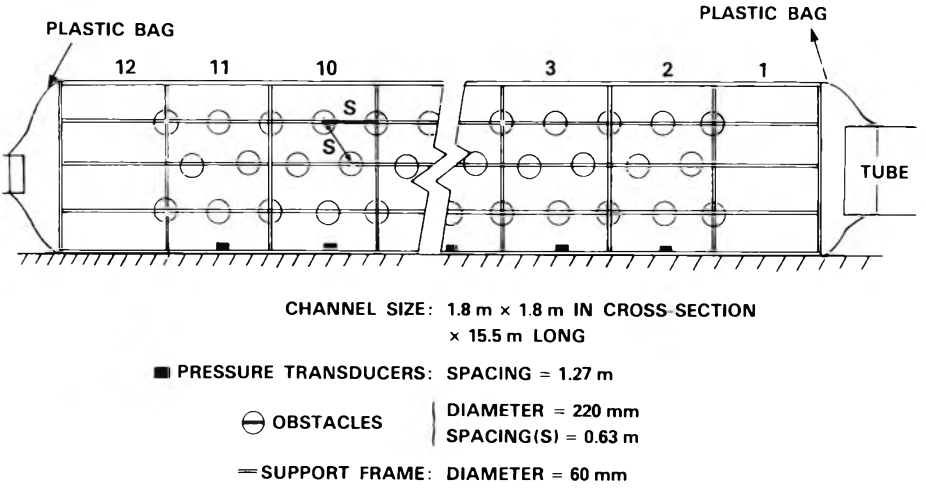

SIDE VIEW OF FLAME ACCELERATION CHANNEL
WITH 220 mm DIAMETER OBSTACLES

Fig. 8. Flame acceleration channel with: 500-mm diameter obstacles; and 220-mm diameter obstacles [4, 47].

With the smaller 220 mm obstacles, transition to detonation occurs about 11 m down the channel, again due to a localized explosion at ground level. The flame speed reaches about 250 m/s prior to a rapid acceleration phase which starts 9 m down the channel and results in a full-fledged detonation with

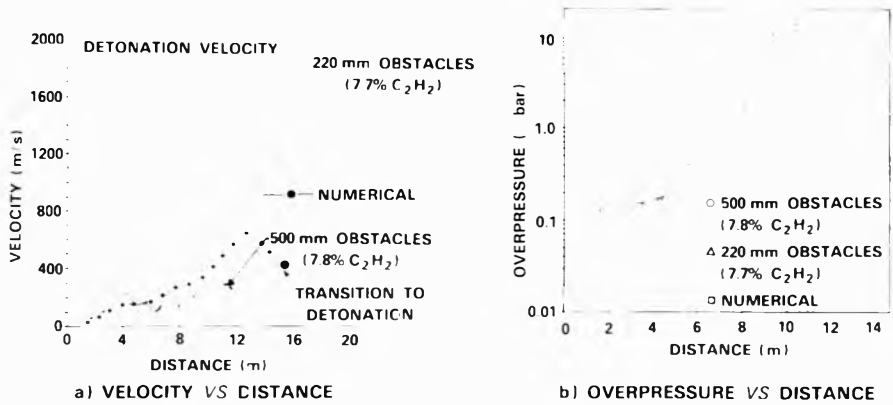

Fig. 9. Experimental and numerical results for acetylene–air mixtures: (a) flame velocity vs. distance; (b) peak overpressure vs. distance [4, 47].

a velocity close to the theoretical value by the end of the channel (see Fig. 9a). Prior to the rapid acceleration phase, the peak pressure is less than 2 bar (0.2 MPa). The peak pressure quickly increases to a detonation-like pressure of about 15 bar (1.5 MPa) at 10.6 m (see Fig. 9b). Selected frames from a high-speed film record showing the flame propagation and transition to detonation are shown in Fig. 1, and described in the Introduction.

The behaviour of flames in propane– and hydrogen sulphide–air mixtures in the same lane with repeated obstacles is much less dramatic. The flame speeds range from about 25 m/s up to 200 m/s, with associated pressures typically less than 5 kPa. The flame speeds observed in propane–air mixtures are up to four times larger than the maximum flame speed observed in the same mixtures in a similar laboratory scale channel (0.9 m long by $0.3 \times 0.15\ m^2$) with repeated obstacles [48].

Similar results are reported by Harris and Wickens [7] in a larger open-sided rig (3 m × 3 m in cross-section and 45 m long) with a similar array of obstacles. Using an 18 m length of the test section, they obtain maximum flame speeds of 70 m/s in cyclohexane–air, 65 m/s in butane–air and 50 m/s in natural gas air, with associated maximum pressures between 3 and 7 kPa. In ethylene–air, flame speeds of over 200 m/s were recorded and maximum pressures were up to 80 kPa. By extending the length of the test section to the full 45 m with obstacles throughout, flame speeds of 230 m/s with pressures up to 70 kPa were recorded in cyclohexane–air. The corresponding values for natural gas–air were 80 m/s and 10 kPa. These values are somewhat higher than those predicted by scaling the results of Moen et al. [4, 47] using the numerical model of Hjertager and co-workers [40, 42]. As seen in Fig. 10, the peak explosion pressure is predicted to increase with scale, but for a channel scaled up by a factor of about 3 in length, the peak pressure in propane–air is predicted to be less than 0.1 bar (10 kPa). Yet these pressure levels are observed in a much less sensitive mixture of natural gas and air.

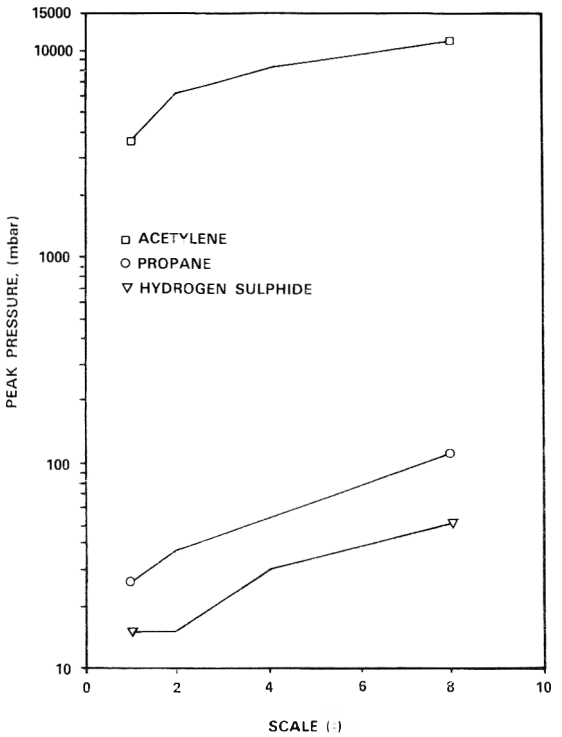

Fig. 10. Variation of peak pressure with linear scale. Scale of one corresponds to 1.8 m × 1.8 m cross-section channel, 15.5 m long, with 500-mm diameter obstacles [4].

Nevertheless, the scaling predictions shown in Fig. 10 indicate that transition to detonation is unlikely in mixtures such as propane–air in configurations with similar obstacle densities, ignition source and confinement to the experimental configuration used by Moen et al. [4, 47]. The fact that flames in acetylene–air and hydrogen–air do produce detonations in such partially confined environments show that the potential for very damaging explosions does exist. However, in order for such explosions to occur in less sensitive mixtures, the cloud must be: (i) more highly confined; (ii) ignited by a strong ignition source (e.g., strong ignition from a confined explosion); (iii) in a denser obstacle environment; or (iv) highly turbulent prior to ignition.

Transition to detonation in propane–air has been observed in highly confined vessels, and by strong ignition from a confined explosion. Bjørkhaug and Hjertager [6] observed transition to detonation in propane–air in a 10 m radial vessel, confined on the top and bottom, with central ignition, and with obstacles blocking 50% of the area between the plates. Harris and Wickens [7] report transition to detonation in propane–air mixtures in their 45 m-long test rig with obstacles when the first 9 m of the rig is covered with solid walls to produce an initial rapid acceleration of the flame. However, transition to

TABLE 3

Transition to detonation in fuel–air mixtures by flame acceleration in partially confined configurations

% Fuel by volume	d_c (m)	V_s[a] (m/s)	Configuration	V_{max}[b] (m/s)	P_{max}[c] (bar)	Reference
Hydrogen (H_2) 24.8%	0.23	14.2	30.5 m × 2.4 m × 1.8 m 13% Top venting	230	0.65	Sherman et al. [3]
Hydrogen (H_2) 36 & 38%	0.23	21.9 23.2	10 m × 3 m × 3 m Open-top lane with fan	220 240	1.0	Pförtner et al. [1]
Acetylene (C_2H_2) 7.8%	0.12	12.1	15 m × 1.8 m × 1.8 m Open top lane with obstacles	435 375	>0.15	Moen et al. [4, 47]
Cyclohexane (C_6H_{12}) 2.3%	—	3.6	45 m × 3 m × 3 m Open-sided lane with obstacles	600	—	Harris and Wickens [7]
Propane (C_3H_8) 4.0%	0.9	3.7	45 m × 3 m × 3 m Open-sided lane with obstacle (first 9 m of lane confined)	600	—	Harris and Wickens [7]
Propane (C_3H_8) 4.0%	0.9	3.7	10 m radial vessel with obstacles	500	—	Bjørkhaug and Hjertager [6]

[a] Laminar flame speed assuming velocity of burned gas is zero.
[b] Maximum flame speed prior to transition to detonation.
[c] Maximum overpressure prior to transition.

detonation in natural gas–air was not observed even with a flame speed of 1000 m/s in the confined region.

The reported observations of transition to detonation in large partially confined fuel–air clouds by flame acceleration are summarized in Table 3. Flame speeds just prior to ignition range from about 230 m/s in hydrogen–air mixtures to between 500 and 600 m/s for propane–air and cyclohexane–air mixtures.

5.3 Ignition of a turbulent pocket

Another mode of transition to detonation was observed by Moen et al. [4, 47] in one of their experiments with acetylene–air in the open-top lane with repeated obstacles. In this experiment, the turbulent pocket at the end of the channel was ignited by a hot wire used to cut the plastic. The phenomena is illustrated in Fig. 11 by a sequence of frames from a high-speed film record. The turbulent burning in the end-pocket (Frames a and b) produces an explosion near ground level (Frames c and d) that leads to a detonation prior to the arrival of the main flame front.

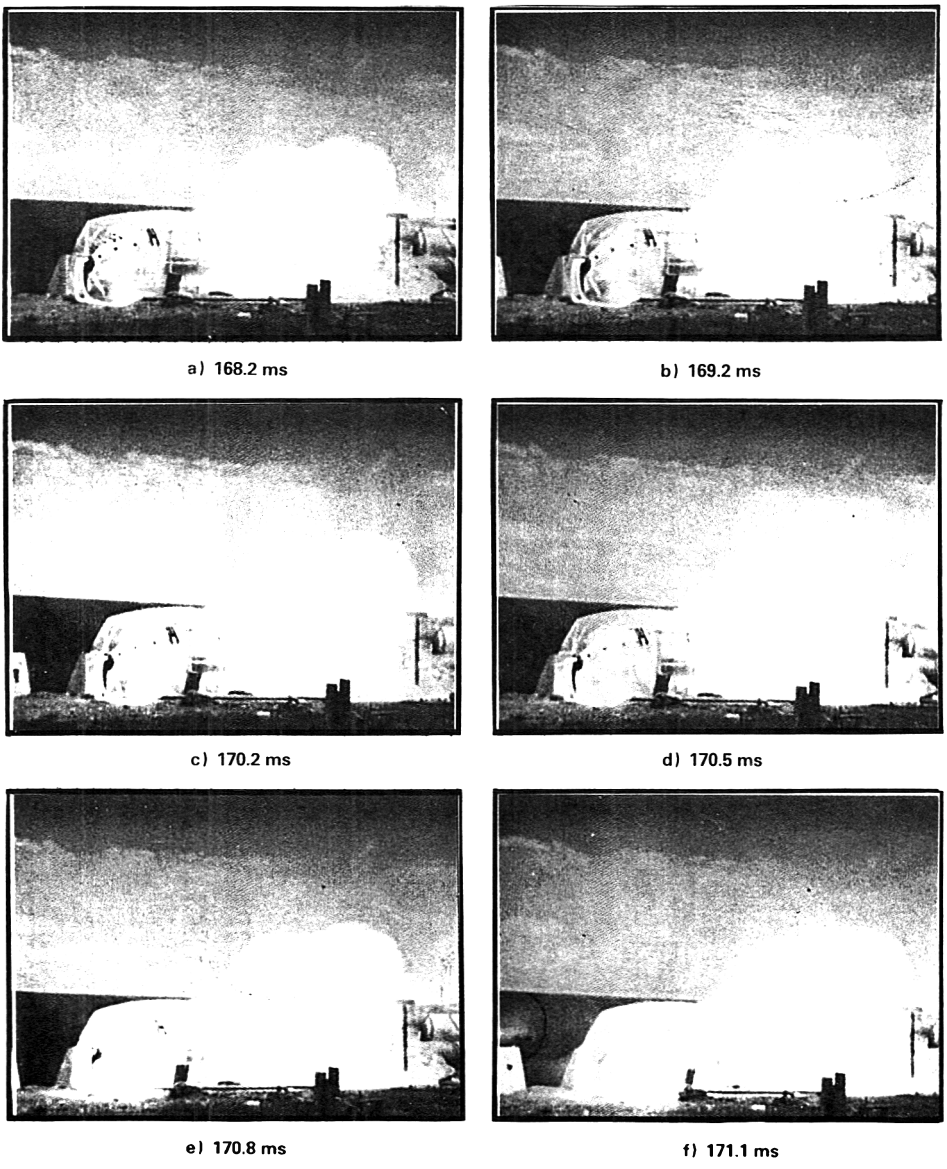

Fig. 11. Selected frames from high-speed film record showing explosion and transition to detonation in a turbulent end-pocket of acetylene–air prior to the arrival of the main flame front [4, 47].

The maximum velocity of the main flame front, prior to the onset of detonation, was 180 m/s with an associated overpressure of 13.2 kPa. Such pressures are much too small for shock reflections to be responsible for the onset of detonation. However, the flame-induced flow produces a pocket of turbulent

flow at the end of the channel. It is the ignition of this pocket which triggers an explosion of a sufficiently large volume to cause transition to detonation.

A similar transition to detonation phenomenon in a less sensitive mixture (5% C_2H_2–air), was observed in a jet-ignition experiment [2]. In that experiment, a fast flame emerging from a 0.64 m diameter tube produced violent turbulent burning in a cloud contained in a 2 m diameter plastic bag. Selected frames from a high-speed movie showing flame propagation, explosion, and transition to detonation are included in Fig. 12. The trajectories of the flame and detonation fronts are plotted in Fig. 13. The first frame in Fig. 12 shows the flame just as it emerges from the tube. The next frame shows the flame 2 ms later. The flame is highly turbulent and unstable, with a flame tongue running ahead at a speed of about 600 m/s near the bottom of the bag. This flame tongue reaches the lower corner at the end of the bag about 5.4 ms after the flame emerges from the tube. The resulting burning in this corner is seen in Frames c and d. In Frame d, a curled up flame vortex can be seen in the corner. The type of burning seen in these last two frames incubates for about 1.2 ms, at which time a localized explosion occurs in the corner (Frame e). The subsequent growth of an explosion bubble into a detonation front propagating backwards along the bottom of the bag can be seen in Frames f and g. As seen in Frame h, the resulting detonation wave engulfs the remaining unburned gas in the bag.

These two observations show that the gradients in temperature and free radicals required for transition to detonation can be established in turbulent eddies or pockets. In both cases, the turbulent eddies are produced ahead of the main flame front and transition to detonation occurs before the main flame front arrives. One of the observations is for a relatively insensitive mixture of 5% acetylene in air, with a critical tube diameter of 0.6 m and a minimum detonation initiation energy of about 20 g of tetryl high-explosive. Both hydrogen and ethylene can produce fuel–air clouds which are more sensitive to detonation, and there is no reason to exclude similar transition to detonation in less sensitive mixtures provided the turbulent pocket is large enough.

5.4 Jet ignition

The first demonstration that the conditions for onset of detonation can be achieved by turbulent mixing between hot combustion products and unburned mixture was made by Knystautas et al. [10]. In their experiment a turbulent jet of combustion products was injected into a cloud of explosive mixture. A sequence of schlieren photographs illustrating the transition to detonation in the flame jet is shown in Fig. 14. The turbulent structure of the hot jet of combustion products is clearly evident in the first four frames (10–95 μs). At 114 μs, a detonation "bubble" resulting from an exploding eddy somewhere within the turbulent mixing region can be seen. This bubble expands and eventually sweeps the entire surface of the turbulent region to form a detonation.

The jet initiation experiments of Knystautas et al. were performed with an initial flame jet diameter of 40 mm, and various turbulence inducing obstacles

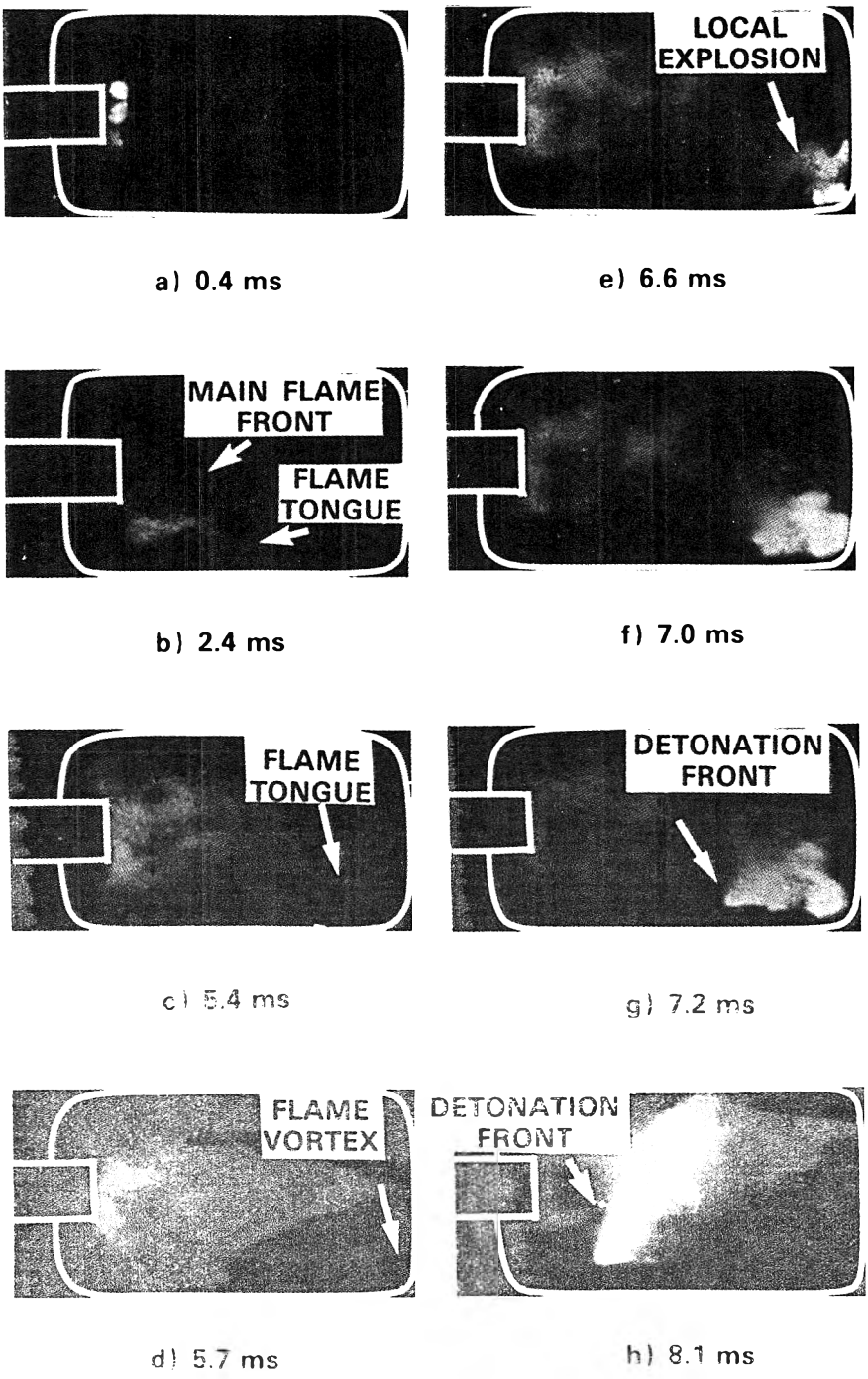

Fig. 12. Flame propagation and transition to detonation in a 2 m diameter plastic bag with ignition by a flame jet emerging from a 0.64 m diameter tube (5% v/v. C_2H_2-air) [2].

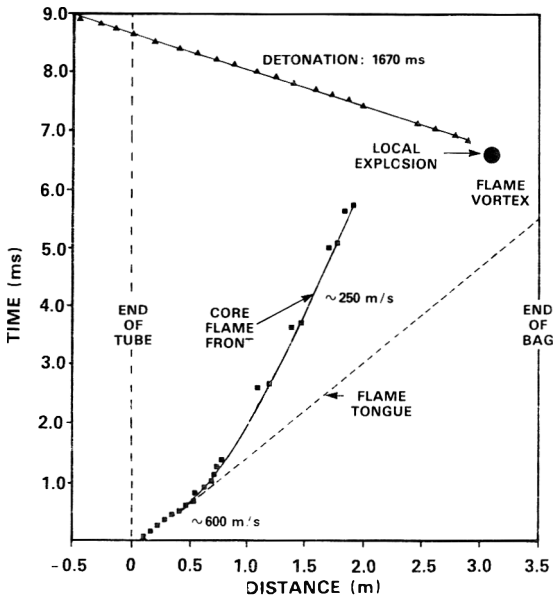

Fig. 13. Trajectories of the flame and detonation fronts in 5% C_2H_2–air mixture ignited by a flame jet [2].

in the orifice plate connecting the flame chamber and the larger detonation chamber. Detonation was obtained in equimolar acetylene–oxygen at an initial pressure of 150 torr. The critical tube diameter for this mixture at this pressure is about 5 mm. The smallest critical tube diameter of fuel–air mixtures is about 80 mm for rich acetylene–air. Based on linear scaling with the critical tube diameter, a minimum jet diameter of about 0.6 m would therefore be required in order to begin observing similar jet initiation phenomena in fuel–air mixtures.

In an investigation of flame-jet ignition in acetylene–air clouds, Moen et al. [5] confirmed that transition also occurs in fuel–air flame jets provided the scale is large enough. The first series of experiments were performed at a large-scale, fuel–air facility at Raufoss, Norway. The experimental configuration consisted of a 0.66 m diameter steel tube, 11 m long, connected to a large plastic bag 2 m in diameter (see Fig. 15). Experiments were performed with the end of the tube connected to the plastic bag completely open, partially blocked by circular discs with diameters 0.55 m and 0.36 m, and with an orifice plate (50 mm holes, open area ratio 0.25).

An example of transition to detonation in a flame jet from an open tube is shown in Fig. 16. In this case, the flame accelerates down the tube producing a flame jet with an exit velocity of almost 600 m/s. The intense turbulent burning in the jet can be clearly seen in the first two frames (0.33 and 1.33 ms). The intensity of the burning appears to increase in the next frame (2.33 ms). At

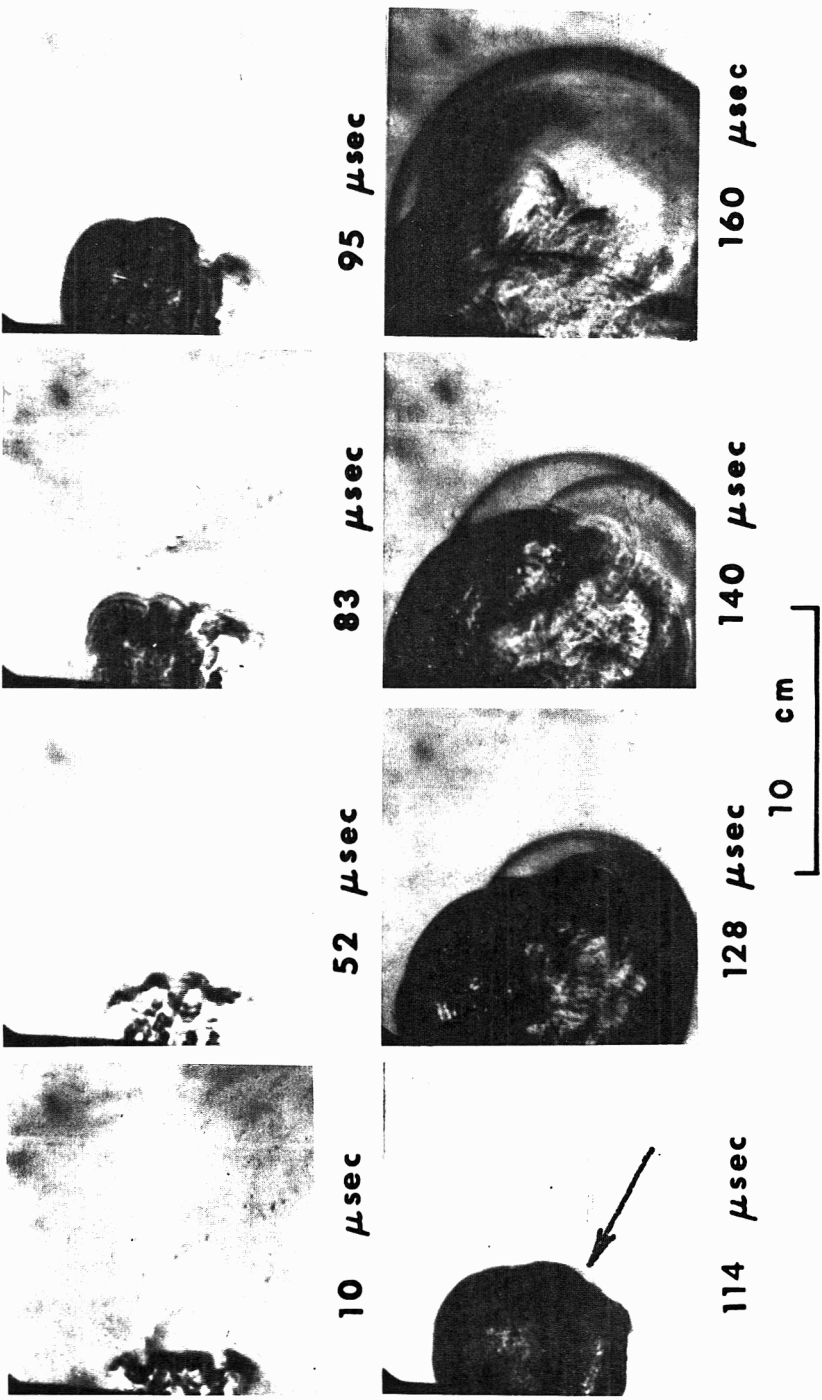

Fig. 14. Sequence of spark schlieren photographs showing the initiation of detonation by turbulent mixing with a hot turbulent jet of combustion products. The mixture is equimolar $C_2H_2 + O_2$ at an initial pressure $P_0 = 150$ torr [10].

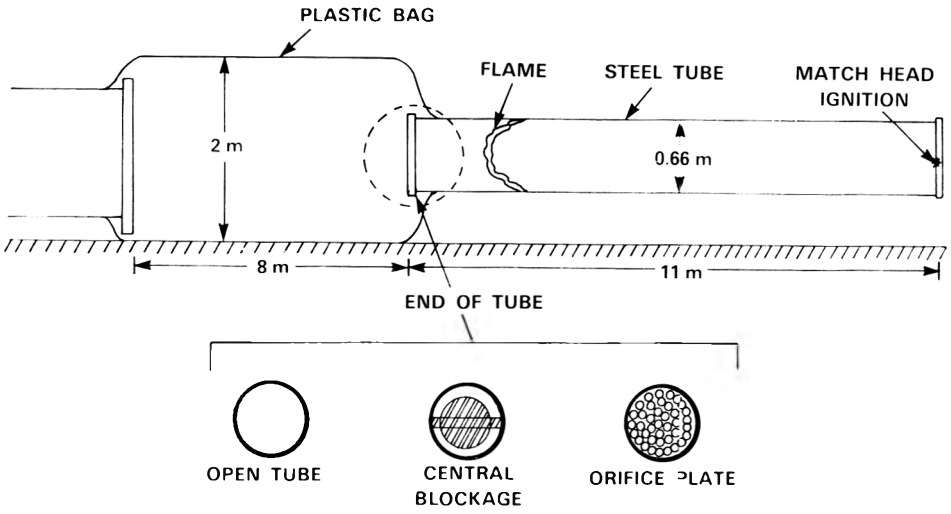

Fig. 15. Sketch of experimental configuration for investigation of flame jet ignition of acetylene–air clouds [5].

2.67 ms, a localized explosion near the tube exit leads to the onset of detonation. This detonation then propagates through the remaining unburned mixture in the bag.

The second series of jet ignition experiment were performed at the Defence Research Establishment (DRES) Fuel–Air Explosive facility [49]. The experimental configuration that was filled with explosive gas is shown in Fig. 17. It consisted of a 7.8 m long tube, 0.9 m in diameter, with a 1.8 m (or 2.4 m) diameter plastic bag, 8 m in length, attached to the open end of the tube. The end of the tube attached to the plastic bag was either unobstructed or partially blocked by a central circular disc 0.43 m or 0.58 m in diameter. Various arrays of obstacles were used to accelerate the flame which was ignited by a spark at the closed end of the tube. The test fuels were acetylene, ethylene, propane and vinyl chloride monomer.

Transition to detonation in the flame jet was observed for a range of acetylene–air concentrations and flame jet velocities. A plot of the flame jet velocity, V_j, versus mixture sensitivity expressed in the form d_c/D, where d_c is the critical tube diameter of the mixture and D is the tube diameter, is shown in Fig. 18. The data indicate that a minimum velocity of about 600 m/s is required for initiation in the most sensitive fuel–air mixtures ($d_c/D \simeq 0.1$). This minimum V_j increases as the mixture sensitivity decreases. At $d_c/D \simeq 0.5$, for example, the minimum flame jet velocity is about 700 m/s.

Some of mechanisms which can trigger transition to detonation were identified from the high speed film records. They include a variety of flame/vortex, flame/flame and flame boundary interactions, some of which are illustrated in the flame and detonation front contours shown in Fig. 19.

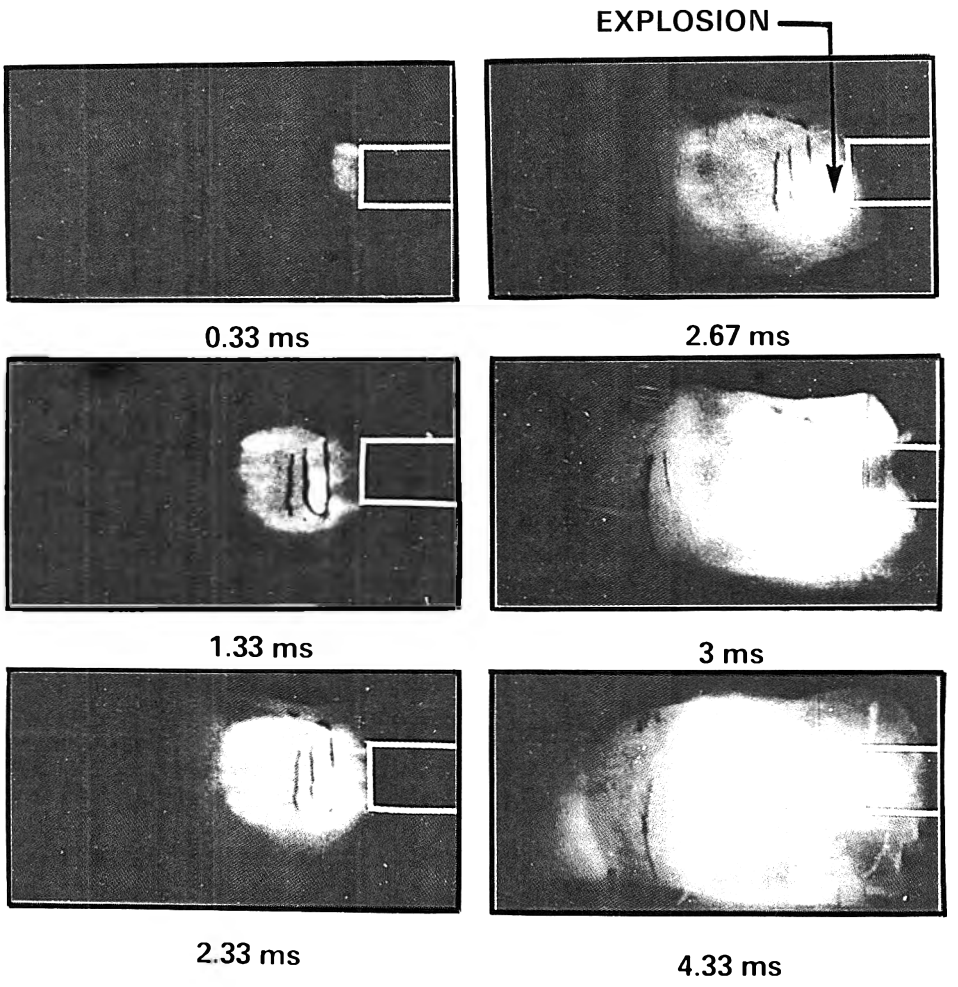

Fig. 16. Sequence from high-speed film showing transition to detonation in the flame jet (7.9% C_2H_2) from an open 0.66-m diameter tube, 11 m long [5].

With etylene-, propane- or vinyl chloride-air mixtures, the critical conditions for transition were not realized in the outside cloud. The flame-jet velocities were too low for transition to occur in these less sensitive mixtures. Even though transition to detonation does not take place, violent explosions were observed in ethylene-air mixtures producing overpressures in excess of 0.5 MPa in the outside cloud, significantly larger than the maximum pressure in the tube.

In summary, the results of these large scale jet ignition tests confirm that the phenomena of transition to detonation in fuel-air mixtures are identical to those in fuel-oxygen mixtures, but on a much larger scale due to the less

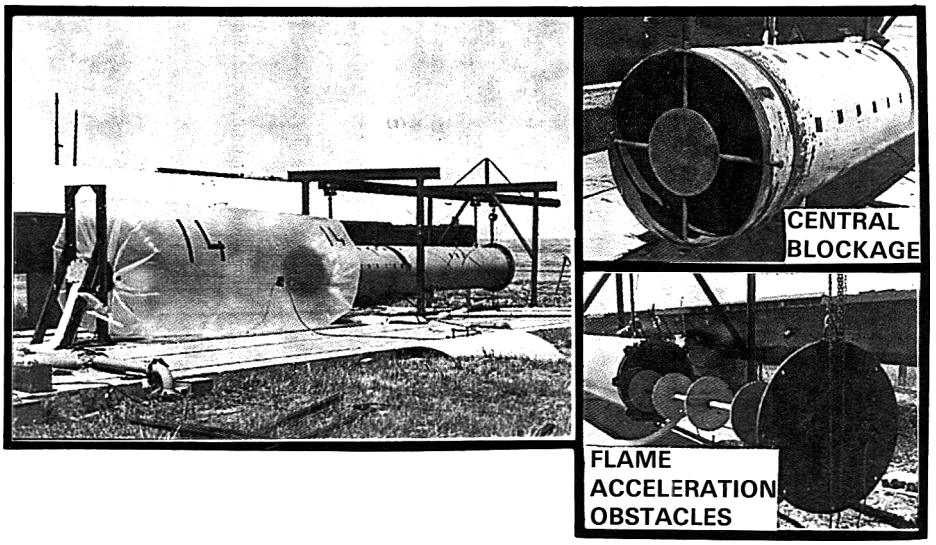

Fig. 17. The experimental apparatus used in flame-jet initiation studies [49].

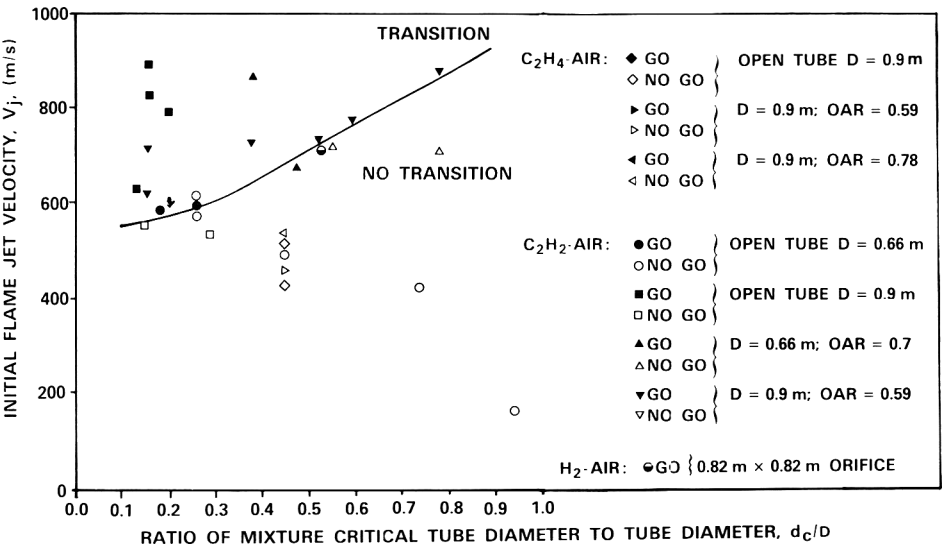

Fig. 18. Plot of initial flame jet velocity against the sensitivity of the mixture to detonation. (Tube diameter $D = 0.66$ m from Ref. [5]; $D = 0.9$ m from Ref. [49]; and 0.82 m × 0.82 m orifice from Ref. [50].)

sensitive nature of the fuel–air mixtures. These results were obtained with acetylene fuel, but there is no reason to exclude similar phenomena in other fuel–air mixtures provided the scale is sufficiently large. With an initial flame jet velocity of 600 m/s, for example, a critical tube to flame jet diameter (d_c/D)

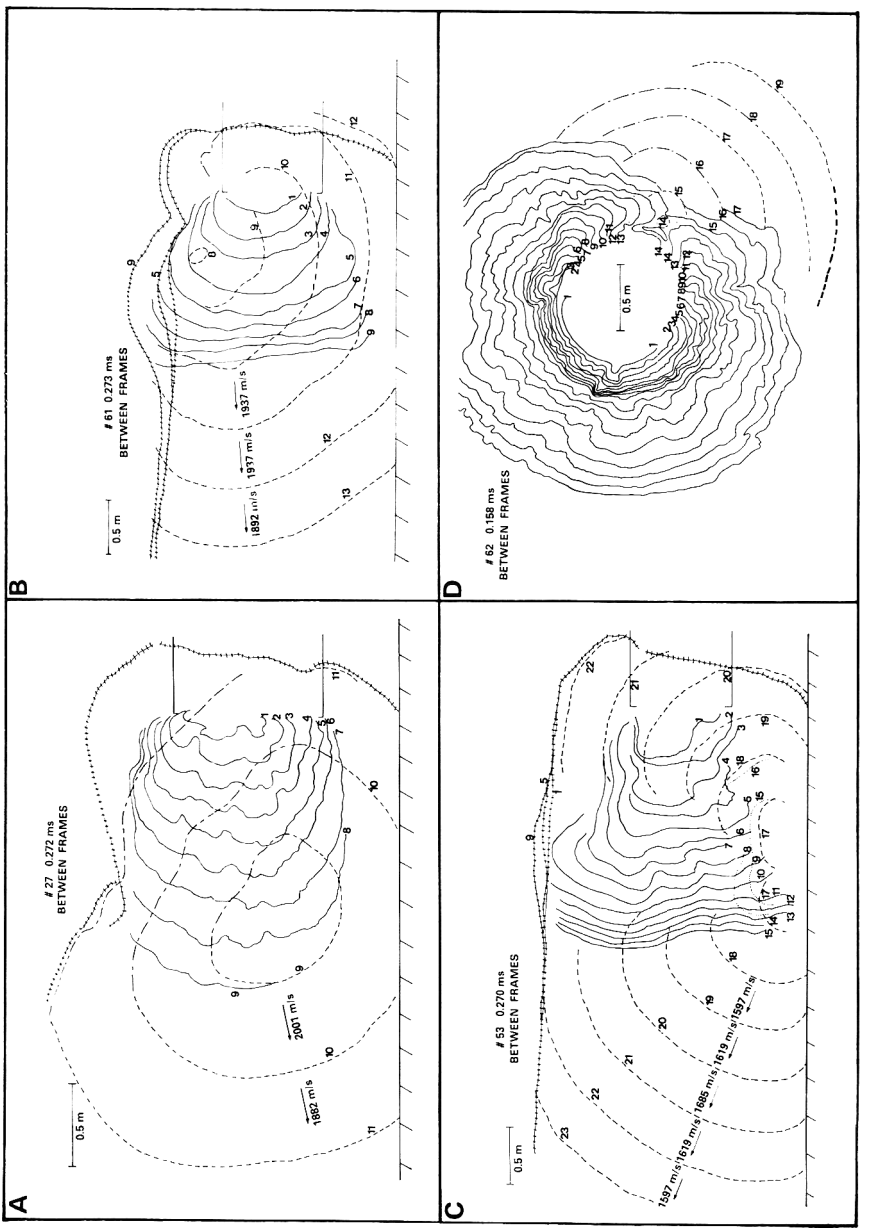

Fig. 19. Flame front and detonation front contour plots taken from the high-speed cinematographic records showing the various modes of transition to detonation: (A) transition in the pre-established flow downstream of a central blockage, (B) transition resulting from a flame/boundary interaction. (C) transition in the wake of the explosion reflecting from the ground, and (D) transition resulting from the collision of flame tongues in an asymmetric flame jet. Solid lines denote flame contours. Dashed lines signify detonation front contours. Cross-hatched lines depict boundaries of the plastic bag [49].

of about 0.1 would be required, as observed in acetylene–air. This corresponds to minimum jet diameters of about 2.0 m, 3.0 m, 9.0 m and 40 m for hydrogen–, ethylene–, propane– and methane–air mixtures, respectively. These scale requirements could be reduced significantly by increasing the flame jet velocity. According to Fig. 18, an increase to 700 m/s, could decrease the minimum flame diameters by a factor of five.

6. Conclusions

Several experimental observations of transition to detonation in fuel–air mixtures have clearly demonstrated that transition phenomena, similar to those identified in more sensitive fuel–oxygen mixtures, can also occur in fuel–air mixtures. This means that the worst case detonation scenario cannot be excluded *a priori* in assessing the hazards from vapour cloud explosions.

The obstacle and confinement environment of the vapour cloud must be taken into account in assessing the potential for DDT. Weak ignition of vapour clouds in an unconfined, relatively unobstructed environment is unlikely to result in DDT, even for relatively sensitive fuel–air mixtures. On the other hand, DDT can be considered likely in highly confined clouds, particularly if there are obstacles present to accelerate the flame. Explosions in confined spaces can also serve as strong ignition sources for external clouds, greatly enhancing the potential for DDT. In partially confined regions, more typical of chemical plants, the potential for DDT is less than in the heavily confined regions, and depends critically on the degree of confinement, the obstacle configuration, the ignition source, the initial turbulence and the fuel–air mixture. Any configuration which can produce large turbulent burning pockets or eddies is susceptible to localized explosions which can trigger transition to detonation.

At the present time, it is not possible to predict whether transition can occur in a given spill scenario, but considerable progress has been made towards quantifying both the flame acceleration processes and the relative detonability of fuel–air mixtures. The qualitative 'picture' of the transition phenomena presented by Lee and Moen [11] in 1980 remains essentially unchanged. New data which lend further support to this 'picture' have been described. Of particular relevance are the observations of DDT in large scale experiments. These observations confirm that the essential requirement for transition is a high rate of energy release associated with rapid burning or explosion of a sufficiently large volume. The minimum volume required depends on the sensitivity of the mixture to detonation. This sensitivity can be characterized by the detonation length scales (i.e., the detonation cell size and the critical tube diameter). Typically, the detonation length scales for fuel–air mixtures are at least an order of magnitude larger than those for fuel–oxygen, so that large scale experiments were required to clarify the potential for DDT in fuel–air mixtures.

Quantitative criteria for the critical turbulent mixing and burning rates required for DDT in a given fuel–air mixture are still lacking. However, it has been shown that the critical conditions can be achieved by: (i) flame acceleration; (ii) ignition of a turbulent pocket; and (iii) jet ignition. Better controlled and diagnosed experiments supported by numerical calculations are required to quantify the mechanisms responsible for DDT. Such investigations are particularly important for clarifying the potential for DDT in less sensitive fuel–air mixtures such as methane–air. Since, the scale of the experiments required to confirm this potential becomes prohibitively large (e.g., 10–40 m diameter flame jets for methane–air) it is recommended that extensive fundamental theoretical, numerical and experimental studies of the DDT mechanisms be performed before such experiments are attempted.

References

1 H. Pförtner and H. Schneider. Explosion von Wasserstoff–Luft Gemischen unter teilverdämmten Bedingungen und unter dem Einfluss einer turbulenten Strömung, FhG-ICI Report, 1984, Pfinztal Berghausen (FRG).
2 I.O. Moen, D. Bjerketvedt, A. Jenssen and P.A. Thibault, Transition to detonation in a large fuel–air cloud, Combustion and Flame, 61 (1983) 285–291.
3 M.P. Sherman, S.R. Tieszen, W.B. Benedick, J.W. Fisk and M. Carcissi, The effect of transverse venting on flame acceleration and transition to detonation in a large channel, AIAA Prog. Astronaut. Aeronaut. 106 (1986) 66–89.
4 I.O. Moen, A. Sulmistras, B.H. Hjertager and J.R. Bakke, Turbulent Flame Propagation and Transition to Detonation in Large Fuel–Air Clouds, 21st Symp. (Int.) on Combustion, The Combustion Institute, Pittsburgh, PA, 1986, pp. 1617–1627.
5 I.O. Moen, D. Bjerketvedt, T. Engebretsen, A. Jenssen, B.H. Hjertager and J.R. Bakke, Transition to detonation in a flame jet, Combustion and Flame, 75 (1989) 297–308.
6 M. Bjørkhaug and B.H. Hjertager, Influence of obstacle shape, fuel composition and obstacle layout on Flame and Pressure Development in a Radial Vessel of 10 m Radius, Chr. Michelsen Institute Report No. 865403-1, Bergen (Norway), 1986.
7 R.J. Harris and M.J. Wickens, Understanding vapour cloud explosions — An experimental study, Communication 1408, 55th Atumn Meeting of the Institute of Gas Engineers, Kensington Hall Town, 27–28 November, The Institution of Gas Engineers, London, 1989.
8 C.K. Chan, Personal communication, 1991.
9 J.E. Lee, R. Knystautas and N. Yoshikawa, Photochemical initiation of gaseous detonations, Acta Astronautica, 5 (1978) 971–982.
10 R. Knystautas, J.H. Lee, I.O. Moen and H.Gg Wagner, Direct initiation of spherical detonation by a hot turbulent gas jet, 17th Symp. (Int.) on Combustion, The Combustion Institute, Pittsburgh, PA, 1979, pp. 1235–1244.
11 J.H.S. Lee and I.O. Moen, The mechanisms of transition from deflagration to detonation in vapor cloud explosions, Prog. Energy Combust. Sci. 6 (1980) 359–389.
12 J.E. Shepherd and J.H.S. Lee, On the transition from deflagaration to detonation, In: M.Y. Hussaini, A. Kunar and R.G. Voight (Eds.), Major Research Topics in Combustion, Springer-Verlag, Berlin, 1992, pp. 439–487.

13 S. Gordon and B.J. McBride, Computer program for calculation of complex chemical equilibrium compositions, rocket performance, incident and reflected shocks and Chapman Jouget detonations, NASA Report SP-273, Washington, DC, 1976.
14 M. Cowperthwaite and W.H. Zwisler, TIGER Computer program documentation, Stanford Research Institute Publication No. Z106, Stanford, CA, 1973.
15 I.O. Moen, P.A. Thibault and J.W. Funk, Blast waves from non-spherical fuel air explosions, Proc. of the 8th Int. Symp. on Military Applications of Blast Simulation, Paper No. I.7, Spiez (Switzerland), June 1983.
16 W. Fickett and W.C. Davis, Detonation, University of California Press, Berkeley, CA, 1979.
17 C.K. Westbrook, Chemical kinetics of hydrocarbon oxidation in gaseous detonations, Combustion and Flame, 46 (1982) 191–210.
18 C.K. Westbrook and P.A. Urtiew, Chemical kinetic predictions of critical parameters in gaseous detonations. 19th Symp. (Int.) on Combustion, The Combustion Institute, Pittsburgh, PA, 1982, pp. 615–622.
19 J.E. Shepherd, Chemical kinetics of hydrogen air–diluent detonations, AIAA Prog. Astronaut. Aeronaut., 106 (1986) 263–293.
20 J.E. Shepherd, I.O. Moen, S.B. Murray and P.A. Thibault, Analyses of the cellular structure of detonations, 21st Symp. (Int.) on Combustion, The Combustion Institute, Pittsburgh, PA, 1987, pp. 1649–1658.
21 I.O. Moen, S.B. Murray, D. Bjerketvedt, A. Rinnan, R. Knystautas and J.E. Lee, Diffraction of detonation from tubes into a large fuel–air explosive cloud, 19th Symp. (Int.) on Combustion, The Combustion Institute, Pittsburgh, PA, 1982, pp. 635–644.
22 I.O. Moen, J.W. Funk, S.A. Ward, M.G. Rude and P.A. Thibault, Detonation length scales for fuel–air explosives, AIAA Prog. Astronaut. Aeronaut., 94 (1983) 55–79.
23 R. Knystautas, C. Guirao, J.H. Lee and A. Sulmistras, Measurement of cell size in hydrocarbon–air mixtures and predictions of critical tube diameter, Critical intiation energy and detonability limits. AIAA Prog. Astronaut. Aeronaut., 94 (1983) 23–37.
24 O. Peraldi, R. Knystautas and J.H. Lee, Criteria for Transition to Detonation in Tube, 21st Symp. (Int.) on Combustion, The Combustion Institute, Pittsburgh, PA, 1988, pp. 1629–1636.
25 R. Knystautas, J.E. Lee, O. Peraldi and C.K. Chan, Transmission of a flame from a rough to a smooth-walled tube, AIAA Prog. Astronaut. Aeronaut., 106 (1986) 37–52.
26 I.O. Moen, A. Sulmistras, G.O. Thomas, D. Bjerketvedt and P.A. Thibault, The influence of cellular regularity on the behaviour of gaseous detonations, AIAA Prog. Astronaut. Aeronaut., 106 (1986) 220–243.
27 T. Engebretsen, Propagation of Gaseous Detonations through Regions of Low Reactivity, Doctoral Thesis, Thermal Energy Division, The Norwegian Institute of Technology, Trondheim (Norway), 1991.
28 G. Dupré, O. Peraldi, J.H.S. Lee and R. Knystautas, Propagation of detonation waves in an acoustic absorbing walled tube, Prog. Astronaut. Aeronaut., 114 (1988) 248–263.
29 Ya.B. Zeldovich, S.M. Kogarko and N.N. Simonov, An experimental investigation of spherical detonation of gases, Sov. Phys.-Tech. Phys., 1 (1956) 1689–1713.
30 D.C. Bull, Concentration limits to the initiation of unconfined detonation in fuel/air mixtures, Trans. Inst. Chem. Eng., 57 (1979) 219–227.
31 W.B. Benedick, C.M. Guirao, R. Knystautas and J.H. Lee, Critical charge for the direct initiation of detonation in gaseous fuel–air mixtures, AIAA Prog. Astronaut. Aeronaut., 106 (1986) 181–202.
32 I.O. Moen and A.J. Saber, Explosion Hazards of Hydrogen Sulphide, Phase II: Flame Acceleration and Transition to Detonation Review, Atomic Energy Control Board Report, Ottawa, Ont., Canada, September 1985.
33 P.A. Urtiew and A.K. Oppenheim, Experimental observations of transition to detonation in an explosive gas, Proc. R. Soc., A295 (1966) 13–28.

34 J.H. Lee, R. Knystautas and C.K. Chan, Turbulent flame propagation in obstacle-filled tubes, 20th Symp. (Int.) on Combustion, The Combustion Institute, Pittsburgh, PA, 1985, pp. 1663–1672.
35 W. Bartknecht, Explosions, Springer-Verlag, Berlin, 1981.
36 H. Steen and K. Schampel, Experimental investigation of the run-up distance of gaseous detonations in large pipes, 4th Int. Symp. on Loss Prevention and Safety Promotion in the Process Industries, Pergamon Press, London, 1983, pp. E23–33.
37 I.O. Moen, J.H.S. Lee, B.H. Hjertager, K. Fuhre and R.K. Eckhoff, Pressure development due to turbulent flame propagation in large-scale methane–air explosions, Combustion and Flame, 47 (1982) 31–52.
38 C. Chan, J.H.S. Lee, I.O. Moen and P.A. Thibault, Turbulent flame acceleration and pressure development in tubes, Proc. 1st Specialist Meeting (Int.) of the Combustion Institute, Bordeaux (France), 20–24 July, 1981, p. 479.
39 B.H. Hjertager, K. Fuhre, S.J. Parker and J.R. Bakke, Flame acceleration of propane–air in a large obstructed tube, AIAA Prog. Astronaut. Aeronaut., 94 (1984) 504–522.
40 B.H. Hjertager, Simulation of transient compressible turbulent reactive flows, Combust. Sci. Technol., 27 (1982) 159–170.
41 B.H. Hjertager, Influence of turbulence on gas explosions, J. Hazardous Mater., 9 (1984) 315–346.
42 B.H. Hjertager, Simulation of gas explosions, Model. Ident. Control, 10(4) (1989) 227–247.
43 M. Berman, A critical review of recent large-scale experiments on hydrogen–air detonations, Nucl. Sci. Eng., 93 (1986) 321–347.
44 C.K. Chan, I.O. Moen and J.H.S. Lee, Influence of confinement on flame acceleration due to repeated obstacles, Combustion and Flame, 49 (1983) 27–39.
45 C.J.M. van Wingerden and J.P. Zeeuwen, Investigation of explosion-enhancing properties of a pipe-rack-like obstacle array, AIAA Prog. Astronaut. Aeronaut., 106 (1984) 53–65.
46 K.H. Orth (Responsible Director), Transition from slow deflagration to detonation, CEC-Research Programme Final Report, Control No. SR-019-80D(B), Technisches Berichtwesen R914/83/045, Kraftwerk Union, Reaktorentwicklung, Erlangen (West Germany), 1983.
47 I.O. Moen and A. Sulmistras, Flame Acceleration and Transition to Detonation in Large Fuel–Air Clouds with Obstacles (U), Suffield Memorandum No. 1159, Defence Research Establishment Suffield, Ralston, Alberta, Canada, April 1986. UNCLASSIFIED.
48 P.A. Urtiew, J. Brandeis and W.J. Hogan, Experimental Study of Flame Propagation in Semiconfined Geometries with Obstacles, Combustion Sci. Technol., 30 (1983) 105–119.
49 D.J. Mackay, S.B. Murray, I.O. Moen and P.A. Thibault, Flame-Jet Ignition of Large Fuel–Air Clouds, 22nd Symposium (International) on Combustion, The Combustion Institute, Pittsburgh, PA., 1988, pp. 1339–1353.
50 H. Pförtner and H. Schneider, Versuche zur Freistrahlzungdung Partiell Verdämmter Wasserstoff–Luft im Hinblick auf die Skalierbarkeit des Ubergangs Deflagration–Detonation, FhG.ICT Report, 1984, Pfinztal-Berghausen, Germany.

Journal of Hazardous Materials, 33 (1993) 193–202
Elsevier Science Publishers B.V., Amsterdam

The history and development of emergency response planning guidelines

George M. Rusch

Allied-Signal Inc., 101 Columbia Road, Morristown, NJ 07962 (USA)

Abstract

In 1988, the Emergency Response Planning Guideline Committee was formed to review a series of documents summarizing chemical toxicity which had been developed by a combined interindustry effort. This Committee, is a part of the American Industrial Hygiene Association and is composed of representatives from academia, government and industry, with backgrounds in industrial hygiene, medicine and toxicology. Since its founding, the Committee has published 35 review documents containing recommendations for emergency exposure planning levels. Currently, the Committee is working on another 25. Most of the chemicals selected for this process are on the SARA Title III Extremely Hazardous Substance List or the OSHA Highly Hazardous Chemical List.

1. Introduction

The tragic accidental release of methylisocyanate in Bhopal, India underscored the need for the chemical industry to pool its resources and work with local and national authorities in the development of emergency response plans [1–3]. These activities have been occurring at many levels around the world. In Europe for example, the European Chemical Industry Ecology and Toxicology Centre (ECETOC) has formed a task force which has produced a guide for reviewing chemicals and estimating the hazard associated with an accidental release [4].

In the U.S., under SARA Title III and similar regulations, local communities are required to set up emergency response plans in locations where potential hazards exist such as nuclear power plants or chemical manufacturing operations [5]. These plans frequently include utilization of emergency response teams which may include fire fighters, first aid professionals, and police. Representatives from industry and members of the community are working together to develop emergency response plans. Where chemicals are involved,

Correspondence to: G.M. Rusch, Allied-Signal Inc., 101 Columbia Road, Morristown, NJ 07962 (USA).

it is important to know the identity of the chemical; the toxicity of the chemical and the amount used or stored at the plant. It is also important to have an idea of the area that could be affected if the chemical is accidentally released, and to have an understanding of air-flow patterns around the area [6, 7]. With this information, local emergency response teams can make estimates of dispersion in the event of a catastrophic release and make appropriate plans for evacuation of the local community, if necessary. In addition, the teams need to know how to monitor for these chemicals in the air; what type of protective equipment is required; what is appropriate breathing protection; when to administer first aid; what constitutes an effective first aid treatment; and if there is an effective way to disperse the cloud or neutralize the chemical.

Much of this information should be well known to the plant safety personnel, especially current information on protective equipment, monitoring, respirator selection, and containment practices. Information on air-flow modeling must be developed locally. Information on the toxicity of the chemical and treatments for exposure should be obtained from expert sources.

There are many references and guides which offer recommendations for maximum permissible exposure levels for a variety of chemicals. For workplace standards, one can refer to the OSHA-Permissible Exposure Levels (PELs) [8], the American Conference of Governmental Industrial Hygiene's Documentation for the Threshold Limit Values (TLVs) [9]; the American Industrial Hygiene Association's (AIHA) Workplace Environmental Exposure Level Guides [10] or the NIOSH Recommended Exposure Levels [11]. None of these, however, are designed for emergency situations or even single, acute exposures, in general. On one hand, they typically consider workers whose health status may be somewhat better than that of the general population. Also, they are designed for long-term exposure scenarios such as 8 to 10 hours per day, 5 to 6 days per week for several years. In contrast, the emergency exposure should, by definition, be a rare event of short duration, possibly at a high or unknown concentration, but one which could involve a heterogeneous population.

Currently, there are two reference sources available for emergency exposures. The first was developed by the National Research Council (NRC) for use by the military. These are called Emergency Exposure Guidance Levels or EEGLs [12]. While these can be very helpful, they have been developed for a population of healthy young adults and are not applicable to the general public. They provide a single value which is the estimate for the highest exposure which will not interfere with one's ability to perform specific tasks. While Short Term Emergency Guidance Levels (SPEGLs) have also been developed by the NRC to address exposures to civilians living in and near military installations, these cover only a few chemicals.

The second series of publications deal with the toxicity associated with potential exposures to acutely toxic chemicals [13], that is, possible community exposure resulting from the accidental release of a chemical. These series of

documents are called Emergency Response Planning Guides (ERPGs) and are published by the American Industrial Hygiene Association's Emergency Response Planning Committee. The development of these decuments will be described in the balance of the paper.

1.1 History

Following Bhopal, the chemical industry increased its efforts to develop comprehensive assessments of the risks from possible chemical exposures resulting from accidental chemical releases. A key component was the development of a comprehensive understanding of the toxicology of the chemical substances in question.

Many companies already had toxicology information on their major products and most had developed contingency plans to address accidents. While much of these data were shared, a forum was needed to aid in the exchange and review of this information and for review and discussion of other information available in the published literature. In this way, companies could pool their information and scientific expertise to develop a comprehensive understanding of the chemicals in question. This forum was provided in 1987 through the Organization Resources Counselors (ORC) [14]. Working through the ORC, member companies sent scientific representatives to form a review committee. The committee discussed the selection of candidate chemicals for review. The criteria considered included quantities produced, number of people and sites using the substance, number of companies using the substance, whether it appeared to be a highly toxic substance, and the physical properties of the chemical (i.e. gas or volatile liquid which could lead to widespread distribution, or a solid with limited potential for dispersion). In addition, the chemicals listed on the Hazardous Substance List from SARA Title III were considered. Recently, consideration has been extended to include those chemicals on the new OSHA list of Highly Hazardous Chemicals [15].

Member companies were then asked to write review documents, modeled after the AIHA's WEEL guides and NRC EEGLs, on compounds for which they had extensive knowledge. They also included recommendations for emergency exposure limits. These documents were then reviewed by the full ORC Committee for completeness, accuracy and quality.

As the process evolved, it was recognized that there would be a significant advantage to having these documents peer reviewed by an interdisciplinary group of occupational health professionals. To this end, the members of the ORC committee worked with the American Industrial Hygiene Association (AIHA) to create a review committee. The AIHA has members from academia, government and industry and broadly represents the area of occupational health. This led to the formation of the AIHA's Emergency Response Planning Committee in 1988, as an *Ad Hoc* Committee within the Workplace Environmental Exposure Level (WEEL) Committee. Two years later, the ERPG Committee was made a full, permanent AIHA Committee.

2. Function of the emergency response planning committee

The Committee is composed of representatives from academia, government and industry. While some members may write Emergency Response Planning documents for their institutions, the Committee is a Review Committee. Its function is to take documents written by others, review them, edit them, and make recommendations for emergency exposure planning levels based on the available toxicology information. The guidelines by which the Committee functions are described in the preface document reproduced below.

PREFACE TO EMERGENCY RESPONSE PLANNING GUIDELINES

The emergency Response Planning Guideline (ERPG) values are intended to provide estimates of concentration ranges above which one could reasonably anticipate observing adverse effects as described in the definitions for ERPG-1, ERPG-2, and ERPG-3 as a consequence of exposure to the specific substance.

The ERPG-1 is the maximum airborne concentration below which it is believed that nearly all individuals could be exposed for up to 1 hr without experiencing other than mild transient adverse health effects or perceiving a clearly defined objectionable odor.

The ERPG-2 is the maximum airborne concentration below which it is believed that nearly all individuals could be exposed for up to 1 hr without experiencing or developing irreversible or other serious health effects or symptoms that could impair their abilities to take protective action.

The ERPG-3 is the maximum airborne concentration below which it is believed that nearly all individuals could be exposed for up to 1 hr without experiencing or developing life-threatening health effects.

The committee recognizes (and all who make use of these values should remember) that human responses do not occur at precise exposure levels but can extend over a wide range of concentrations. The values derived for ERPGs should not be expected to protect everyone but should be applicable to most individuals in the general population. In all populations there are hypersensitive individuals who will show adverse responses at exposure concentrations far below levels where most individuals would normally respond. Furthermore, since these values have been derived as planning and emergency response guidelines, *not* as exposure guidelines, they do not contain the safety factors normally incorporated into exposure guidelines. Instead, they are estimates, by the committee, of the thresholds above which there would be an unacceptable likelihood of observing the defined effects. The estimates are based on the available data summarized in the documentation. In some cases where the data are limited, the uncertainty of these estimates is large. Users of the ERPG values are strongly encouraged to review carefully the documentation before applying these values.

In developing these ERPGs, human experience has been emphasized to the extent data are available. Since this type of information is rarely available, however, and, when available, usually is only for low level exposures, animal exposure data most frequently form the basis for these values. The most pertinent information is derived from acute inhalation toxicity studies that have included clinical observations and histopathology. The focus is on the highest levels not showing the effects described by the definitions of the ERPG levels. Next, data from repeat inhalation exposure studies with clinical observations and histopathology are considered. Following these in importance are the basic, typically acute, studies where mortality is the major focus. When inhalation toxicity data are either unavailable or limited, data from studies involving other routes of exposure will be considered. More value is given to the more rigorously conducted studies, and data from short-term studies are considered to be more useful in estimating possible effects from a single 1-hr exposure. Finally, if mechanistic or dose-response data are available, they are applied, on a case by case basis, as appropriate.

It is recognized that there is a range of times that one might consider for these guidelines; however, it was the committee's decision to focus its efforts on only one time period. This decision was based on the availability of toxicology information and a reasonable estimate for an exposure scenario. Some using these guideline levels will prefer other, usually shorter, exposure periods and will seek ways of extrapolating ERPGs for other exposure durations. The usual method for such extrapolation is to use the Haber relationship, expressing the constancy of the product of exposure concentration and exposure duration ($Ct = K$). However, users are cautioned against such extrapolation. The Haber relationship, with or without some of the proposed modifications, does not hold over more than small differences in exposure time.

Use of these ERPG values for exposure periods shorter than 1 hour should be safe; use for longer periods is not. Extrapolation to higher guidance levels for shorter exposure periods should not be attempted by use of the Haber relationship or modifications thereof without specific validating data. This caution about extrapolations applies to exposures to most toxic substances that are dose-limiting substances, but not generally to sensory irritants that are concentration-limiting substances. With some of these latter substances, exposure should be limited to a given concentration regardless of the exposure time because of the sensory response produced.

Initially, the Committee was exclusively reviewing documents prepared by the ORC member companies. However, from the outset, it was felt that the Committee should consider documents from all reliable sources. The decision to review a document would be based on: (1) The need for a document on the substance in question; these criteria are similar to those used by ORC. (2) The existence of adequate toxicology information to develop exposure guidelines. (3) The quality of the document submitted for review. The Committee has also taken a practical, advocacy role. It has reviewed both the SARA Title III and OSHA Highly Hazardous Chemical lists and is encouraging members of the ORC and the Chemical Manufacturers Association as well as other organizations to draft documents on the most important chemicals on these lists.

Additionally, the Committee is working with the Department of Energy, reviewing Emergency Response Planning Guides developed by DOE on substances of concern to them. The Committee has also reviewed documents written by some of its members, but in those cases the author does not serve in any direct review capacity.

The scope of the Committee was described in "Concepts and Procedures for the Development of Emergency Response Planning Guidelines", published by the AIHA in December, 1989 [16]. The exposure parameters to be included in the development of these guides were considered at great length. Two key questions were: (1) the number of time intervals, and (2) criteria for and number of exposure levels. There were good arguments for considering both short and long time intervals. The Committee recognized that, while no one time interval would accommodate all needs, nor would two or three. Therefore, it is decided to consider a single one-hour exposure interval. As most acute inhalation toxicity studies utilize exposure periods of from one to four or six hours and most accidental exposures are for periods of less than one hour, the one-hour interval represented a time period that would combine reasonable precision of experimental data with community need.

In considering the number of exposure levels to be defined, the Committee agreed on three. These have been defined in our preface, and correspond to the threshold for recognition of adverse exposure (ERPG-1); the threshold for possible toxic action resulting from exposure (ERPG-2); and the threshold for possible lethal effects (ERPG-3). In cases where the threshold for toxicity occurs at or below the odor threshold or other ERPG-1 criteria, an ERPG-1 is not defined. Otherwise, the three values are defined for all chemicals.

While all available toxicity information is considered during the review process, emphasis is on those endpoints that can be associated with single short term exposures. Thus, acute toxicity and lethality data, which rarely are critical in the risk assessment process, are central in estimating the ERPG levels.

The Committee has been asked to consider possible environmental effects resulting from chemical release. While there is no question that this is a major concern, the Committee did not feel it had the expertise or resources needed to adequately address this issue.

3. Review process

The procedure followed during the reviewing process is outlined in Fig. 1. The reviewers check the references, style and accuracy of information. If necessary, they confer with the author and make revisions before sending it for full Committee review. Additionally, suggestions may be made by either the author or one of the reviewers for ERPG levels.

The Committee's initial review begins with a consideration of the chemical's physical properties. How likely is it to become airborne and in what form and what level? Gases and vapors from highly volatile liquids represent the greatest exposure potential. Some substances can form fumes which can also travel large distances, while other fumes quickly coalesce and settle out.

Next, the acute toxicity data are considered. Of greatest importance is any information on inhalation toxicity. Using this information, the Committee attempts to estimate the one-hour lethal threshold and slope of the dose response curve. Data from all species and time intervals are considered and compared for consistency. The greater the consistency, the greater the confidence one has in the data. Naturally, more recent studies and those with good analytical data are considered first. Unless there is something unique about a particular animal model, it is assumed that man will be as sensitive as the most sensitive specie tested.

After a review of the acute data, subacute and subchronic data are evaluated. Subacute and subchronic studies are conducted for much longer time periods than covered by ERPGs, therefore, their primary use is in the identification of possible target organs. This provides better insight on the possible effects that could result from exposure to the chemical. These data can also provide the physician with help in determining treatment. This information is compared to any information on systemic toxicity in the acute studies to see if the target organs are the same.

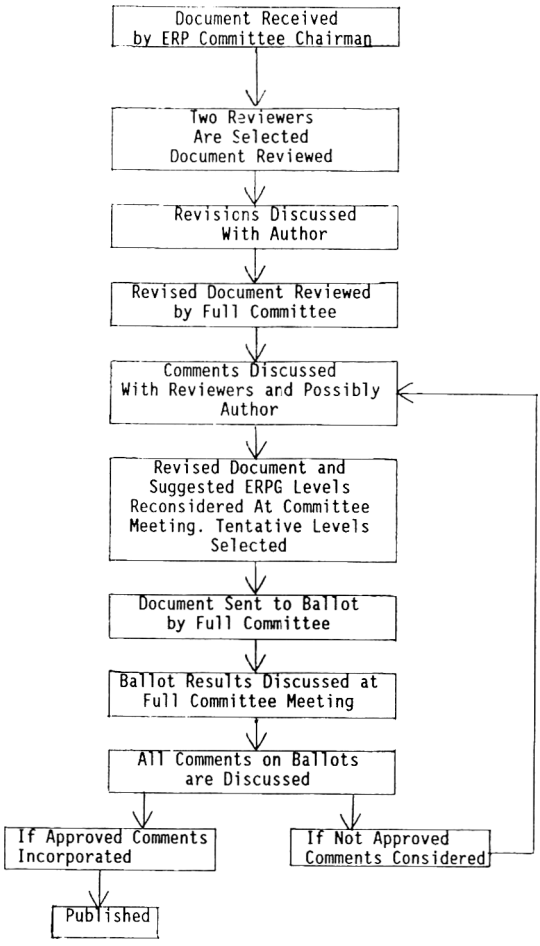

Fig. 1. Emergency response planning guideline review process.

Next, any information on reproductive or developmental toxicity and possible teratogenicity is considered. Because birth defects may arise from a relatively short term exposure to high levels of a chemical, these findings are of great concern and the studies are used in determining the ERPG-2 level. Other information on reproductive or developmental toxicity is considered more generally, along with the subchronic data. If, however, one noted signs of severe embryo toxicity or lethality, it would be considered carefully in the development of estimates of exposure levels for both ERPG-2 and ERPG-3 levels.

Mutagenicity data is generally used only to enhance understanding of the chronic data when it is available. If there are no chronic data, a high, reproducible level of mutagenic activity would be taken as a caution sign. Chronic data again serve primarily to help identify target organs, and to a lesser degree, to look for cumulative effects. Compounds that show carcinogenic activity are

TABLE 1

Currently approved ERPGs (1992)

Chemical	ERPG-1	ERPG-2	ERPG-3
Acrolein	0.1 ppm	0.5 ppm	3 ppm
Acrylic acid	2 ppm	50 ppm	750 ppm
Allyl chloride	3 ppm	40 ppm	300 ppm
Ammonia	25 ppm	200 ppm	1000 ppm
Bromine	0.2 ppm	1 ppm	5 ppm
1,3-Butadiene	10 ppm	50 ppm	5000 ppm
Carbon disulfide	1 ppm	50 ppm	500 ppm
Chlorine	1 ppm	3 ppm	20 ppm
Chloroacetyl chloride	0.1 ppm	1 ppm	10 ppm
Chloropicrin	NA[a]	0.2 ppm	3 ppm
Chlorosulfonic acid	2 mg/m^3	10 mg/m^3	30 mg/m^3
Chlorotrifluoroethylene	20 ppm	100 ppm	300 ppm
Crotonaldehyde	2 ppm	10 ppm	50 ppm
Diketene	1 ppm	5 ppm	50 ppm
Dimethylamine	1 ppm	100 ppm	500 ppm
Epichlorohydrin	2 ppm	20 ppm	100 ppm
Formaldehyde	1 ppm	10 ppm	25 ppm
Hexachlorobutadiene	3 ppm	10 ppm	30 ppm
Hydrogen chloride	3 ppm	20 ppm	100 ppm
Hydrogen fluoride	5 ppm	20 ppm	50 ppm
Hydrogen sulfide	0.1 ppm	30 ppm	100 ppm
Isobutyronitrile	10 ppm	50 ppm	200 ppm
Methyl iodide	25 ppm	50 ppm	125 ppm
Methyl mercaptan	0.005 ppm	25 ppm	100 ppm
Monomethylamine	10 ppm	100 ppm	500 ppm
Perfluoroisobutylene	NA	0.1 ppm	0.3 ppm
Phenol	10 ppm	50 ppm	200 ppm
Phosgene	NA	0.2 ppm	1 ppm
Phosphorus pentoxide	5 mg/m^3	25 mg/m^3	100 mg/m^3
Sulfur dioxide	0.3 ppm	3 ppm	15 ppm
Sulfuric acid (oleum, sulfur trioxide, and sulfuric acid)	2 mg/m^3	10 mg/m^3	30 mg/m^3
Tetrafluoroethylene	200 ppm	1000 ppm	10 000 ppm
Titanium tetrachloride	5 mg/m^3	20 mg/m^3	100 mg/m^3
Trimethylamine	0.1 ppm	100 ppm	500 ppm
Vinyl acetate	5 ppm	75 ppm	500 ppm

[a]NA = not appropriate.

evaluated using the multistage linear model at a risk level of one in ten thousand. Since the actual exposure period is so short, one hour in a lifetime, carcinogenicity is rarely a significant factor.

Any human experiences are also considered. While one would like to rely heavily on this type of information, rarely does one have a good estimate for exposure level and much of the data is, therefore, anecdotal. This information

is compared, where possible, to the animal data to look for consistency of target organs or any unique responses. Also, data on odor threshold or irritation thresholds can be very helpful in estimating the ERPG-1 level.

Although occupational exposure limits are generally developed for exposures of eight hours or more per day, and for extended periods of time, the basis for these is reviewed very carefully. Frequently, they, along with information on human exposure experiences, are very helpful in determining ERPG-1 levels.

As the review process is going on, the Committee considers all the data in light of the definitions for ERPG-1, -2 and -3. Each value is independently considered, and is based on the data most suitable for that level. For example, irritation data could be used for an ERPG-1 level, developmental or subchronic toxicity data for an ERPG-2 level and acute lethality data for an ERPG-3 level. While many people would like to see a straightforward formula for deriving one ERPG value from the others, considering the definitions associated with each category the slope of the dose response curve, and the variety of effects seen, each value must be independently considered.

Accomplishments

Since its inception in 1988, the ERP Committee has developed planning guides for 35 chemicals and is currently working on another 25. Table 1 lists the chemicals for which ERPGs have been developed and the corresponding ERPG values for these chemicals. Table 2 lists compounds for which ERPGs are being developed.

In developing these values, the Committee had to try to be as precise as possible. If the recommendations were too high, people could be injured. Also, if the levels were set too low, the consequence could be unnecessary fear and concern or even large scale, unnecessary disruption associated with an evacuation. By providing this information and making it available to local communities, they can make better informed decisions in the event of an emergency.

ERPGs are not designed as exposure guides, but as planning guides. The exposure limits together with the supporting information are intended to be one part of a package used by emergency response teams.

TABLE 2

ERPGs currently under review

Acrylonitrile	Dimethyldisulfide	Methanol	Nitrogen dioxide
Arsine	Dimethylformamide	Methylbromide	Perchloroethylene
Benzyl chloride	Dimethylsulfide	Methylchloride	Phosphene
Carbon monoxide	Ethylene oxide	Methylisocyanate	Styrene
Carbon tetrachloride	Hexafluoroacetone	n-Butylacrylate	Toluene
Chlorine trifluoride	Hydrogen cyanide	Nitric acid	Trichloroethylene
			Uranium hexafluoride

Acknowledgements

The success of this program is the result of the combined effort of the entire ERPG Committee. I would like to thank all of the other current members: Jim Barnett, Jonathan Borak, David Brown, Barbara Callahan, Finis Cavender, LeRoy Garcia, Larry Gephart, James Grapenthien, Doan Hansen, Brian Hardin, Keith Jacobson, David Kelly, Stephen Paul, Frank Renshaw, Richard Schlesinger, John Spencer, Marlene Swank and Richard Thomas.

References

1 U.S. Environmental Protection Agency, Health Assessment Document for Methyl Isocyanate. Environmental Criteria and Assessment Office, Research Triangle Park, NC (Final Draft), December 27, 1988.
2 L.A. Gephart and S. Moses, An approach to evaluate the acute impacts from simulated accidental releases of chlorine and ammonia, Plant/Operations Prog., 8(1) (1989) 8–11.
3 L.A. Gephart, B. Gorton, M.G. Schurger and T.S. Ely, Three tier emergency action levels for 20 chemicals. American Industrial Hygiene Association Conference Abstract No. 176, 1986.
4 ECETOC, Emergency Exposure Indices for Industrial Chemicals, Technical Report No. 3, Avenue Louise 250, B. 63, B-1050 Brussels, Belgium, 1991.
5 List of Extremely Hazardous Substances and Their Threshold Planning Quantities. 40 CFR Section 355, Appendix A. Government Printing Office, Washington, DC, 1987.
6 M.T. Fleischer, Mitigation of Chemical Spills: An Evaporation/Air Dispersion Model for Chemical Spills on Land. Shell Development Company, Houston, TX, 1980.
7 S. Hanna and P. Drivas, Guidelines For Use of Vapor Cloud Dispersion Model. Center For Chemical Process Safety (CCPS), Am. Inst. Chem. Eng., New York, NY, 1987.
8 Occupational Safety and Health Standards, Code of Federal Regulations, Title 29, Pt. 1910.1000 Table Z-1, Government Printing Office, Washington, DC, 1985.
9 American Conference of Governmental Industrial Hygienists, Documentation of Threshold Limit Values and Biological Exposure Indices. American Conference of Governmental Industrial Hygienists, Cincinnati, OH, 1987.
10 American Industrial Hygiene Association, Workplace Environmental Exposure Level Guide Series. American Industrial Hygiene Association, Akron, OH, 1986.
11 National Institute for Occupational Safety and Health Testimony on the Occupational Safety and Health Air Contaminants Rule, CFR 54 (2) (19 January 1989), Government Printing Office, Washington, DC, 1989, p. 2482.
12 National Academy of Sciences, Guideline for Short Term Exposures of the Public to Air Pollutants. National Research Council, Committee on Toxicology, National Academy Press, Washington, DC, 1987.
13 Emergency Response Planning Guidelines, American Industrial Hygiene Association, ERPG Committee, 345 White Pond Drive, Akron, OH 44320, 1992.
14 Organization Resources Counselors, Inc., 1910 Sunderland Pl., N.W., Washington, DC, 1992.
15 Occupational Safety and Health Administration. Process Safety Standard. CFR 57 (No. 36) 1910.119 List of Highly Hazardous Chemicals, Toxics and Reactives (February 24, 1991).
16 Concepts and Procedures for the Development of Emergency Response Planning Guidelines (ERPGs), American Industrial Hygiene Association, ERPG Committee, 345 White Pond Drive, Akron, OH 44320, 1989.

Journal of Hazardous Materials, 33 (1993) 203–214
Elsevier Science Publishers B.V., Amsterdam

Reactive monomer tank—A thermal stability analysis

T. Chakravarty[a], Harold G. Fisher[b] and Laura A. Voyt[b]

[a] *Bechtel Corporation, Houston, TX 77252 (USA)*
[b] *Union Carbide Chemicals and Plastics Company Inc., South Charleston, WV 25303 (USA)*

Abstract

Chemical production processes should always be examined to identify and, when needed, modified to prevent runaway reactions. A thermal stability analysis was therefore conducted on an existing process for producing a reactive monomer. Thermal decomposition kinetics were developed from Accelerating Rate Calorimeter (ARC) data. Due to a low Self-Accelerating Decomposition Temperature and short Time to Maximum Rate, the prevention of a runaway reaction due to a process upset was found to be more important than providing the normal fire exposure protective insulation. Runaway reaction computer simulations demonstrated that an uninsulated vessel would have a lower risk of venting toxic and flammable materials than an insulated vessel. Lessons learned from this analysis will be discussed.

1. Process description

A primary alcohol A is reacted with a reactive chemical R in a batch kettle at moderate temperature and pressure to form a reactive monomer M. The byproduct acid gas G is scrubbed and excess alcohol is refluxed to the kettle. Upon completion of the batch, the contents of the kettle are neutralized.

Excess alcohol is stripped from the kettle, condensed and collected in a lights receiver. The alcohol, however, forms an azeotrope with the product and also reacts with the product to form another bifunctional monomer T and a flammable gas H. The lights, which are a reactive mixture of the primary alcohol and the monomer, are transferred to a portable dumpster for incineration. The remaining product is transferred to intermediate storage. All process equipment is vented to prevent the build-up of non-condensible gas pressure at production conditions. Emergency relief was also to be provided for all process equipment to prevent overpressure due to a runaway reaction. Figure 1 is a schematic of the process.

Correspondence to: Dr. T. Chakravarty, Bechtel Corporation, Houston, TX 77252 (USA).

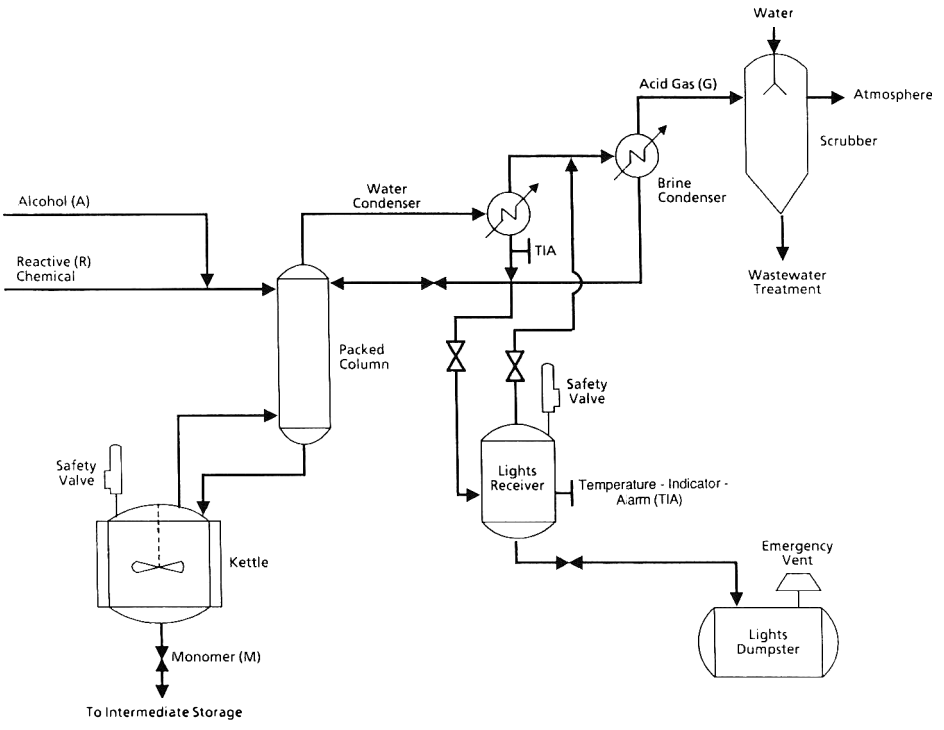

Fig. 1. Process flow sketch.

2. Process hazards

The product M is a flammable, toxic material of moderate volatility (NBPT 85 °C). A rapid, exothermic, uncatalyzed reaction between the alcohol and the product occurs at around 55 °C. A highly flammable, non-condensible gas H and a heavy product T are produced. The operating conditions are such that a process upset is more likely than fire exposure to induce a runaway reaction in the lights receiver.

3. Objective

Emergency relief was to be designed [1] for the lights receiver based upon a model of the thermal runaway reaction of the product with the primary alcohol. Our investigation into the safety of the process led us to conclude that various reactive mixtures in the lights receiver could undergo a runaway reaction at abnormally high process or ambient temperatures. Our goal was to reduce the risk of venting toxic and flammable materials. We therefore wanted to quantify the conditions where mixtures of various composition in the lights

receiver could undergo a runaway reaction so that a preventive strategy could be developed [1].

4. Kinetic model development

A kinetic model for the runaway reaction between the monomer and the alcohol was developed. We also developed thermal stability criteria for reactive mixtures in the lights receiver. Development of the kinetic model and the thermal stability criteria for these reactive mixtures are discussed below.

To develop a kinetic model for the reaction, several Accelerating Rate Calorimeter (ARC) tests [2] were conducted with the stoichiometric amount of alcohol and monomer. The tests show that a peak heat rate of several hundred degrees C/min and pressure of a few thousand psig can be generated in an industrial vessel.

A second order kinetic model for the thermal runaway reaction was developed using the ARC data. The rate of the uncatalyzed reaction was assumed to be first order with respect to the concentrations of alcohol and monomer, respectively.

$$\text{Reaction Rate (lb mol/ft}^3\text{ h)} = k C_A C_M \tag{1}$$

where k is the specific rate constant (ft^3/lb mol h), C_A is the alcohol concentration (lb mol/ft^3), and C_M is the monomer concentration (lb mol/ft^3).

Arrhenius kinetic parameters obtained from regression [3, 4] of the raw ARC data are shown in Table 1.

These kinetic parameters, the heat of reaction value and our physical property models were then checked by simulation of the ARC data using the UCC&P Runaway Reaction Emergency Relief Sizing Program. This digital simulation computer program uses numerical integration to solve the mass and heat balance differential equations, kinetic models and physical property relationships required to model plant production processes and provide solutions to the equations required to size emergency relief systems. The DIERS SAFIRE computer program [5, 6] has similar capabilities.

Figures 2, 3 and 4 compare the predictions of the heat rate, temperature and pressure, respectively, with the raw data. Our computer simulation agrees well

TABLE 1

Summary of kinetic parameters for the reaction A + M → T + H

$A\left(\frac{ft^3}{lb\ mol\ h}\right)$	E (cal/mol)	ΔH (Btu/lb mol)
1.89×10^{14}	23630	31770

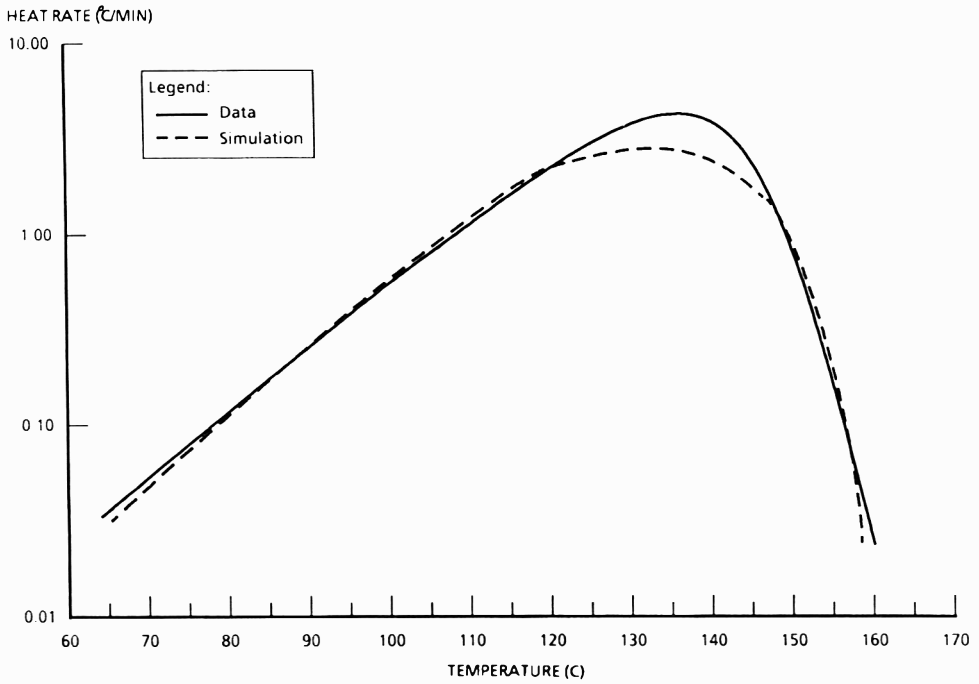

Fig. 2. Experimental data vs. simulation stoichiometric A + M → T + H(g) (PHI = 1.7).

with the experimental data and accounts for the variable thermal inertia (heat capacity effect) of the ARC bomb. Nevertheless, a few comments are worth making regarding fitting of the data.

1. The kinetic parameters were fitted based upon the assumption that the reaction rate is equal to $kC_A C_M$.
2. The kinetic model was not verified against isothermal rate data.
3. The assumption of equimolar decomposition stoichiometry and a negligible gas solubility fit the pressure data.
4. Extrapolation of model results beyond the temperature range of the data must be done with caution.

5. Effects of contamination

Possible effects of contaminants such as the acid gas and iron in ppm quantities have also been investigated. ARC tests conducted using tantalum bombs show significant effects of iron on the experimental onset temperature as well as on the peak heat rate. The experimental onset temperature of the iron catalyzed reaction is lowered by approximately 50 C and the peak heat rate increased tenfold. The effect of iron is believed to be catalytic. The

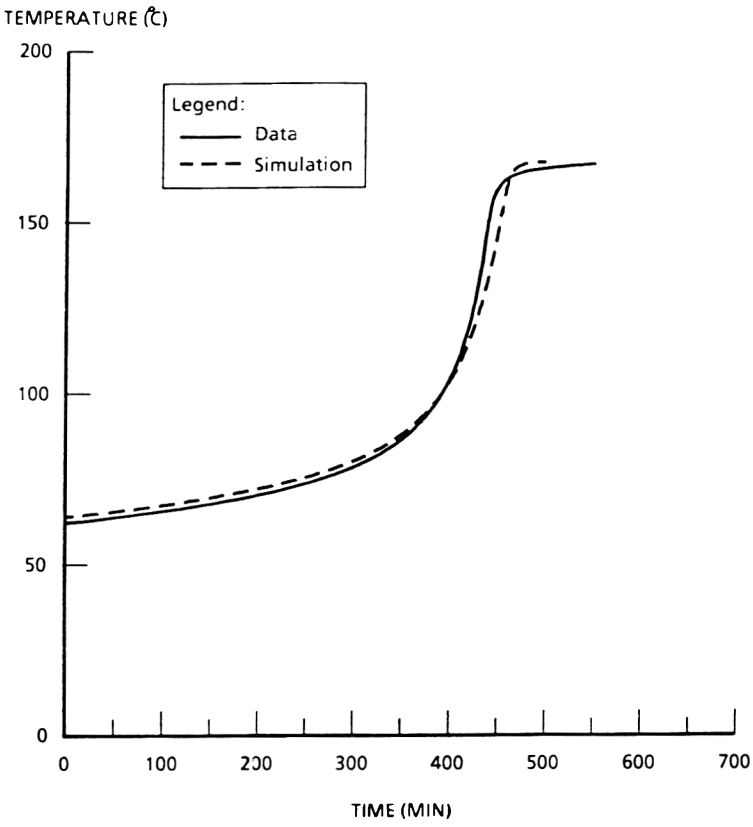

Fig. 3. Experimental data vs. simulation stoichiometric A + M → T + H(g) (PHI = 1.7).

presence of acid gas, on the other hand, tends to raise the onset temperature, perhaps by preferentially reacting with the primary alcohol.

The best means to avoid a runaway reaction due to contamination is to avoid the presence of any contaminants. Because the penalty from contamination with iron is so great, we decided to design the system with materials such that iron contamination is not possible. Since acid gas contamination is beneficial, no action has been taken to avoid its presence.

6. Thermal stability analysis

The kinetic parameters presented above were used to determine the stability of the reactive mixture in terms of the Self-Accelerating Decomposition Temperature (SADT) and the Temperature of No Return (T_{NR}). The SADT and T_{NR} and their relation to thermal stability have been discussed by Townsend and Tou [3], Wilberforce [7] and Fisher and Goetz [8] and are based on the

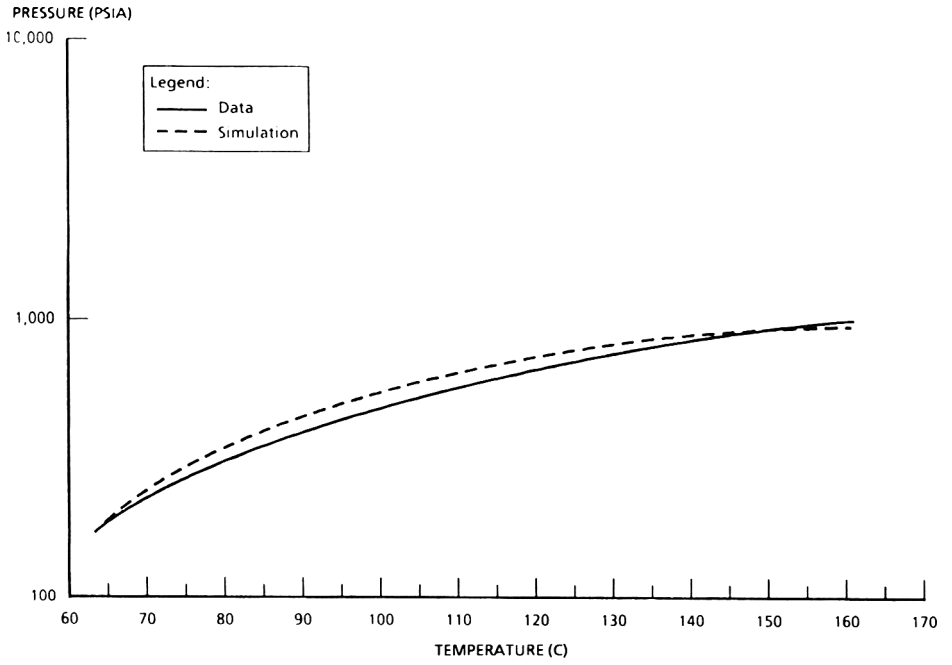

Fig. 4. Experimental data vs. simulation stoichiometric A + M → T + H(g) (PHI = 1.7, fill ratio = 0.3).

Semenov theory of thermal explosions [9]. The relations used to calculate the SADT and T_{NR} are briefly described below.

SADT is the minimum ambient air temperature at which a reactive material of specified stability decomposes in a specified commercial package in a period of seven days or less. While the term SADT applies strictly to commercial packages, the thermal stability concepts discussed herein also apply to commercial vessels.

At the temperature of no return (T_{NR}) the heat generation from an exothermic reaction equals the heat loss from the vessel. A runaway reaction is expected whenever either the process temperature exceeds the T_{NR} or the ambient air temperature exceeds the SADT.

The following equations can be used to calculate the T_{NR} and SADT.

$$T_{NR}^2 = \frac{E(\Delta H)(V)A\exp(-E/(RT_{NR}))C_{A0}C_{M_0}}{R(U)(1.8)S} \tag{2}$$

$$\text{SADT} = T_{NR} - \frac{R(T_{NR})^2}{E} \tag{3}$$

where T_{NR} is the temperature of no return (K), E the activation energy (cal/mol), ΔH the heat of reaction (Btu/lb mol), V the initial volume of the

reactant mixture (ft^3), A the pre-exponential factor (ft^3/lb mol h), R the universal gas constant (1.987 cal/mol K), C_{A0} the initial concentration of alcohol, (lb mol/ft^3), C_{M0} the initial concentration of monomer (lb mol/ft^3), U the heat transfer coefficient (Btu/h ft^2 °F), S the heat transfer area (ft^2), and SADT the self-accelerating decomposition temperature (K).

Another quantity of interest is the Time to Maximum Rate (t_m), which is a measure of how long the reaction takes to reach the peak rate. The following equations can be used to calculate t_m.

$$k_0 = M(V)(A \exp(-E/(RT_0))C_{A0}C_{M_0} \tag{4}$$

$$t_m = \frac{m(R)(T_0)^2 C_P}{E(\Delta H)k_0} \tag{5}$$

where k_0 denotes the initial decomposition rate (lb mol/h), t_m denotes the time to maximum rate (h), m denotes the mass of monomer (lb), T_0 denotes the initial temperature (K), and C_P denotes the specific heat (Btu/lb °C).

Parameters such as the temperature of no return, SADT and time to maximum rate can be used to select alarm levels and "never exceed points" for a process.

7. Safety investigation

At the end of a production reaction in the kettle, the azeotropic mixture of alcohol and monomer is taken overhead and condensed into the lights receiver. After all of the primary alcohol is stripped from the reaction mixture, the volatile monomer boils over to the lights receiver. Table 2 summarizes the thermal stability parameters for the lights receiver. Calculations were done for both stoichiometric and azeotropic mixtures because the material in the lights receiver can vary in composition from azeotropic (55 wt% monomer) to stoichiometric (79 wt% monomer). The T_{NR}, SADT and t_m thermal stability parameters for the lights receiver using the relationships (eqs. 2–5) discussed previously are summarized in Table 2.

The Semenov theory of thermal explosions assumes zero order kinetics (i.e. reaction rate is independent of the concentration of the reactants). The accuracy of the predictions decreases as the kinetic activation energy and/or heat of reaction decrease. The effect of reactant depletion on the thermal stability parameters for the lights receiver as determined by digital simulation is shown in Table 3.

Each of the temperatures increases about 4 °C compared to the results from Semenov theory (Table 2). The critical temperature difference, $T_{NR} - R(T_{NR})^2/E$, remains constant, however, at about 8 °C. The combined effects of higher temperatures and depletion of reactants decrease the time to

TABLE 2

Lights receiver thermal stability parameters from Semenov theory

Parameter	Stoichiometric mixture (79% M)		Azeotropic mixture (55% M)	
	Insulated	Uninsulated	Insulated	Uninsulated
T_{NR}, °C	28.0	45.7	24.7	42.0
SADT, °C	20.4	37.2	17.2	33.6
t_m, h, @ T_{NR}	75.2	9.4	52.6	6.6

TABLE 3

Lights receiver thermal stability parameters from digital simulation

Parameter	Stoichiometric mixture (79% M)		Azeotropic mixture (55% M)	
	Insulated	Uninsulated	Insulated	Uninsulated
T_{NR}, °C	32	50	29	46
SADT, °C	24	41	21	38
t_m, h, @ T_{NR}	68.0	8.5	65.2	9.1

maximum rate (t_m) for the stoichiometric mixture and increase the value for the azeotropic mixture.

Tables 2 and 3 serve to quantify the responses anticipated for this system. The values of T_{NR} and SADT are higher and t_m is shorter for an uninsulated compared to an insulated vessel. Also, the azeotropic mixture has a shorter t_m and lower T_{NR} and SADT in a given situation. This means that if indeed we have an azeotropic mixture, the possibility of a runaway reaction is increased. Driving the composition toward stoichiometric, however, means a greater loss of product.

The effect of the mixture composition on the t_m is shown in Fig. 5. The azeotropic mixture reaches the peak reaction rate faster than the stoichiometric mixture. The values for t_m shown in Fig. 5 are different than those from Table 3 because we selected a common initial temperature of 50°C and an adiabatic condition for the comparison.

8. Prevention approaches

Because the SADT is low compared to abnormal process or high ambient temperatures and the time to maximum rate is short, several measures were considered to prevent a runaway reaction in the lights receiver.

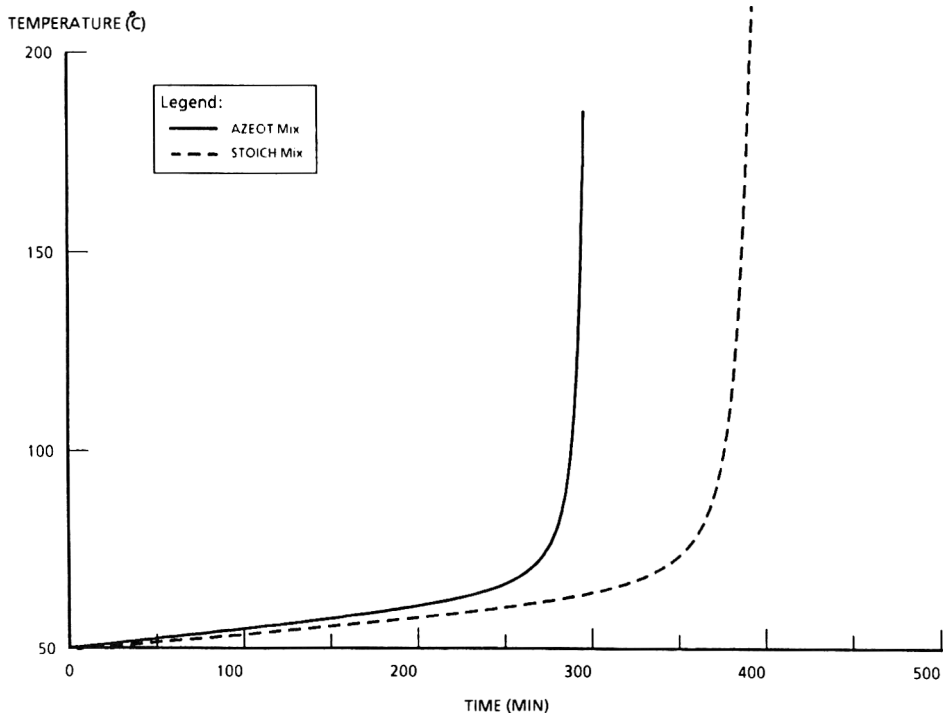

Fig. 5. Time to max rate comparison for an azeotropic vs. stoichiometric mixture of A and M (Adiabatic condition – initial temperature 50 °C).

1. Remove insulation from the lights receiver to facilitate heat loss and increase the values of T_{NR}, SADT and t_m.
2. Install temperature-indicator-alarms (TIA) in the condensate line from the water condenser and in the lights receiver to warn of high process temperatures.
3. Limit the amount of reactive mixture in the 200 gallon lights receiver to 10–20 percent of the capacity to improve the surface to volume ratio.
4. Use a cooling medium in the jacketed lights receiver to minimize the reaction rate.
5. Dilute the reactive mixture (the concept of quenching) with a nonreactive solvent or the primary alcohol.
6. Add a reaction inhibitor upon determination that a runaway reaction is occurring.
7. Convert the lights receiver into a reactor to reduce the alcohol and monomer concentration in a controlled manner.

We will discuss each of these measures separately. Of course, the most effective measure(s) will be adopted.

A fault-tree risk analysis established that the threat of a runaway reaction from an abnormal process or a high ambient temperature was more probable than one related to fire exposure. Therefore, removal of the fire protection insulation was recommended. However, it should be noted that adequate emergency relief protection was provided for the uninsulated vessel in the event of a fire.

Use of temperature-indicator-alarms will provide a warning of high process temperatures and allow time for corrective action.

The effect on thermal stability of reducing the amount of reactive material (increasing the effective surface to volume ratio) in the lights receiver was considered. Figure 6 shows the variation of T_{NR} and SADT with inventory in the vessel. The plot shows that reducing the inventory increases the values of T_{NR} and SADT thus increasing the thermal stability of the reactive mixture. However, the plots also show that removing the vessel insulation has a much greater effect on the thermal stability of the mixture than reducing the inventory.

Cooling the vessel to maintain a low temperature introduces the need for temperature control and raises the question of cooling failure. We decided to consider other measures and return to this option if necessary.

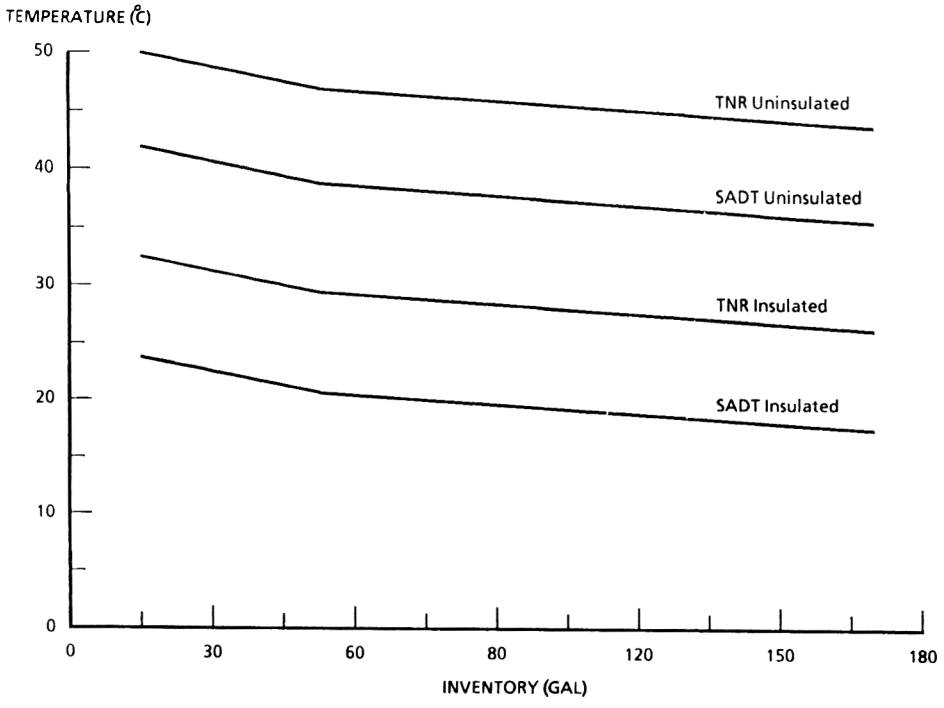

Fig. 6. Variation of T_{NR} and SADT with lights receiver inventory azeotropic mixture of A and M.

TABLE 4

Lights receiver reaction of azeotropic mixture of A + M → T + H

Temperature (°C)	Residence time (h)
70	39
100	2.5
150	0.25

The concept of quenching the reaction with a non-reactive solvent or excess alcohol did not prove to be an attractive approach from both an operational and a cost viewpoint. This approach was not pursued further.

An effective inhibitor was known for this reaction. But this was not a cost-effective measure. First, the inhibitor addition system was expensive. Second, the inhibitor generates an additional hazard by creating toxic fumes when incinerated.

We used digital simulation and our kinetic model to design an isothermal recirculating batch reactor for the reaction of the alcohol with the monomer utilizing the lights receiver. Table 4 shows the residence times required to complete the reaction at various temperatures. The time required to complete the reaction is only acceptable at temperatures above 100 °C.

9. Conclusions

Now that we understood how different process parameters affect the thermal stability of the system, we can select the option to reduce the runaway reaction hazard. Removing the insulation along with reducing the vessel inventory will minimize the risk of having to vent toxic and flammable materials. This recommendation is independent of whether the composition of the mixture in the lights receiver is azeotropic or stoichiometric. Furthermore, by using our kinetic model in runaway reaction simulations, we can show that either reaction mixture will be inherently stable at ambient temperature if the lights receiver is filled to no more than 20 percent of its capacity.

The principal conclusion of this study is that a detailed investigation of a process can allow straightforward selection of cost-effective solutions to improve process safety by identifying and preventing runaway reactions. Our recommendations will reduce the risk of venting toxic and flammable materials. The predicted thermal stability differences between Semenov theory and digital simulation are not significant for the cases investigated.

Acknowledgements

The Specialty Chemicals Division of the Union Carbide Chemicals and Plastics Company Inc. funded this work and preparation of this paper. The Safety Research Laboratory (G.E. Snyder) provided the ARC data.

References

1 H.G. Fisher, A perspective on emergency relief system design practice, Plant/Operations Prog., 10(1) (1991) 1–12.
2 D.W. Smith, M.C. Taylor, R. Young and C. Stephens, Accelerating rate calorimetry, Am. Lab., (1980) 51–66.
3 D.I. Townsend and J.C. Tou, Thermal hazard evaluation by an Accelerating Rate Calorimeter, Thermochim. Acta, 37 (1980) 1–30.
4 M. Ahmed, H.G. Fisher and A.M. Janeshek, Reaction kinetics from self-heat data — correction for the depletion of sample, Proc. of the CCPS Int. Symp. on Runaway Reactions, Cambridge, MA, AIChE, Center Chem. Process Saf., 1989, pp. 331–349.
5 M.A. Grolmes and J.C. Leung, Code method for evaluating integrated relief phenomena, Chem. Eng. Prog., 81(8) (1985) 47–52.
6 D.A. Shaw, SAFIRE Program for design of emergency pressure relief systems, Chem. Eng. Prog., 86(7) (1990) 14–17.
7 J.K. Wilberforce, The use of the Accelerating Rate Calorimeter to determine the SADT of organic peroxides, Columbia Scientific Industries Corp. Internal Report, July 1981.
8 H.G. Fisher and D.D. Goetz, Determination of self-accelerating decomposition temperatures using the Accelerating Rate Calorimeter, J. Loss Prev. Process Ind., 4(4) (1991) 305–316.
9 N.N. Semenov, Some Problems of Chemical Kinetics and Reactivity, Pergamon Press, Elmsford, NH, 1959.

Journal of Hazardous Materials, 33 (1993) 215–227
Elsevier Science Publishers B.V., Amsterdam

Toxicological assessments in relation to major hazards

S. Fairhurst and R.M. Turner

Health and Safety Executive, Magdalen House, Stanley Precinct, Bootle, Merseyside, L20 3QZ (UK)

Abstract

This paper outlines a general approach for determining the toxicological hazard posed by the release of a substance from a Major Hazard. The aim of the toxicological assessment is to derive a "toxic load" value and relationship which will be representative of all sets of exposure conditions predicted to produce a chosen Specified Level of Toxicity (SLOT). This "toxic load" can then be used as the basis for calculating the risk from the Major Hazard. Such risk calculations are currently an integral part of the assessment of Major Hazards carried out by the Health and Safety Executive of Great Britain. Emphasis is placed on the importance of obtaining and evaluating data from original reports and on maintaining a sound biological basis for the assessment. The approach is a pragmatic one, in that it is intended to represent the best that can be achieved under the usual prevailing circumstances of sparse data, with little or no direct information on human effects. The limitations of the approach and the assumptions made in its adoption are discussed. and reference is made to toxicological assessments produced for specific substances.

1. Introduction

In the United Kingdom, a considerable number of installations (chemical plants, warehouses, etc.) are designated as Major Hazards because of the presence of substantial quantities (individual or aggregate) of one or more substances having the potential to produce significant toxicological effects in the surrounding general human population in the event of an accidental release. Having identified that such a potential exists at a particular site, the crucial issue is then that of the likelihood that such a release could occur. Estimations of the likelihood of accidental releases and their consequences have obvious implications in relation to, for example, the operation of the site,

Correspondence to: S. Fairhurst, Health and Safety Executive, Magdalen House, Stanley Precinct, Bootle, Merseyside, L20 3QZ (UK).

proposed developments in the vicinity of the site, provision of information to the general public, and arrangement/planning of emergency services. In order to provide advice in these areas, the Health and Safety Executive (HSE) in Great Britain is making increasing use of quantified risk assessment. This entails the calculation of numerical values for the risks to an individual or a community of being exposed to amounts of released substance(s) which would result in certain levels of toxicity.

One of HSE's principal concerns in this field is the calculation of risks in the vicinity of Major Hazard sites in order to provide advice for land-use planning decision-making [1]. This paper focusses on the assessment and provision of toxicity data such that it can be used as the basis for calculating these risks.

We are aware that some aspects of the approach described in this paper are not universally accepted or routinely adopted by others working in this field. With this in mind, we feel that it is appropriate to state at the outset three principles which we feel are very important:

(i) The toxicological assessment should be regarded as a regulatory toxicology issue and on this basis the approach adopted should follow as closely as possible the best principles and standard, widely accepted practices of "mainstream" toxicology.

(ii) The results of risk analyses are frequently used as a basis for decision by people who are not experts in the fields of toxicology or risk analysis. Therefore, the various steps used in the analysis should be transparent and the end-result of each part of the analysis. including the toxicological assessment, should be easy to trace back to the original supporting data. This is also an essential element in achieving harmony between different risk analysts.

(iii) The objective of the toxicological assessment is to derive a prediction of toxicity in order to facilitate decision-making by the regulatory authority. Failure to make such decisions is not an available option. Clearly, we recognise that frequently the extent of the data available falls well short of ideal, and various assumptions are required if the above objective is to be realised.

This paper only addresses direct effects on human health arising from a substance released into the atmosphere. Adverse effects on the environment or indirect effects on human health mediated via the environment are not discussed.

2. Criteria defining the level of toxicity on which risk calculations are based

Calculations of individual risk from Major Hazards are based on the likelihood of a defined member of an affected population receiving an exposure equal to or greater than that required to produce a Specified Level of Toxicity

(SLOT). The particular SLOT on which risk calculations are based may vary, depending on the situation under consideration, and in some cases risk calculations relating to several different SLOTs may be appropriate.

Inevitably there must be a degree of compromise in the selection of the most appropriate SLOTs for various Major Hazard situations. In the case of land-use planning, criteria defining a SLOT which were based solely on lethality may not be sufficiently stringent; there would be no allowance made for any serious but sublethal effects on health, which may be of great concern (effects such as marked impairment of organ or tissue function or serious disfigurement). On the other hand, if risk calculations were based on only a low level of sublethal effects within the population, this approach could appear to be too stringent, especially for an accidental release which is in itself a rare phenomenon.

Such considerations indicate that for land-use planning, criteria defining the appropriate SLOT which are based on serious injury, as well as on death itself, are appropriate. The SLOT which HSE uses in this situation has therefore been defined as one where there is:

(i) Severe distress to almost everyone in the area;
(ii) A substantial fraction of the exposed population requiring medical attention;
(iii) Some people being seriously injured, requiring prolonged treatment;
(iv) Highly susceptible people possibly being killed.

The choice of these criteria, reflecting a range of individual health effects and a somewhat imprecise level of overall effect on the population, is set out in terms intended to be understood readily by the general public and in particular by those involved in the decision-making process. Some flexibility is necessary to account for variations in the toxic properties of different substances, in that some chemicals may produce more serious sublethal effects than others. These criteria also avoid creating a spurious impression of accuracy, particularly when one reflects on the extent and quality of toxicity information available for most of the substances that need to be considered.

We feel that the level of toxicity given above is a more comprehensive description of the likely overall impact on a population and allows greater flexibility, particularly when faced with poor quality data, when compared with probit expressions generated from and descriptive of mortality data only [2, 3]. Furthermore, the future trend in acute toxicity testing will be towards studies in which the maximum level of toxicity produced should be serious sublethal effects with, at most, only a small percentage of deaths [4]. Consequently, an approach based on a SLOT such as the one described above will be more receptive than a mortality-based probit approach to the type of data likely to emerge from future acute toxicity studies.

In defining a level of toxicity on which risk calculations will be based, attention has focussed on toxic effects which become apparent soon after exposure. It should be acknowledged that there is also the possibility of effects being produced, the consequences of which only become manifest a long-time

after exposure. In animal studies germ cell mutations, teratogenicity and even cancer have arisen following a single exposure to certain substances [5–7]. However, for almost all substances with such properties, single exposure dose-effect data are not available. In addition, at least for carcinogenicity, in view of the envisaged mechanisms of tumour production it is likely that for most substances the risk of cancer arising from a single exposure is very low. Therefore it is generally not possible to include these aspects of toxicity in the overall quantitative approach described here.

3. Identification of appropriate toxicological data for use in the assessment

In considering the human health hazard created by a postulated release into the air of a toxic substance from a Major Hazard, attention will be focussed primarily on effects arising from a single exposure to the airborne substance. It is necessary to attempt to relate the estimated atmospheric concentrations and durations of exposure following a release to the level of toxicity produced within the surrounding population. The data used should therefore be principally those contained in reports of accidental single exposure of humans to the airborne substance, or generated in single exposure inhalation studies in animals.

Toxicity data relating to routes of exposure other than inhalation should be used only with great caution. For example, in the absence of sufficient inhalation data it may be possible, in some instances, to make use of oral exposure data and to relate these values to "equivalent" inhalation exposure conditions. However, care should be taken to ensure that the toxicokinetics (absorption, distribution, metabolism and excretion) and sites of toxic action are (or are judged likely to be) comparable for the two routes. Such comparisons between routes cannot be made if substantial differences in toxicokinetics appear possible, or if the sites of toxic action differ between the two routes; the latter point is particularly important for substances exhibiting predominantly local effects (e.g. irritation, corrosion) on the respiratory or digestive tracts.

Some issues must be raised concerning the quality of toxicological data used in the analysis. Experience has shown that commonly used secondary sources of information may be unreliable, in that the toxicological values given may be inaccurate representations of the original results, or that the primary sources of such values are either difficult to verify or of doubtful quality. Therefore, in a thorough assessment all the data used should be obtained from the original reports. In obtaining these reports, it will also then be possible to consider the quality and reliability of the studies and hence of the results generated. Such considerations form an important aspect of the overall assessment process, and greater emphasis should be given to values for which the underlying scientific evidence is strongest.

Many of the points made in this paper, in relation to appropriateness and validity of toxicological data, are echoed in a recent European chemical industry publication [8].

4. The "TOXIC LOAD" concept

The purpose of the toxicological assessment is to define all the sets of exposure conditions (all pairs of values for atmospheric concentration and exposure duration) predicted to produce the SLOT of interest. This requirement can be satisfied most easily by developing a functional relationship between the exposure concentrations (c) and durations (t) producing the SLOT, such that the end-product of this relationship is a constant numerical value, i.e.

$$f(c,t) = \text{constant} \quad \text{(in appropriate units)} \tag{1}$$

The form of this equation and the units of the constant will vary according to the substance under consideration. The value emerging is not invariably equivalent to the administered "dose" which, in inhalation toxicology, is expressed as concentration × time. Therefore the above numerical constant has been termed the "TOXIC LOAD". Furthermore, the toxic load relating to the particular SLOT used by HSE in land-use planning considerations has been designated the "DANGEROUS TOXIC LOAD" (DTL).

The Dangerous Toxic Load relationship and constant are used by HSE in risk analysis, in terms of calculating the probability that the Major Hazard could create conditions satisfying the DTL in the area surrounding the site.

5. Deriving the toxic load and the relationship between c and t, for the chosen "SLOT"

5.1 Interpretation of results in humans and in animals

In theory, at least, the ideal assessment of the toxicity of Major Hazard substances would be based on accurate observations of effects in humans. However, for most substances, existing reliable data on acute effects arising from a single exposure in humans are sparse. In some cases, information is available on sublethal effects (e.g. carboxyhaemoglobin levels produced by exposure to carbon monoxide, sensory irritation to eyes or mucous membranes by irritant gases). In addition, for a few substances some information is available from their use in warfare (e.g., chlorine, phosgene), although the usefulness of the available information has been disputed [9, 10]. However, for most substances the data are limited to a few reports of accidental exposures, often involving only a few people and rarely containing accurate measurements or even estimates of exposure concentrations and times.

Consequently, heavy reliance has to be placed on the results of experiments on animals in attempting to predict the responsiveness of a human population. Knowledge of the toxicokinetics and toxicodynamics (the relationship between concentration in the body and adverse effects) of a substance at low exposure levels in humans and animals, and at higher exposure levels in animals, would be the best way of extrapolating to effects in man at higher exposure levels. However, at present there are insufficient data for Major Hazard substances to enable such approaches to be used in practice.

Another possible approach in animal-to-human extrapolation is the use of scaling factors based on physiological parameters to develop a relationship which can then be extrapolated to man by incorporating the appropriate value(s) for humans. However, the generality of such relationships and the validity of extrapolation is often in doubt.

Thus in general, extrapolation from laboratory animals to humans with any assurance of accuracy and reliability is fraught with difficulties, principally because of the absence of adequate information. Hence considerable caution and judgement are required in adapting animal results for use in risk analysis. For many substances it may be necessary to make the assumption that results from animal experiments will be representative of effects on the human population, in terms of both the nature of the effects produced and the dose–effect relationships observed.

The approach described in this paper is therefore a pragmatic one, representing the best that can be achieved under the usual prevailing circumstances of sparse data, with little or no information on human effects. In some cases the paucity of data on certain substances will make any analysis extremely tenuous, and in these situations further experimental work by manufacturers or their trade associations would be advisable if important decisions depend on the results. The need for further toxicological research in this area has also been emphasised elsewhere [8].

5.2 Gathering animal LC_{50} data

For the vast majority of Major Hazard substances the most readily available information on the toxic effects of the airborne substance is the atmospheric concentrations and exposure times producing deaths in laboratory animals. For certain substances, particularly where studies have been conducted to current internationally-agreed protocols, there may be more complete details relating exposure conditions to both death and to more specific toxicological end-points. However, some of the older toxicity studies contain only lethality information.

Therefore, the first stage in the process should be the gathering of animal LC_{50} values, each with an associated exposure time. Most animal experiments involve the use of small groups. The response of the group at the 50% mortality level will most accurately reflect the likely response of the population from which the group is drawn.

Collation of these LC_{50} and exposure time values will permit comparisons to be made between different species and between different strains within the

same species. From the available data, the most sensitive animal species and strain should normally be used to represent the prediction of human responsiveness, unless there is information indicating that other animal results will serve to model human responsiveness more reliably.

5.3 Transition from the LC_{50} and t values in the animal model to c and t values representing one set of exposure conditions for the chosen SLOT in the same animal model

Most acute inhalation toxicity studies have been (and are still) performed under conditions where the exposure concentration has been (is) varied but the exposure period has been (is) fixed. In the Major Hazard context one is concerned primarily with the scenario of exposure for a period of perhaps up to 60 minutes, although the nature and limitations of the data usually available means that one must attempt to make use of information from studies employing a duration of exposure which may fall anywhere in a range from a few (5–10) minutes up to several (4–6) hours.

Therefore, at this point in the toxicological assessment we will have selected an animal model represented by an LC_{50} value and associated exposure period. The next stage is to extrapolate from the exposure concentration producing 50% mortality to that producing a degree of toxicity comparable to the chosen SLOT, for the same exposure period and in the same animal species and strain. In the case of land-use planning considerations, this entails deriving a pair of c and t values estimated to produce serious toxic effects and a low percentage (normally taken to be 1–5%) of deaths in the animal model.

As exposure conditions producing a low mortality level within a population cannot, in practice, be observed directly because of the very large groups of animals required, the conventional method of deriving such parameters is by probit analysis [11]. Note that here we are referring to subjecting to probit analysis data from a specific study, where the exposure period is fixed and one is simply moving along a concentration axis from one level of effect to another.

With probit analysis, "best estimate" values relating to a low percentage mortality should be used, because the size of the confidence interval is very much influenced by factors inherent in the design and conduct of experimental studies, in addition to influence from the results obtained.

If the data on the selected animal species and strain are inadequate for such probit analysis, then the extrapolation to a set of c and t values relating to the SLOT in these animals must be approached more empirically, from a simple visual examination of the data.

Occasionally, substances may be encountered where the only available information is a tabulated LC_{50} value, with an associated exposure time. In such cases a possible approach is to estimate, for the species and strain under consideration, the ratio between the LC_{50} and LC_x, where x is a lower percentage of deaths, i.e. around 1–5% in the case of the SLOT used for land-use planning. The slope of the dose-effect curve, and hence this ratio, will vary depending on the substance and on the heterogeneity of the test animals.

Nevertheless, in a study of the acute toxicity of a large number of pesticides in rats of the same strain, sex and age, examined under fixed experimental conditions, many pesticides had an LC_{50}/LC_1 ratio of between 1.5 and 4 [12]. Ratios of a similar magnitude have also been obtained in studies with various lung damaging gases [cf.13–15]. In addition a new classification system for acute toxicity has recently been proposed, in which the criterion determining classification was a dose level producing serious toxic effects but minimal lethality, rather than the LC_{50}. In a subsequent study designed to examine the proposal, most of the substances considered were placed in the same category using either criterion, when the boundaries for classification on the basis of LD_{50} were four to five times the corresponding boundaries for classification on the basis of serious toxic effects but minimal lethality [16].

However, ratios of this type should be used to extrapolate from a dose producing 50% mortality to one producing a lower level of toxicity only in the absence of any other useful data, and even then only with full acknowledgement of their very general and approximate nature.

5.4 Adaptation of one set of c and t values relating to the chosen SLOT in the selected animal model to corresponding values relating to the same SLOT in the general human population

Having derived one set of c and t values relating to the appropriate SLOT in the chosen animal model, it is then necessary to examine whether such values can be considered representative of the corresponding parameters in the general human population.

At this stage any collateral evidence available on effects in humans, usually in the form of isolated case reports of accidental exposures or anecdotal statements relating to the experiences of medical practitioners in particular industries should be considered. Such evidence can be used to assess whether the derived c and t values relating to the SLOT are consistent with the almost invariably scant information available on human responsiveness, or whether some adjustment of the c and t values is required on the basis of such information.

Another issue to be raised at this point is that of population heterogeneity. Animal experiments, particularly those performed in more recent years, will have been conducted using groups of animals bred especially to limit the variability in response. In general such animals will be healthy young adult members of that population. By comparison, the general human population is extremely heterogeneous. Therefore if, for example, the LC_{50} in the general human population has been equated with the LC_{50} in a particular species and strain of animal, then given the increased spread in responsiveness within the human population it may be suggested that for levels of toxicity significantly below 50% mortality, the exposures producing these levels of effect may be lower for the human population than for the animal model.

Several reports have included proposals in the proportion of the human population that should be considered to be particularly vulnerable to health

effects from the release of a toxic substance [17,18]. Generally these are people at the extreme ends of the age range and people with physiological disabilities which may increase their sensitivity to the substance. It has been estimated that such people constitute about 25% of the general population.

However, such issues are mainly conjectural, in that there are no data on the relative sensitivities of different groups within the human population towards most, if not all, Major Hazard substances. In practice, the need to compensate for the heterogeneity of the human population must remain one of toxicological judgement, depending on the particular case under consideration. To a large extent the approach will be dependent on the amount of data available. Adjustment of the toxicity values to account for human population heterogeneity appears unnecessary where data exist for several animal species and strains, the most sensitive of which is taken to represent human responsiveness, as this in itself is a conservative approach. In contrast, some adjustment may be necessary where data are available in only one or two animal species/strains, and where the observed dose–response curve is particularly steep.

At the end of this stage in the analysis, one value will have been derived for c and one for t which, taken together, should represent an estimate of one set of exposure conditions predicted to produce the particular SLOT in the human population. It is then necessary to deduce the relationship between c and t, such that, if possible, the end-product of this relationship (the "toxic load") can be represented by a constant numerical value. This constant, together with the relationship between c and t , can then be used to predict all sets of exposure conditions (c and t values) for the chosen SLOT.

5.5 Derivation of the toxic load equation and constant

Theoretical considerations indicate that there are several forms of expressions relating the toxic load to a function of c and t [19]. The manner in which c and t are functionally related in producing a toxic load value for a particular SLOT should only be examined within a collection of data from the same study involving the same animal species and type of toxic effect. In addition, the toxic effect should be the same as that on which the c and t values are based. These are very important points. If data from different studies and/or different animal species are combined in a single analysis, then inter-species, inter-strain and inter-laboratory variation (factors which have already been taken into account earlier in the process) will also exert an unknown degree of influence on the derived relationship between c and t. In fact, the relationship thus obtained may be predominantly an expression of such variations and far removed from an expression of the true toxic load relationship. The importance of maintaining a constant type of toxic effect (such as mortality) lies in the fact that different toxic effects may show different degrees of dependency on c, relative to t. For instance, sensory irritation of the eyes and mucous membranes may be much more heavily dependent on c, relative to t, than lethality.

There has been little experimental work in this area. Acute inhalation toxicity experiments in laboratory animals, performed in the early years of this

century on a limited number of gases, obtained mortality results suggesting the following relationship [20]:

$$\text{Toxic Load} = c \times t \tag{2}$$

(The Haber Rule)

More recently, a literature survey of more than 30 substances, for which LC_{50} values had been determined in the same species for at least three different exposure periods, suggested two groups of substances, showing empirical relationships of [21]:

$$\text{Toxic Load} = ct \tag{3a}$$

$$\text{Toxic Load} = c^2 t \tag{3b}$$

Overall, experimental observations suggest that in many cases the following general relationship may hold for acute lethality [8,22]:

$$\text{Toxic Load} = c^n t \tag{4}$$

A recent review of acute inhalation studies on various substances, using lethality as an end-point, derived values for n ranging from 0.8 to 4.9 for individual studies on particular substances and animal species, although the strength of evidence underlying some of these values is questionable [22]. To introduce a note of caution, some of the values of n quoted in the risk assessment literature for particular substances must be regarded as very dubious [3, 18, 23]. Such values have often been derived from studies using non-lethality end-points or from combined treatments of vaguely-defined data.

The requirement at this stage is, therefore, a knowledge of the value of n which will relate variations in c and t to a constant, experimentally observed level of mortality within an individual animal species. The most suitable reference point is usually 50% mortality, since exposure conditions relating to this level of mortality are most readily available. A simple (logarithmic) plot of $\ln c$ against $\ln t$, each pair of c and t values relating to the production of 50% mortality, may permit derivation of n from the slope of the resulting line $(-1/n)$, since:

$$c^n t = \text{constant}, k \tag{5}$$

can be rearranged to:

$$\ln c = -\frac{1}{n} \ln t + \frac{1}{n} \ln k \tag{6}$$

However, it must be recognised that the general applicability of the $c^n t$ relationship is based on empirical observation more than fundamental biological principles. If the data available for a specific substance do not appear to fit such a relationship, then there may be very good reasons why this is the case

(e.g. the particular mechanism(s) of toxicity operating) and these should be explored further.

An alternative approach at this stage is to use probit analysis and the method of Maximum Likelihood to produce a description of the relationship between c, n and t in the form of a probit equation [11, 22]. For the reasons given above, each such analysis must be restricted to data relating to the same study, animal species and toxic effect. The simpler graphical method may be preferable because there is no requirement for computer programmes and visual presentation of the data allows one to readily observe deviations from a $c^n t$ relationship. However, the method of Maximum Likelihood will allow all experimental data points to be taken into account, whether or not reliable LC_{50} values can be calculated. It may therefore be applicable to a wider range of data sets and provide a more comprehensive description of the relationship between c, n and t.

Occasionally, sufficient data may be available on a particular substance to permit the derivation of several values for n, representing values for different animal species, or values from different studies in the same species producing very different sets of results which cannot be combined readily or justifiably. In this situation, comparison of the relative standards of the studies under consideration may suggest that one of the values for n is much more reliable than the others, based on strength of experimental evidence, and this value should be used. Otherwise an overall values for n may have to be derived, by taking an average of the values derived for individual species.

In some cases the data available on a substance may be insufficient to permit the derivation of n. In such situations, although use of the Haber Rule has been common practice in toxicology, consideration of the mechanism of toxicity of the substance in question and its similarity in this respect to other substances with better defined $c:t$ relationships may be a better basis for choosing a value for n. On occasion, it may also be appropriate to perform and compare separate risk analyses based on toxic load expressions obtained using the two values of n (1 and 2) commonly observed.

We now have one c and one t value representing one set of exposure conditions predicted to produce the chosen SLOT. We also have the exponent n which can be used to define a "toxic load" equation describing variation in c and t in relation to the production of this SLOT. Insertion of the values for c, t and n into the equation:

$$\text{Toxic Load} = c^n t \tag{7}$$

will produce a numerical value for the "toxic load" constant

6. Use of this approach to toxicological assessment

Detailed assessments for a number of specific substances (acrylonitrile, ammonia, chlorine, hydrogen fluoride, hydrogen sulphide, nitrogen dioxide,

sulphuric acid mist) have been prepared using the approach described in this paper. The "dangerous toxic load" (DTL) values so derived have been used in quantified risk analyses of Major Hazards and the toxicological assessments have been (or are soon to be) published [24–30].

Disclaimer

The comments expressed in this publication are the views of the authors and may not necessarily be the views of HSE.

Acknowledgement

The authors wish to thank all colleagues within HSE who contributed to various discussions during the development of this approach.

References

1 Health and Safety Executive, Risk criteria for land-use planning in the vicinity of major industrial hazards, HMSO, London, 1989.
2 R.M.J. Withers and F.P. Lees, The assessment of Major Hazards: The lethal toxicity of chlorine. J. Hazardous Mater., 12 (1985) 283–302.
3 P. Davies and I. Hymes, Chlorine toxicity criteria for hazard assessment, Chem. Eng., June (1985) 30–33.
4 A.D. Dayan, Chemical hazards and acute toxicity tests, Biologist, 37 (1990) 72.
5 D.W. Arnold, G.L. Kennedy, M.L. Keplinger and J.C. Calandra, Dominant lethal studies with alkylating agents: dose–response relationships, Toxicol. Appl. Pharmacol., 38 (1976) 79–84.
6 F.W. Sunderman, P.R. Allpass, J.M. Mitchell, R.C. Baselt and D.M. Albert, Eye malformations in rats; induction by prenatal exposure to nickel carbonyl, Science, 203 (1979) 550 553.
7 H.E. Driver, I.N.H. White and W.H. Butler, Dose–response relationships in chemical carcinogenesis; renal mesenchymal tumours induced in the rat by single dose dimethylnitrosamine, Br. J. Exp. Pathol., 68 (1987) 133–143.
8 ECETOC (European Chemical Industry Ecology and Toxicology Centre), Emergency Exposure Indices for Industrial Chemicals, ECETOC Technical Report No. 43, ECETOC, Brussels, 1991.
9 R.M.J. Withers and F.P. Lees, The assessment of major hazards: The lethal toxicity of chlorine. Part 3: Cross checks from gas warfare, J. Hazardous Mater., 15 (1987) 301–342.
10 V.C. Marshall, The prediction of human mortality from chemical accidents with special reference to the lethal toxicity of chlorine, J. Hazardous Mater., 22 (1989) 13–56.
11 D.I. Finney, Probit Analysis, Cambridge University Press, London, 1971.
12 T.B. Gaines, Acute toxicity of pesticides, Toxicol. Appl. Pharmacol., 14 (1969) 515–534.
13 M. Schlagbauer and D. Henschler, The toxicity of chlorine and bromine with single or repeated inhalation, Int. Arch. Gewerbepathol. Gewerbehyg., 23 (1967) 91–98.
14 S.D. Silver and F.P. McGrath, A comparison of acute toxicities of ethylene imine and ammonia to mice, J. Ind. Hyg. Toxicol., 30 (1948) 7–9.
15 J. Wohlslagel, L.C. Dispasquale and E.H. Vernot, Toxicity of solid rocket motor exhaust: Effects of HCl, HF and alumina on rodents, J. Combust. Toxicol., 3 (1976) 61–70.

16 M.J. van den Heuvel, A.D. Dayan and R.O. Shillaker, Evaluation of the BTS approach to the testing of substances and preparations for their acute toxicity, Human Toxicol., 6 (1987) 279–291.
17 J.I. Petts, R.M.J. Withers and F.P. Lees, The assessment of major hazards: The density and other characteristics of the exposed population around a hazard source, J. Hazardous Mater. 14 (1987) 337–363.
18 N.A. Eisenberg, C.J. Lynch and R.J. Breeding, Vulnerability model: A simulation system for assessing damage resulting from marine spills, USCG Report CG-D-137-175, available as NTIS Report AD-A015-245, 1975.
19 H.J. Klimisch, R. Bretz, J.E. Doe and D.A. Purser, Classification of dangerous substances and pesticides in the European Economic Community Directives: A proposed revision of criteria for inhalation toxicity, Reg. Toxicol. Pharmacol., 7 (1987) 21–34.
20 R. Flury and F. Zernik, Harmful Gases — Vapours, Fog, Smoke and Dust Varieties, Springer, Berlin, 1931.
21 J.E. Doe and G.M. Milburn, The relationship between exposure concentration, duration of exposure and inhalation LC_{50} values, Human Toxicol., 2 (1983) 564–565.
22 W.F. ten Berge, A. Zwart and L.M. Appelman, Concentration–time mortality response relationship of irritant and systemically acting vapours and gases, J. Hazardous Mater., 13 (1986) 301–309.
23 W.F. ten Berge and M. Vis van Heemst, Validity and accuracy of a commonly-used toxicity assessment model in risk analyses, In: 4th Int. Symp. on Loss Prevention and Safety Promotion in the Process Industries, Inst. Chem. Eng., London, 1983, pp. 11–19.
24 R.M. Turner and S. Fairhurst, Toxicology in substances in relation to Major Hazards: Acrylonitrile, HMSO, London, 1989.
25 R.M. Turner and S. Fairhurst, Toxicology of substances in relations to Major Hazards: Chlorine, HMSO, London, 1990.
26 M.P. Payne, J. Delic and R.M. Turner, Toxicology of substances in relation to Major Hazards: Ammonia, HMSO, London, 1990.
27 R.M. Turner and S. Fairhurst, Toxicology of substances in relation to Major Hazards: Hydrogen fluoride, HMSO, London, 1990.
28 R.M. Turner and S. Fairhurst, Toxicology of substances in relation to Major Hazards: Hydrogen sulphide, HMSO, London, 1990.
29 R.M. Turner and S. Fairhurst, Toxicology of substances in relation to Major Hazards: Sulphuric acid mist, HMSO, London, 1992.
30 M. Meldrum, Toxicology of substances in relation to Major Hazards: Nitrogen dioxide, HMSO, London, 1992.

Journal of Hazardous Materials, 33 (1993) 229–259
Elsevier Science Publishers B.V., Amsterdam

Risk analysis of the transportation of dangerous goods by road and rail

Grant Purdy

DNV Technica Ltd., Highbank House, Exchange Street, Stockport SK3 0ET, Cheshire (UK)

Abstract

In any debate about the transport of dangerous goods where the effectiveness of existing legislative controls is challenged, it is very important that there is a full understanding of the magnitude of the risks involved and the causes and major contributors so that properly informed decisions can be made. This paper gives details of the methodology developed for the analysis of the risks arising from the carriage, in bulk, of toxic and flammable substances by road and rail as part of a major study into the risks faced by the British population from the transport of dangerous substances. This paper concentrates on the novel aspects of the study and in particular consequence and human impact modelling. Models are given for the interaction of passenger and dangerous goods trains taking into account the ability of signals and other systems to detect and stop approaching trains. In the case of road transport, the models allow for the characteristics of different road types and the behaviour of motorists to be simulated. The relative risks of transporting hazardous materials by road or rail are explored and it is shown that the inclusion of motorist and rail passenger populations significantly affects the calculated risk levels. It is concluded that the safe routing of materials with large hazard ranges may be more easily achieved by road. While, the natural separation afforded by the rail system may make this mode more suitable for lower hazard materials. However, it is concluded that in Britain, there appears to be no evidence to support, on safety grounds, a general transfer of hazardous goods from road to rail or the reverse.

1. Introduction

In recent years the issue of whether or not the transport of dangerous goods by road is less safe than by rail or inland waterway has been raised in Europe. A series of road vehicle accidents in Germany in the late 1980's prompted that

Correspondence to: G. Purdy, DNV Technica Ltd., Highbank House, Exchange Street, Stockport SK3 0ET, Cheshire (UK).
The views expressed in this paper are the author's and do not necessarily represent those of DNV Technica or of the Health and Safety Executive.

country's government to implement measures aimed at transferring certain long-haul dangerous good traffic from the road to the railways and inland waterways. This initiative has also prompted the European Community to review the road versus rail safety issue and for member states to consider the need for further legislation dealing with 'safe routing', placarding, driver training and vehicle standards. This legislative activity is, in some cases, being pursued without the benefit of a rigorous study of the risks or benefits involved and much research is now starting to be undertaken in this area. In most cases, methods and models derived for onshore chemical plant risk analysis are now being deployed but those who are undertaking this work soon find that there are crucial differences which need to be respected when the risk from a transport activity is analysed.

This paper is an attempt to express some of those differences; to show where, in the author's opinion, greater care in modelling is necessary and where, conversely, more precise treatments are not warranted. This understanding is based on the experience gained during participation in a five-year study into the transport of dangerous goods in Britain. That study, by a subcommittee of the UK's Health and Safety Commission's Advisory Committee on Dangerous Substances, considered the risks to the British population from the carriage of dangerous goods by rail, road and by sea in the light of the present regulatory and voluntary controls and the need for and possible nature of additional controls [1].

This was the first occasion when the risk to a nation from the transport of hazardous materials had been measured to such a degree and the study involved considerable research in order to develop suitable methods of analysis. Further research was also needed to understand the results which the analysis produced. While studies looking at the risks from transporting hazardous materials have been and are being carried out elsewhere (and all these were reviewed), none of these methodologies were found to be fully appropriate for the UK study. In general this was because:

- elements of the methodology could be considered 'obsolete';
- they had been developed to reflect a transport system or a system of regulatory control that was somewhat different to that in the UK;
- they had been developed specifically to investigate one aspect of transportation, for example, the safe routing through a city area, and did not have wider applicability.

For these reasons a 'new' approach was necessary: specific to the British situation, which sought to minimise uncertainty while providing 'transparency' of the risk calculation process so that the decision makers could understand and have confidence in the results. It also had to allow for assumptions to be easily changed so that the models could be used as 'testbeds' for the gauging the effectiveness of changes to the system of control. The approach was developed by two technical working parties (one for marine, the other for land

based transport) on which sat members of the Health and Safety Executive, its contractors, industry, the emergency services and academia.

This paper is concerned with the work of a technical working party for land-based transport and the modelling associated with the transport of non-explosive substances in bulk (called 'the UK Study' throughout the rest of this paper). While the techniques of analysis were developed in the context of the British situation, many of the lessons learnt and insights gained have much wider application. The paper especially addresses the question of whether it is safer to convey hazardous substances by road or by rail.

2. Objectives of the risk analysis

The choice of consequence and impact models and indeed the manner of conducting a risk analysis depends on the eventual use of the results; who will use them and for what purpose. Both the needs of the user and the needs and capabilities of the analyst need to be considered. In the case of the UK Study, it would not have been useful to expend effort developing complex and indepth analyses where, for example, there were great uncertainties in frequency data or the decision making process could not accommodate significant levels of precision. This is one of the most important principles which guided the development of models and techniques for this work, for while we sought methods of analysis which optimised accuracy, this was often at the expense of unnecessary precision.

Similar considerations applied to the types of risk measured and the presentation of the results. Some transportation studies have concentrated on individual risk calculations, presenting the results as contours or risk transect diagrams showing individual risk against distance from the transport route. While such studies may be useful for routing exercises, where a new transport corridor is being selected, unless there is good evidence on the relative distribution of failure events along the route (i.e., 'high spots'), individual risk results can add little to the understanding of risk from a transport operation. The risk numbers produced are normally so small as to be beyond the normal range of human comprehension. Most importantly, this type of treatment fails to address the public's (and the politician's) major concerns; not the risk to individuals, but that to society at large: the risk of a disaster. This involves not only consideration of the potential for transported hazardous substances to cause multiple fatalities but also the likelihood that these might occur because a loss of containment accident coincides in time and space with a human population. Societal risk is therefore not only a more appropriate measure but it also seems to yield more useful results. It leads naturally, via the generation of expectation values (average number of lives lost), to consideration of the need for, and cost benefit, of risk reduction measures. Societal risk analysis does involve many generalising assumptions and averaging but these are not

inconsistent with the 'smeared out' nature of the risk associated with transport along a route.

3. Frequency analysis

For those countries or regions with a history of hazardous goods accidents, consulting the historical record is normally the first step in any study of risk. Indeed, if enough incidents have (unfortunately) occurred, the modelling of the possible consequences and impact of such events may be of secondary importance. In Britain, however, we have suffered few such incidents. Those that have occurred have normally involved flammable liquids and no person has yet died as the consequence of a leak from a damaged tanker (road or rail) holding liquefied flammable or toxic gases such as LPG or chlorine. For this reason, the UK Study adopted a somewhat different approach to obtaining the release frequencies for hazardous substances in transit.

One approach possible would have been to use an event tree such as that in Fig. 1. This is similar to that developed by Hubert et al. [2] from French data. This builds on data from all road accidents, and in particular, those involving other goods vehicles, to synthesise a puncture rate for a hazardous goods tanker. However, there is no evidence to suggest that the drivers of hazardous goods vehicles will act in a similar manner to drivers of other vehicles nor that such vehicles will suffer equipment and other failures at the same rate as other similar vehicles containing other bulk materials. The value given to the critical probability associated with 'escalation' to puncture is critical yet very uncertain. Even for countries where good data exist there are always the uncertainties associated with under-reporting.

An analysis of the available UK data on rail and road incidents involving tankers containing hazardous materials showed that releases could occur from two sources, firstly by puncture or rupture following collision, roll-over or derailment, or secondly, from failure or maloperation of the tanker equipment. For the rail mode there was sufficient data on 'thin walled' wagon accidents to generate a frequency for punctures and equipment leaks directly. Over six years, 80 cases of spills due to 'equipment leaks' and four incidents involving substantial spillage following puncture were found. These data suggested a puncture frequency of 6.3×10^{-8} per tank wagon km.

For road transport, 25 incidents were found over a four year period. Analysis of these data yielded a spill frequency of 1.4×10^{-8} per loaded tanker km for large spills (> 1500 kg) from collisions etc and 0.7×10^{-8} per loaded tanker km for large spills arising out of equipment failure.

While motor spirit spill frequencies could be obtained directly from this analysis, there are no incidents recorded in the UK where properly designed road or rail tankers for pressurised liquefied flammable or toxic gases have been punctured. For these it is therefore necessary to adopt a synthetic approach to deriving appropriate spill frequencies; a rate generated by

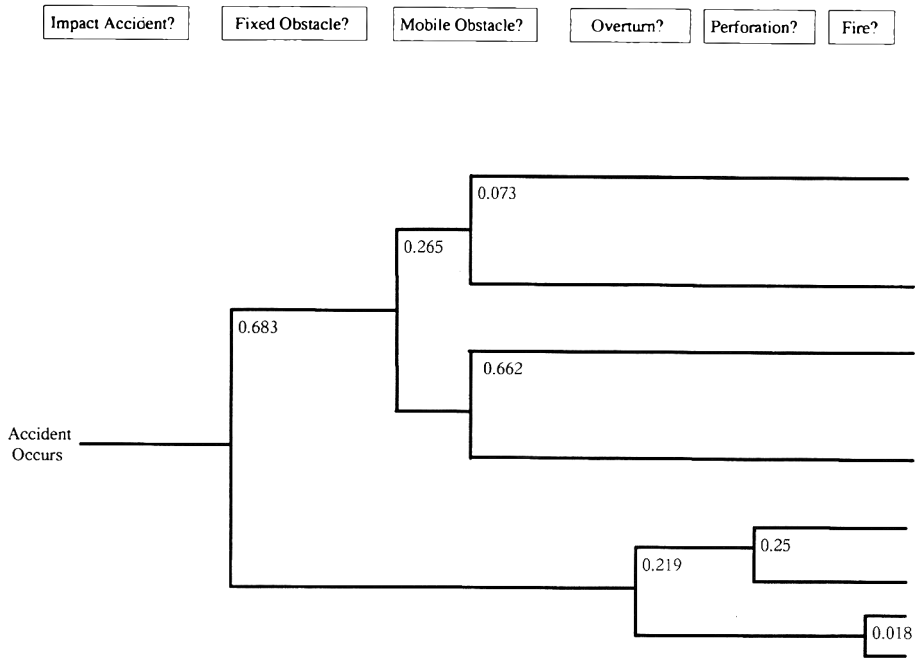

Fig. 1. Incident data analysis after Hubert et al. [2].

statistical techniques from an 'accident free' history provides a useful 'upper bound' check. For transport by rail, the technical working group considered a study by ICI Transport Engineering Division and agreed spill frequencies for ammonia, chlorine and LPG. This study considered the historical accounts of puncture of 'thin walled' wagons and estimated in each case the conditional chance of failure if the vessel concerned had been a 'thick walled' LPG/ammonia or chlorine containing vessel.

Although data on US rail incidents are easily available, it was felt the differences between the design standards and operating practices made these data inapplicable to the British situation. However, for road transport, the differences were less important and could be identified with some confidence. Because of this, US road data could be used and, by appropriate modification to exclude those events which could not or were unlikely to occur in Britain, spill frequencies were derived. Fault tree analysis was used to develop the possible causes and events which could lead to equipment leaks. These were then used to derive appropriate equipment spill frequencies for both rail and road transport of LPG, ammonia and chlorine.

In summary, the spill frequencies and ignition probabilities listed in Tables 1 and 2 were derived for this work.

Table 1 gives base event frequencies. For flammable events, it is also necessary to consider the probability that a spill will then be ignited and whether

this will take place initially or at some later time once a flammable cloud has developed. In some cases it was possible estimate ignition probabilities from accident data, but the under-reporting of spills which have failed to ignite makes these figures unreliable. In most cases, ignition probabilities have to be estimated using synthetic techniques or by expert judgement. This is simplified in transport situations as often the spill-causing event involves sufficient energy to cause ignition, or other sources (for example other road vehicles) are nearby. For the UK study we used the values as listed in Table 2.

TABLE 1

Frequency of spills against cause, substance and transport mode

Substance	Road transport		Rail transport	
	Puncture/ rupture ($\times 10^{-10}$ per wagon km)	Equipment leak ($\times 10^{-10}$ per wagon journey)	Puncture/ rupture ($\times 10^{-10}$ per wagon km)	Equipment leak ($\times 10^{-10}$ per wagon journey)
Motor spirit[a]	190	70	630	–[b]
Chlorine	0.8	36	9	310
Ammonia	4.8	70	25	130
LPG	4.8	52	25	83

[a] For large spills only.
[b] Not considered as such small spills are unlikely to affect members of the public.

TABLE 2

Ignition probabilities for flammable substances

Substance	Type of ignition	Rail		Road	
		Small spill	Large spill	Small spill	Large spill
Motor spirit	Immediate	0.1[a]	0.2[a]	0.03	0.03
Motor spirit	Delayed	0.0	0.1	0.03	0.03
Motor spirit	None[b]	0.9[a]	0.7	0.94	0.94
LPG	Immediate	0.1	0.2	0.1	0.2
LPG	Delayed	0.0	0.5	0.5	0.8
LPG	None[b]	0.9	0.3	0.4	0.0

[a] Derived from historical data.
[b] Derived from: 1 – (Immediate + Delayed).

4. Consequence analysis

As with all forms of such quantified risk analysis, the selection of a representative set of failure cases and assignment of the corresponding spill sizes/rates are the most important steps to producing an accurate characterisation of risk. An optimum set of cases has to be found which while minimising computational effort does not unduly compromise accuracy. Fortunately in the transport situation there are several constraints which act to limit the range of possible events:

- for multi-compartment tankers, the simultaneous loss of contents from all compartments is extremely unlikely;
- small releases of flammable material are unlikely to ignite or cause hazard as they are rapidly dispersed as the tanker moves and even when stationary, the normal 'open' aspect of a transport situation will aid dilution;
- above a certain hole size, either the release of pressurised, liquefied gas will be so rapid that it can be considered equivalent to an instantaneous release on vessel rupture, or the hole will be sufficiently large to lead to a propagating failure of the pressure vessel;
- in the rail environment, ignited jets of LPG are unlikely to create significant hazard unless they impinge on other LPG tankers which then BLEVE. However, the BLEVE frequency used should normally include such a cause.

For the UK transport study three failure cases were used. These were vessel rupture, a large hole and a nominal equipment leak. Taking such a small number of cases does lead to some coarseness and lack of accuracy in the risk analysis but was justifiable given the limited data available here to suggest how the overall failure rate could be partitioned between difficult failure cases. In the absence of any corroborative data, it was assumed that 10% of the releases from pressure vessels were instantaneous and could be modelled as the entire loss of contents. Sensitivity testing to a 99%/1% split or a 50%/50% split showed that this assumption was not critical. In the case of toxic materials the cloud was assumed to contain 100% of the tanker contents, for LPG twice the adiabatic flash fraction was assumed to enter the vapour cloud.

Particular care is needed to take into account the physical aspects of the spill environment when the consequences are modelled. Factors such as the containment effect of roads and drains can significantly affect the shape and dimensions of the hazard zone. This is particularly true of spills of flammable liquids where the hazard zone is only slightly greater than the area of confinement provided by the road or rail corridor. Furthermore, on the road, surface water drains will limit the size of any liquid pool.

For motor spirit spills we therefore considered two cases: either the tanker remained on the highway or rail corridor in which case the spill was confined by kerbs, drains etc. or the tanker left the road or rail line and was modelled as a circular pool. The pool will (in both cases), if ignited reach a maximum size

where the regression rate is equal to the spill rate. Spreading pool expressions such as those given by Shaw and Briscoe [3] can be coupled with a 'drain model' and a fire model [4] to estimate the maximum area of road affected. As the thermal hazard decays rapidly as a receptor moves away from a burning pool, most people who were exposed outside the pool could escape and the area of the pool can be taken as the hazard zone. For example, we calculated that a 25 kg s^{-1} continuous release from a leaking rail wagon (32 te) would produce a pool of radius 24 m. The release would persist for about 20 minutes. If the vapours ignited during this time, the pool size would regress to 12 m. Table 3 shows similar results for road tanker spills.

These results for road tankers take into account loss of the motor spirit into drains and therefore the pool sizes are reduced from their theoretical maximum.

The immediate ignition cases were calculated by assuming that the release occurred over a finite time and that the pool size was the maximum possible after regression. In the delayed case, the pool was allowed to spread to its maximum before ignition took place. These seemed to be realistic assumptions.

The possibility of a 'soft' BLEVE fireball due to heating of a motor spirit tanker in a fire has been considered but does not seem likely. Analysis of the Summit Tunnel Fire incident [5] has shown that even under severe heating conditions, motor spirit tankers will not rupture if three out of four relief valves work or will take at least an hour of prolonged heating if only two operate.

For LPG the type and extent of the hazard depends on the mode of release and whether and when it is ignited. Figure 2 in an example, for continuous LPG releases, of the event trees which can be drawn to rationalise this potential for escalation. Similar trees exist for instantaneous releases of LPG and for spills of motor spirit.

For LPG, standard consequence modelling approaches can be adopted. However, when applied to transportation accidents, certain special considerations apply:

TABLE 3

Motor spirit tanker pool areas

Spill size	Pool area (m^2)	
	Immediate ignition	Delayed ignition
25 kg s^{-1}	314	908
4000 kg	707	1018
8000 kg	1385	1964
12000 kg	2124	3019

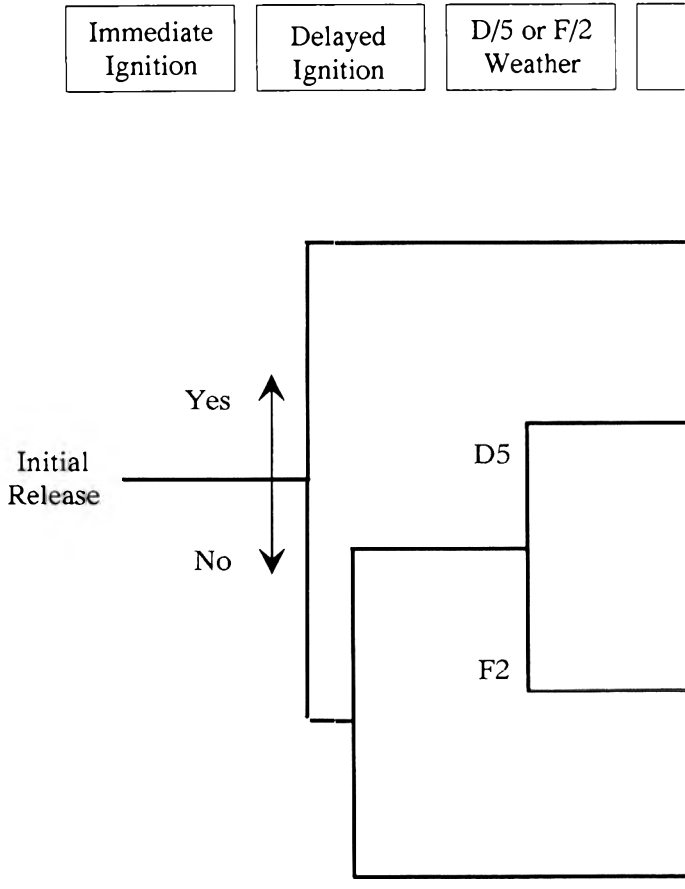

Fig. 2. Event tree for continuous LPG releases.

VCE
Flame Impingement
Remedial Action
Outcome
Torch
BLEVE
Torch
VCE (D5)
Flashfire and torch
Flashfire and BLEVE
Flashfire and torch
VCE (F2)
Flashfire and torch
Flashfire and BLEVE
Flashfire and torch
Unignited release

- for BLEVEs, the resulting fireball will contain a large proportion of the vessel contents as the vessels are always conveyed full;
- BLEVEs are much less likely on the road as one of the primary causes, jet fire impingement from one tanker to another, is highly improbable;
- Vapour Cloud Explosions (VCEs) are very unlikely on both road or rail given the open aspect and limited amount of confinement available. Given the small contribution they will therefore make to the overall risk, a simple consequence model (such as TNT equivalence) is appropriate;
- outside the flammable cloud, the probability of death due to the effects of overpressure from a VCE is low and can be ignored.

The risk from released toxic gases such as ammonia and chlorine is very dependent on the accuracy of the dispersion modelling. As societal risk is to be calculated, the crosswind extent of the cloud is as important as the downwind hazard range. The societal risk estimation involves the calculation of the numbers of fatalities from the areas of land which experience more than a critical toxic load. The use of simple Gaussian models which do not allow for negative buoyancy effects such as cross and up wind spreading will therefore produce inaccurate (likely to be optimistic) results for both toxic and flammable gas clouds. The release orientation in relation to the wind direction can be an important consideration and the modelling of the initial momentum driven jet seem important pre-requisites to the use of an accurate dense gas dispersion model.

There is also a strong dependency between the crosswind and downwind extent of the cloud and the level of atmospheric turbulence. This is characterised by the use of appropriate parameters to represent different Pasquill stability categories. For the UK Study, only two categories; D with a windspeed of $5\,m\,s^{-1}$ and F at $2\,m\,s^{-1}$, were used for reasons of computational efficiency. This choice may have had a significant effect on accuracy, and more categories — four or six are usual — are to be preferred for toxic gases. Given the relatively short range of flammable hazard zones, two categories are probably adequate in this case.

The above discussion only applies strictly to above ground, open air releases on a flat, unobstructed terrain. There has been considerable interest recently about the carriage of hazardous materials through tunnels, and the assessment of the associated risks needs special consideration. In the confined space of a tunnel, the spread of the hazardous consequences is very much affected by the air flow and the channelling effect of the tunnel. For example, the blast wave from a vapour cloud explosion could be expected to be transmitted largely undiminished along a tunnel. One of the most serious hazards arises from the hot, often poisonous smoke and products of combustion which can travel significant distances along the roof of the tunnel away from a fire. The UK Study did not pay particular attention to tunnels as they did not constitute a large proportion of any of the routes studied and, in general, the only members of the public who would be affected would be those using the same road or rail tunnel. Further work is required to refine the current analysis

methods so that a more accurate estimate can be made of the contribution of tunnels to an overall route risk. At present, few decisions involving the control of dangerous goods through tunnels seem to be based on any form of risk assessment.

5. Impact analysis

While the modelling of consequences and the estimation of frequencies are important components of the risk analysis approach, of equal importance is the estimation of the number of people who will be killed or injured by a particular hazardous event; societal risk places equal emphasis on both the frequency of occurrence and the number of fatalities. However, we find that this aspect of analysis has been little developed elsewhere and it was given particular attention in the UK Study. In particular, it seemed important to us to include *all* the population who may be affected by a dangerous goods incident. This includes motorists on a road where an incident occurs, or members of the public travelling as passengers on trains which become involved in an accident. If only those people who live near the transport route are considered in the analysis, an incomplete picture may be presented of the risk and its major contributors. This could lead to erroneous conclusions about the nature of, and benefits from, risk reduction strategies.

5.1 Off-route population density measurement

For long transport routes, the population distribution along the route has to be characterised by a limited number of population categories, each representing an average situation. For the UK study we chose the four categories shown in Table 4.

The length of the transport route alongside which each category of population exists can be obtained using computerised techniques for handling census and other demographic information. Much use is now being made of Geographical Information Systems (GIS) to handle such data, although we found

TABLE 4

Off-route population categorisation scheme

Population category	Average density (km^{-2})
Urban	4210
Sub-urban	1310
Built-up rural	210
Rural	20

that a manual technique, using maps, provided a level of accuracy that was acceptable given the many other uncertainties in this work. One refinement of the approach was to note those lengths of track or road alongside which population of the same class exists on both sides, and those where, for instance, the rail line or road has formed a natural barrier and there is one side of urban development while the other is rural. To prevent 'double counting', in the 'one sided' case, for directional hazards — for example a torch flame or toxic cloud — the frequency of the event is halved and, for events with circular hazard ranges such as BLEVE fireballs, the number of fatalities is halved.

It is also important to take into account the natural separation that occurs between off-route populations (typically residential) and the road or rail line. In Britain, there are very few locations where there is a residential population within 25 m of a rail line and so when the impact of an event is being calculated, this 25 m 'swathe' must be excluded. This approach also acts to 'screen out' small, low consequence events from the analysis.

5.2 Off-road and motorist population modelling

In the road situation there is a smaller but nevertheless important separation between the road and the off-road population. The width of the separation depends essentially on the class of road. It may be only the width of a pavement on an urban single carriageway road, but it may be much larger for a motorway. Furthermore, there are large sections of some routes where 'ribbon development' in a narrow strip alongside the road produces a very high population density (for example shopping areas), with open, low population density land beyond. To accommodate all these situations, and to encompass the variation in the on-road road user population density, a zoning scheme was developed. This is shown in Fig. 3 for a dual carriage way road. The zone structure is described in Table 5.

This scheme also allowed us to model the response and density variations in the motorist population following an accident involving the release of hazardous material. We find that even at night, on main roads and especially motorways and dual carriageways, traffic rapidly builds and behind an accident leading to a very high population density on that carriageway. On the opposite carriageway, the traffic slows down due to the 'ghoul' effect; again increasing the population density. By assuming that 10% of traffic comprises heavy goods vehicles that occupy 20 m of lane length while other vehicle are 4 m long, an average vehicle population of 1.5 gives a Zone d population density of $0.056\ m^{-2}$ for motorways and $0.05\ m^{-2}$ for other roads. Zone d ahead of the accident is essentially clear. For the other carriageway, we have assumed that the curiosity of the motorists produces a density of 0.5 that of Zone d, but in both directions.

This scheme also allowed us to model those events which have directionality, for example a toxic gas release influenced by wind direction and its

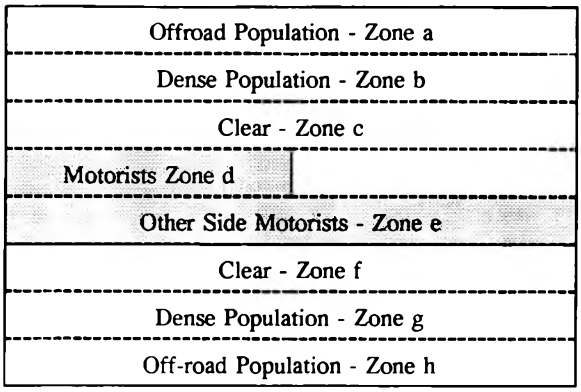

Fig. 3. Population zoning scheme for dual carriage-way roads.

TABLE 5

Population zoning structure for roads

Zone	Name	Description
a	Off-route population	This is similar to that used in the rail study but may be 'depleted' if there is ribbon development
b	Dense population	This allows for a high population density immediately adjacent to the road
c	Clear zone	Motorways and Dual Carriageway roads are likely to have a significant gap between the road edge and the population
d	Motorists, accident side	Road user population which 'backs-up' behind the accident
e	Motorists, other side	Road user population on other side of carriageway
f	Clear zone	Same as Zone c
g	Dense population	Same as Zone b
h	Off-route population	Same as Zone a

momentum driven phase. There are, of course, an infinite range of possible directions, but these can be reduced to the four cases shown in Figs. 4a and 4b. The cloud is represented as either travelling perpendicular to or along the carriageway. In the along the carriageway case, the plume can either travel in the direction of the affected carriageway or opposite to it. For the perpendicular case, the plume either travels off the road from the accident or across the other carriageway. There is a further complication with instantaneous releases of dense gas where we would predict some gravity driven movement of the cloud up-wind.

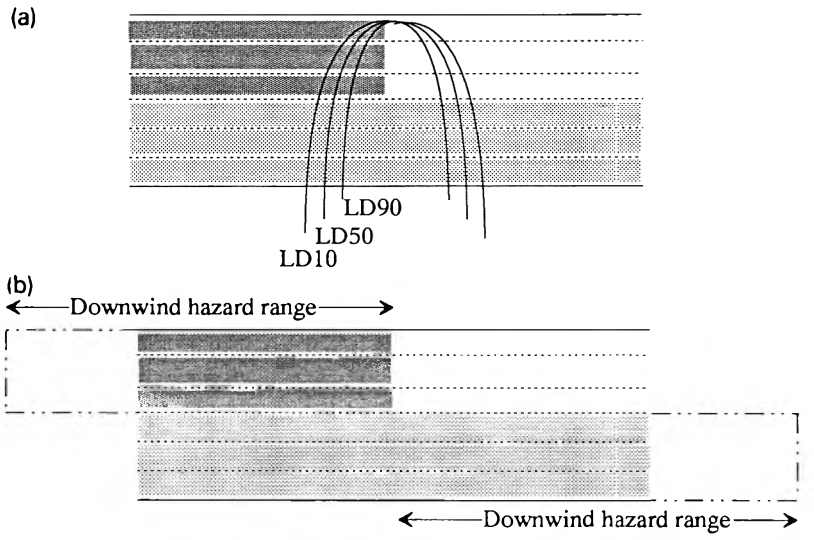

Fig. 4. Model for motorist fatalities, wind across (a) and along (b) carriageway.

5.3 Human impact measurement — Flammable substances

For flammable and explosive events, we find that consequence models predict a fairly sharp cut-off between the point where people exposed will suffer very serious injuries which are likely to be fatal. For flammable events we therefore adopted an impact model which had two 'steps':

- within the LD_{50} hazard range, all die;
- between the LD_{50} and LD_{01} ranges 25% of people die;
- beyond the LD_{01} range all survive.

Where the LD_{50} and LD_{01} are very close together, this can be simplified to a single step where everyone inside the LD_{50} hazard range dies. This is particularly true for motor spirit where only those within the pool fire are assumed to die.

This approach is only true for the impact of overpressure events and thermal events on people out-of-doors. For non-continuous thermal events such as flash-fires, people indoors are assumed to survive; even if their homes catch on fire.

For motorists, it can be assumed that vehicles provide very little protection against fires and explosions. Those in cars are effectively trapped, and escape from the road is not easy in congested traffic.

5.4 Human impact measurement — Toxic gases

To allow for the accurate representation of the variation in human susceptibility, and to enable the implementation of the zoning schemes for on and

off-route populations, it was necessary to use a graduated approach to dose–effect modelling for toxic gases. The normal manner of doing this is to use 'probit' equations which seek to represent that variation in the percentage of a population that will die against a received 'toxic load' assuming a log-normal relationship. These have the general form:

$$Pr = a + b\ln(C^n t) \tag{1}$$

We used three levels of impact, LD_{90}, LD_{50} and LD_{10} for this study, and assumed that the proportion of the population that will die in the area between LD_X and LD_Y will be $(X+Y)/2\%$.

It has been shown [6] that going, or being, indoors provides considerable mitigation against the effects of toxic gases. The impact on people indoors can be calculated by using a simple gas infiltration model which allows for the exponential build up of concentration indoors (C(I)) while the gas cloud is present outside:

$$C(\mathrm{I}) = C(\mathrm{O})[1 - \exp(-\lambda t)] \tag{2}$$

where C(O) is the outside concentration, λ is the ventilation rate and t the duration of exposure. This is followed by a decay phase once the cloud has passed but people still remain indoors:

$$C(\mathrm{I}) = C(\mathrm{M})(-\lambda t) \tag{3}$$

where C(M) is the maximum indoor concentration reached. The integration of these expressions with respect to time with the concentration raised to a power n (taken from the probit equation) yields a toxic load ($\int C^n \mathrm{d}t$). This can be compared with the probit relationship to give an expected percentage fatalities.

Figure 5 shows some of the potential options available to a person who is affected by a toxic gas. For people out-of-doors this can be rationalised into a simple model:

- at or above a concentration (C_1) a person will be unable to take any action and is likely to die;
- below this concentration, down to C_2, there is a chance that he or she can escape indoors. C_2 can be set so that this chance is (say) 0.2;
- below that concentration there is a higher probability of escape, but of those who remain outside the proportion who die is given by $(X+Y)/2$ where the area falls between the LD_X and LD_Y hazard ranges.

This model is shown in Fig. 6. Therefore, for hazardous event E in weather j, the number of people out-of-doors likely to be killed is:

$$N_{\mathrm{O}.E.j} = D_q P_{\mathrm{O}.j}[A_{C1} + A'_1(1 - P_{e1}) + (1 - P_{e2})(0.95A'_2 + 0.7A'_3 + 0.3A'_4)] \tag{4}$$

where $P_{\mathrm{O}.j}$ is the proportion of the people who might be out of doors in weather j, P_{e1} is the chance of escape within concentration C_2, P_{e2} is the chance of

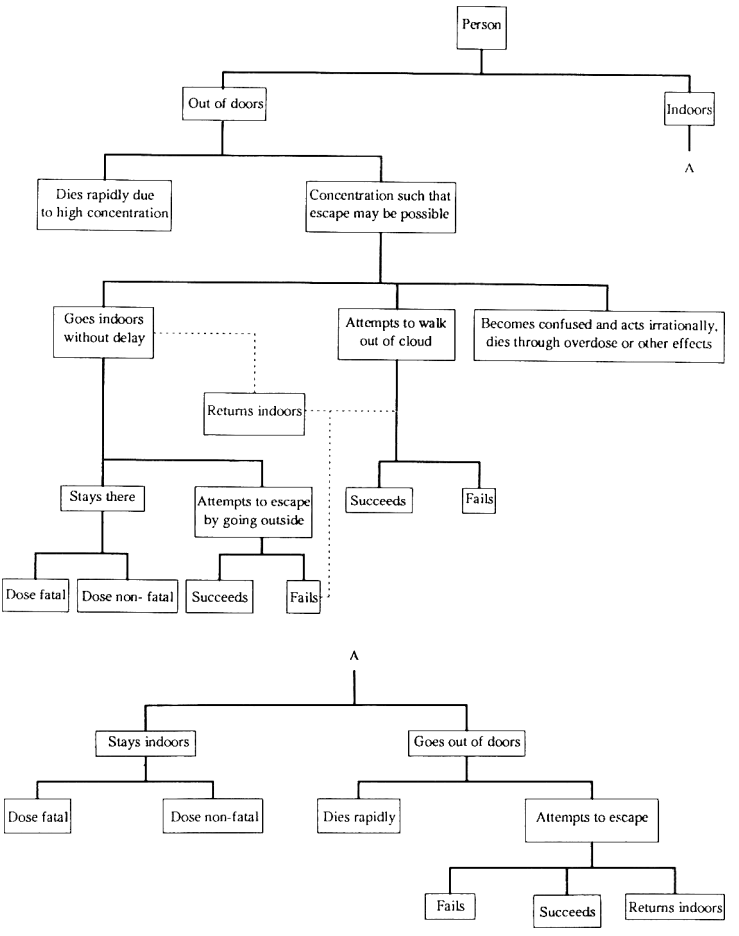

Fig. 5. Range of options available to individual affected by toxic gas.

escape within concentration C_3, area A'_1 is $A_{C2} - A_{C1}$, A'_2 is $A_{C3,90} - A_{C2}$, A'_3 is $A_{C3,50} - A_{C3,90}$, A'_4 is $A_{C3,10} - A_{C3,50}$, and D_q is the population density.

In reality, this expression is more complex as for some releases, $A_{C3,90} \leq A_{C2}$ or even $A_{C3,90} \leq A_{C1}$ and $A_{C3,50} \leq A_{C2}$.

Once people have escaped indoors, they may still be subjected to a fatal toxic load of gas. The number of fatalities indoors therefore comprises those who are already indoors and perish together with the proportion of the 'escapees' who also die. It is given by:

$$N_{I,E,j} = D_q(1 - P_{O,j}) + D'_q(0.95A_{D,90} + 0.7A'_5 + 0.3A'_6) \tag{5}$$

where $A_{D,90}$ is the area covered by the indoor LD_{90} isopleth, A'_5 is $A_{D,50} - A_{D,90}$, and A'_6 is $A_{D,10} - A_{D,50}$.

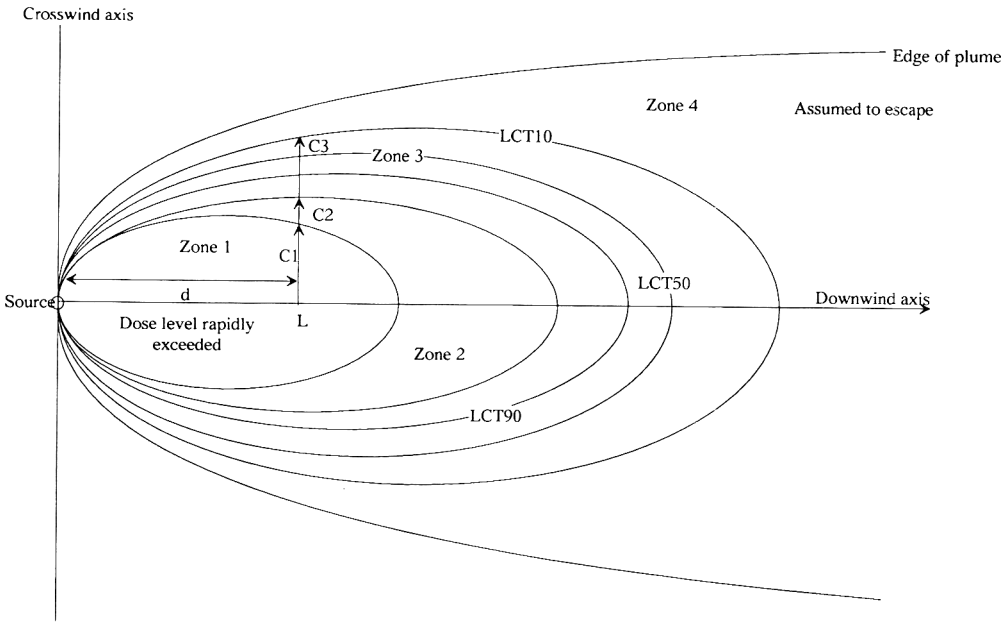

Fig. 6. Model for toxic gas impact.

The proportion of those who escape indoors who subsequently die will depend on whether they escape from $\geq C_1$ concentration, i.e. P_{e2} go indoors, or $\geq C_3$ concentration, i.e. P_{e2} go indoors. D'_q is the average population density of escapees.

For motorists, the protection afforded by their vehicles is very limited. Work by Cook [7] shows that the 'Ram' effect of the car, even without a fan switched on, provides a very high level of ventilation. Therefore we have assumed that these people are effectively out-of-doors and the expression given above, without the terms for escape, can be used:

$$N_{M.E.j} = D_M[0.95A_{90} + 0.7(A_{50} - A_{90}) + 0.3(A_{10} - A_{50})] \quad (6)$$

where D_M is the motorist population density, and A_x is the area of carriageway (one side) which will experience toxic load LD_x or more. This area is given by:

$$\text{Area } A_x = \text{hazard range to } LD_x \times \text{carriageway width} \quad (7)$$

5.5 Rail users (passengers) interactions

In Britain, the rail network is used for both goods and passenger transport. This raises the possibility that one or more passenger trains may interact with a hazardous goods incident causing fatalities on the passenger train. Most other studies have failed to consider this 'extra' population but our work shows that they can make a significant contribution to the risk and that steps to prevent and minimise such interactions need to be considered.

On British Rail, the signalling system is principally concerned with preventing collisions between trains running on the same track. Signalling failure was the cause of one of the UK's most serious transport incidents involving a hazardous substance. This occurred at Eccles, near Manchester, in December 1984 when a passenger train ran into the back of a 14-wagon goods train hauling 'gas oil'. Three tanks ruptured forming pool fires and a 'fireball' which caused three fatalities and 76 injuries.

Despite this incident, we would expect such collisions to be rare events and, in the case of flammable liquids, to cause, at worst, only a few fatalities. Events involving LPG and liquefied toxic gases have the potential to cause many more fatalities and our analysis has mainly considered the interaction of passenger trains with incidents involving rail tanks containing these materials. These materials have long range effects which could affect a passenger train properly stopped by the signalling system, the so called 'obedient' train. Moreover, there is a possibility, although more remote, that the passenger train might collide with the hazardous goods train and cause the release, or might collide with a previously derailed train, or might, as this is specifically not prevented by the signalling system, be affected as it attempted to pass by the scene of a hazardous goods incident on an adjacent line.

This is a complex study which requires that the signalling and emergency systems on British Rail be understood and adequately represented. Using a combination of fault and event trees, the PASSTRAM model was developed to allow the frequency and consequences of such interactions to be calculated for a route that involves sections along which different passenger train types, of different frequencies and passenger numbers, travel at different times of the day. This model is fully described in the Appendix to this paper.

6. Case study — A comparison of transporting chlorine by road and by rail

To demonstrate the use of the models described in this paper and to bring out many of the points made above, we have carried out calculations of the societal risks associated with the transport of the same annual tonnage of chlorine between two locations by road or by rail. At present, this trade is conducted by road between these two sites, approximately 100 km apart. However, a change of mode is a realistic possibility.

The route, in the northwest of England, is at present served by road tankers several times a day. This one route constitutes a significant proportion of the national annual tonnage of chlorine transported by road in Britain. The journey is 103 km long, of which 80 km is motorway, and the rest is mostly single carriageway. The route travels past, but not through, three large towns, and only about 1 km of the route has 'urban' population on at least one side with 19 km with suburban population on one or both sides. Most of the rest is rural. The exact breakdown is shown in Table 6.

TABLE 6

Population distribution along study road route

Road type	Population type	Density (km^{-2})	No. of sides	Length (km)
Motorway	Urban	4210	2	0.0
			1	1.0
	Sub-urban	1310	2	1.0
			1	13.0
	Built-up rural	210	2	2.0
			1	17.5
	Rural	20	2	45.5
			1	31.5
Single carriageway	Urban	4210	2	0.0
			1	0.0
	Sub-urban	1310	2	4.0
			1	1.0
	Built-up rural	210	2	4.0
			1	0.5
	Rural	20	2	13.5
			1	1.5

The road tankers which travel this route make 1,743 journeys a year carrying 17.5 te each time.

The alternative delivery by rail would require 1,052 29-te tankers a year. The rail route is about 97 km long but passes through 3 major towns with populations of 176,000, 81,700 and 126,000, respectively. The route includes 6 km of urban and 20 km of sub-urban population. Most of the route is also used extensively by passengers trains; part is the West Coast main line between London and Scotland. The passenger train traffic is shown in Table 7.

Using the techniques described above, we have calculated the following levels of societal risk for the different modes in Tables 8 and 9.

TABLE 7

Passenger train traffic on study route

Section	Intercity		Provincial	
	Day	Night	Day	Night
Warrington	47	18	32	3
Kirkham	10	1	125	11

TABLE 8

Societal risk results — Transport by rail

Group at risk	Frequency of N or more fatalities ($\times 10^{-6}$ y^{-1})					
	1	10	30	100	300	1000
Passengers	39.5	39.5	39.5	10.6	0.0	0.0
Off-rail population	105.0	47.8	27.8	26.8	11.9	5.2
Total	107.3	68.0	56.8	41.5	13.6	5.7

TABLE 9

Societal risk results — Transport by road

Group at risk	Frequency of N or more fatalities ($\times 10^{-6}$ y^{-1})					
	1	10	30	100	300	1000
Motorists	16.7	10.5	8.8	4.8	1.7	0.0
Off-road population	15.5	5.9	2.9	1.4	0.9	0.0
Total	19.0	13.6	10.3	6.2	2.6	0.1

These results are also shown in Fig. 7 as FN curves.

It can be seen that:

- the risk by rail is approximately five times that by road;
- the risk to rail users is about double that to motorists;
- the risk to off-rail population is approximately 8 times higher than that to the off-road population;
- the road risk is dominated by that due to motorist involvement.

These results are due to a common factor in British transport systems; most of our rail system was built over 100 years ago and was intended to go from town to town while most of our major roads have been built over the last 20 years and have been specifically routed to take traffic away from centres of population.

It would be possible to construct a route which would be more favourable to rail, but in reality the historical legacy of our transport systems will always tend to produce lower risks for the transport by road of materials with long hazard ranges. The risks from the transport of these substances will be lower if the route followed avoids centres of population and this is more easily achieved in Britain by road rather than rail. Substances with a shorter range effect such as motor spirit, should normally be more safely transported by rail since there is already a very worthwhile separation between the rail line and people who

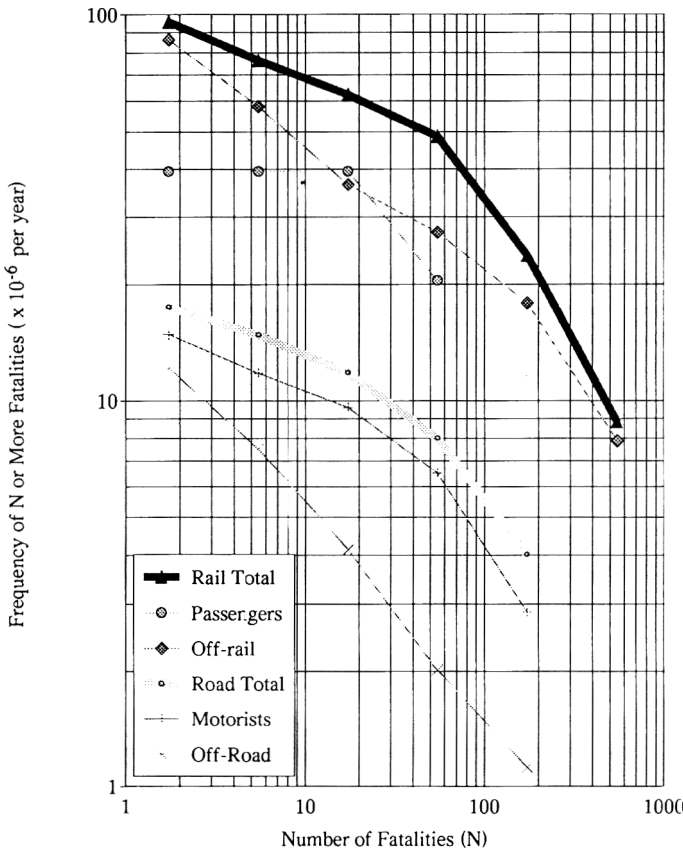

Fig. 7. Societal risk result for road/rail comparison.

live nearby, and passenger train involvement is likely to be restricted to direct collisions when, at worst, only a few passengers may be affected.

It is clear that in Britain it is not possible to say that transport of hazardous substances by rail is safer than by road or, indeed, vice versa. However, there seems to be no case on grounds of safety alone for the British Authorities to enforce modal transfer. This contrasts with the situation in other countries such as Germany, where legislation now requires transfer to rail for longer journeys.

7. Conclusions

Throughout Europe, concern is being voiced about the transport of dangerous goods and the risks posed to members of the public. Legislators are widening their attention from the problems of fixed major hazard installations to identify the most appropriate means to control the risk from hazardous materials in transit.

It is very important that there is a full understanding of the magnitude of the risks involved, and the causes and major contributors, so that properly informed decisions can be made. In this paper we have described the methodology that was developed as part of a major study into the risks faced by the British population from the transport of dangerous substances.

We have concentrated on the novel aspects of the study and in particular consequence and human impact modelling. In the case of consequence models, we have suggested that the choice of model and the depth of the analysis must be driven by an understanding of the overall uncertainties of the risk analysis, and the contribution each element makes to that uncertainty. Where it matters, the most accurate models are appropriate; for less sensitive elements, a more simple and less rigorous approach may be justifiable. The final arbiter of the degrees of complexity and precision necessary is the end user; in this case a decision making body. The analysis methodology must be sufficiently transparent so that the results can be understood and used with confidence.

The modelling of human impact has been a feature of this paper reflecting the need perceived by those conducting the UK Study to be more rigorous in the treatment of this aspect of hazardous goods transportation risk analysis. Other workers have not dealt with this in such detail before but our work has shown that the inclusion of motorist and rail passenger populations can significantly affect the calculated risk levels, and can therefore have a profound effect on any conclusions which are drawn on the need for further legislative controls and the nature of those controls.

In support of these points, and to demonstrate the use of the models that were built, the relative risks of transporting chlorine by road or rail have been explored in a realistic case study. From this it can be concluded that the safe routing of materials with large hazard ranges may be more easily achieved by road. For materials with a smaller hazard range, the natural separation afforded by the rail system may make this mode more suitable. However, in Britain, there appears to be no evidence to support, on safety grounds, a *general* transfer of hazardous goods from road to rail or the reverse.

The potential hazards from the transport of dangerous substances is a very emotive issue; the hazards are brought close to where people live, work and play, and they have no fixed location. This is a case where any risk which is imposed is truly 'involuntary' in that we are unlikely to derive any immediate benefit from the tanker passing our homes, but we can do little to dissociate ourselves from the risks it may present. It is therefore essential that any debate about the level of the risks, their tolerability, and the possible need for risk reduction, is conducted with the benefit of a full understanding of those risks based on a rigorous and appropriately accurate analysis. It is also incumbent on the analyst to consider how best the results of his analysis can be communicated to prevent mis-understanding; this may well influence the manner in which he conducts the analysis.

To ensure consistency and to stimulate quality in such studies, it would seem that some form of code of practice is desirable. This was one of primary

conclusions of a recent International Consensus Conference on the Transportation of Dangerous Goods held in Toronto whose participants agreed that the code should consider:

- standards for the definition, measurement and reporting of risk;
- a standard approach to risk analysis for the transport of dangerous goods;
- the need for any results to be compared with observed data to prove realism;
- a standard approach to:
  - (i) release rate and size estimation;
  - (ii) loading and unloading risks;
  - (iii) weather modelling;
  - (iv) inclusion of all affected populations;
  - (v) the use of standardised incident and other databases;
- an explicit statement about the size and sources of uncertainty in any analysis;
- the need to match the complexity and precision of any analysis to the needs and capabilities of the end user;
- criteria for quality review and assurance of the risk analysis process.

Acknowledgements

The author would like to thank the Directors of DNV Technica for their support in preparing this paper, and also would also like to acknowledge the very considerable contributions made to this work over many years by past colleagues in HSE, notably Geoff Grint, Nigel Riley, Linda Smith and Stewart Campbell and by the members of the technical working party.

References

1 Health and Safety Commission, Major Hazard Aspects of the Transport of Dangerous Substances, Advisory Committee on Dangerous Substances, HMSO, ISBN 0-118-85676-6, 1991.
2 P. Hubert et al., Les risques d'accident majeurs dans les transports de maitre dangereuses, Centre d'Etude sur L'évaluation de la Protection Nucleaire, D 114, France, 1985.
3 P. Shaw and F. Briscoe, Evaporation from spills of hazardous liquids onto land and water, UKAEA, Safety and Reliability Directorate, R210, Culcheth, 1978.
4 G.A. Mitzner and J.A. Eyre, Large scale LNG and LPG pool fires, In: The Assessment of Major Hazards, I. Chem. E., Rugby, 1982, pp. 146–164.
5 A. Jones, The Summit Tunnel Fire, IR/L/FR/85/86, HSE Report, Health and Safety Executive, 1985.
6 G. Purdy and P.C. Davies, Toxic gas incidents — some important considerations for emergency planning, In: Multistream, The Subject Group Symposium, I. Chem. E., Rugby, 1985, pp. 257–268.
7 M. Cooke, Risk Assessment Safety: A Case Study of Two Chlorine Plants, Thesis for M.Sc., UMIST, Manchester, 1988.

Appendix

PASSTRAM — A model to calculate the frequency and impact of hazardous goods events on passenger trains

Background

In Britain, the signalling system on the railways has been developed over many years to prevent accidents due to the collision of trains running on the same set of tracks. However, in the event of an incident involving a train conveying hazardous goods, the correct operation of the signalling system may not, in itself, prevent passenger trains being affected. It is entirely possible, although unlikely, for releases of materials with long hazard ranges to affect trains properly stopped at signals up the line from the hazardous goods incident.

Normally, a following train would not be allowed into a section of track until the first train has cleared an average 200 yards 'overlap' beyond the next set of signals. However, events with hazard ranges greater than this could impact on trains behind which have properly stopped.

In the event of an incident, the train crew's duty is to protect their train from approaching trains on their track. Many routes in Britain are equipped with automatic 'track circuiting' that detects the presence of a train and will prevent other trains entering that section of track by not clearing the signal protecting that length of track. 'Clips' are also carried which can be applied to nearby tracks to simulate the presence of a train and so provide further protection. In addition, the train crew can place detonators on the rail, can wave red flags to slow approaching trains, and can by walking to the nearest signal post or other means of communication warn. If these safeguards fail, passing passenger trains on adjacent tracks may still enter the hazardous area and become affected. Furthermore, the passenger train (PT) itself may be in collision with a hazardous goods train (HGT) under normal running conditions or after a derailment and this could itself lead to a loss of containment with consequential impact on the passenger train population.

Possible interactions

The range of possible interactions can be rationalised into:

- the collision of a PT and a HGT leading to tank rupture, this includes the case of a previously derailed PT;
- the PT entering a hazard zone after an earlier puncture incident (a 'passing' train or a 'disobedient' train which has passed a 'stop' signal);
- the PT collides with a previously derailed HGT and causes a puncture;
- the PT enters a hazard zone caused by an equipment leak on the HGT; and
- the hazard range from a punctured tanker on the HGT affects a PT properly stopped at signals (an 'obedient' train).

This can be further expanded into six impact cases which take into account directionality:
Case 1 – PT drives into the cloud, the wind is along the track
Case 2 – PT drives into the cloud, the wind is across the track
Case 3 – PT collides with a derailed HGT and punctures a tank
Case 4 – PT collides with HGT and, as a consequence of the collision, a tank is punctured
Case 5 – PT enters the cloud produced by an equipment leak
Obedient long – The PT is stopped at signals but is affected by a HG release nearby, the wind is along the tracks
Obedient perp – The PT is stopped at signals but is affected by a HG release nearby, the wind is across the tracks

The frequency of N or more fatalities — Toxic materials

Cases 1 to 4 above concern the passenger train entering the 'Affected Section of Line' (ASL), the length of track between two sets of signals where the HG incident occurs. In Britain, the length of the ASL will vary between 3/4 and 20 miles. For non-track circuited line, there is an average of five miles between stations or signal boxes. The likelihood of causing passenger train fatalities in Cases 1 to 5 is a function of the spill or puncture frequency, the probability of a particular wind direction, and the probability that given an HGT incident the PT will enter the ASL and, furthermore, will not stop until it is within the hazard range. Figures 8, 9 and 10 show event trees that have been used to derive an interaction frequency for Cases 1 to 5 above. The probability that the PT will enter the ASL (P2) can be derived from quantifying the fault trees shown in Fig. 11 (for track circuited) or Fig. 12 (for non-track circuited line). The value of the top gate probability (G1) is calculated from the probability that the PT will fail to stop at signals (G2, which is a constant for all similar lines) and the probability that a PT will be 'nearby' when the HG incident occurs (E5, which is a function of the PT traffic along that line). For this study we obtained values of G2 of:

- 0.011 for track circuited line;
- 0.22 for non-track circuited line.

Therefore, the frequency of PT fatalities in Cases 1 to 5 are given by:

$$F_{\text{Case 1}} = F_1 P_1 P_2 P_3 P_4 \tag{8}$$

$$F_{\text{Case 2}} = F_1 P_1 P_2 (1 - P_3) P_5 \tag{9}$$

$$F_{\text{Case 3}} = F_1 (1 - P_1) P_2 P_6 P_7 \tag{10}$$

$$F_{\text{Case 4}} = F_2 P_8 \tag{11}$$

$$F_{\text{Case 5}} = F_1 P_2 P_3 P_{10} \tag{12}$$

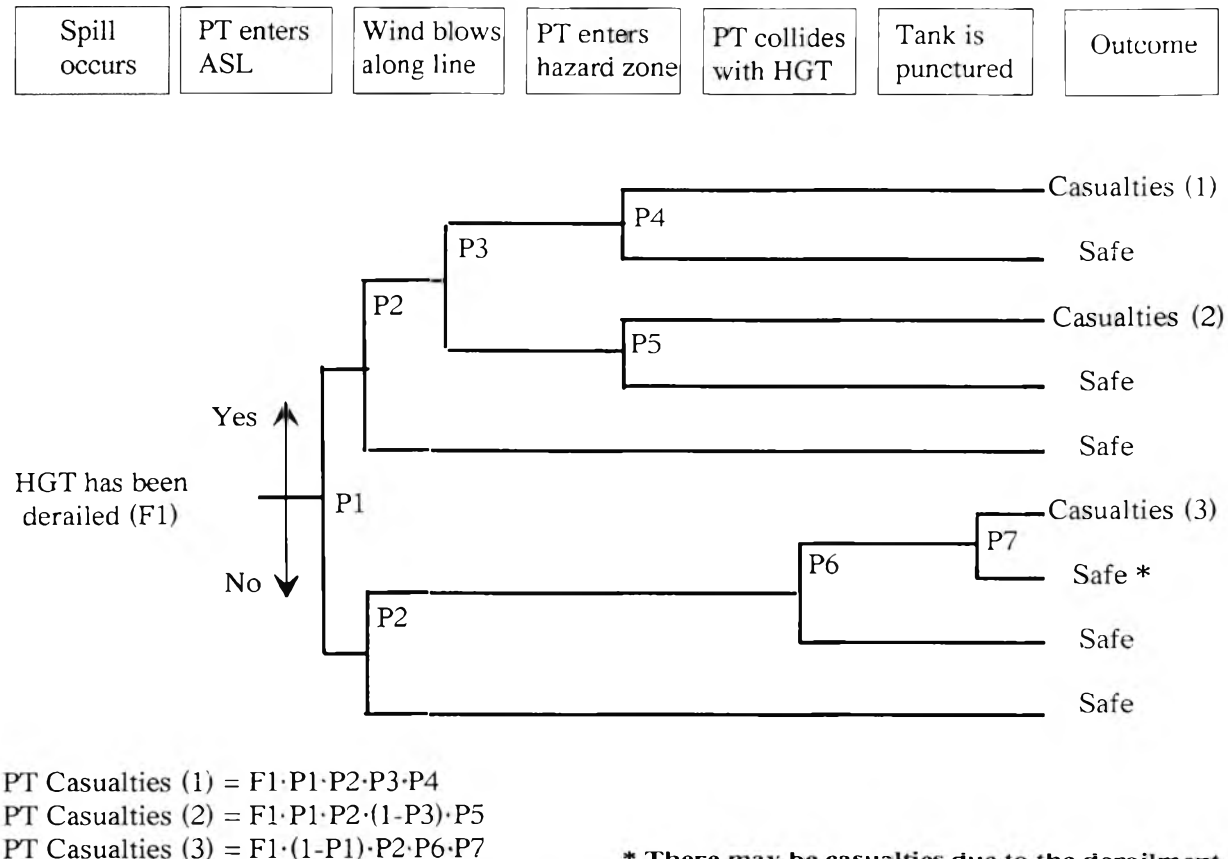

Fig. 8. Event tree for PT interaction with derailed HGT.

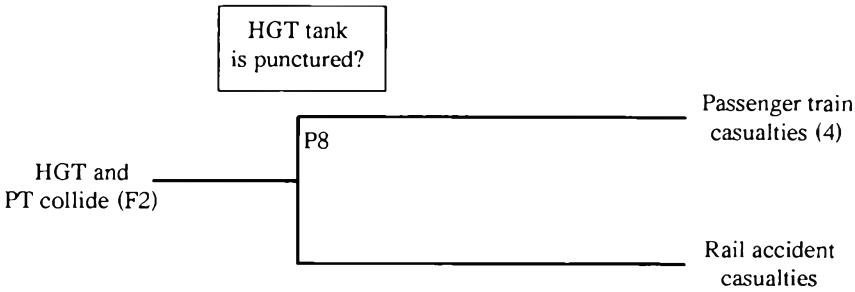

PF casualties (4) = F2·P8

Fig. 9. Event tree for running collisions.

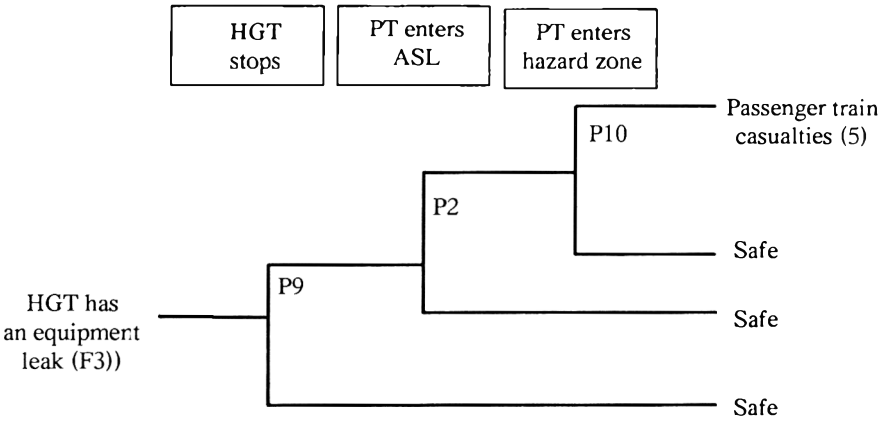

PT casualties (5) = F3·P2·P9·P10

Fig. 10. Event tree for PT interaction with equipment leak.

The number of fatalities in each case depends on the proportion of the PT within the hazard range, the outside concentration, the ventilation rate into the train carriage, and the duration of exposure. Rail passengers are effectively 'indoors' and are provided with a measure of protection against the ingress of toxic gases. Modern British trains are, however, provided with mechanical ventilation and the controls are not accessible to train staff (other than the driver) or to passengers. The ventilation rate at 13 air changes an hour is relatively high, and the protection afforded is significantly less than they would experience in a normal house. Train drivers are provided with an extremely high air exchange rate and can effectively be considered as 'out of doors'.

For Case 1, the fraction of the train affected is given by:

$$X_A = L_H / L_T \tag{13}$$

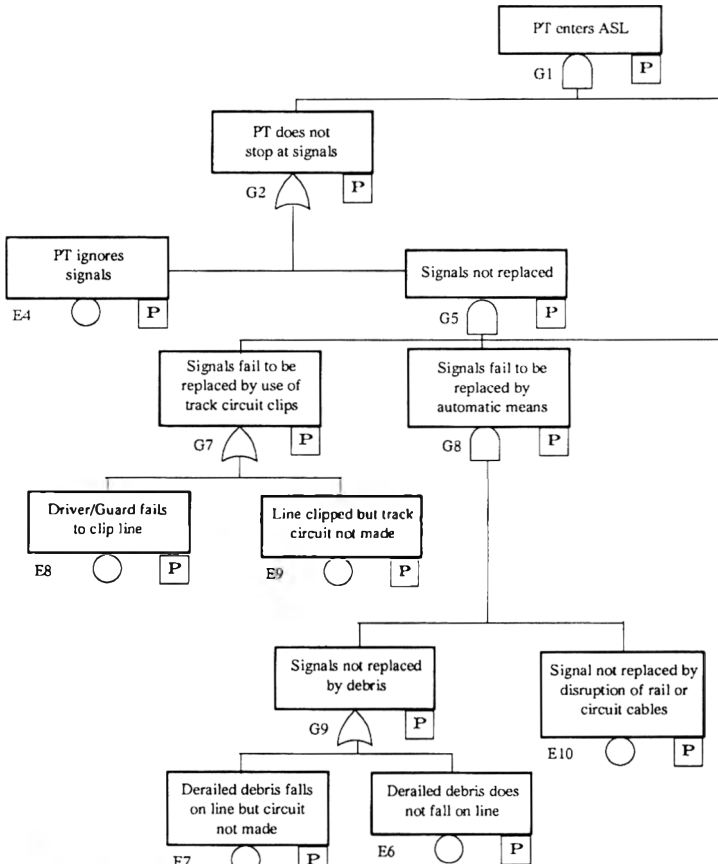

Fig. 11. Fault tree for PT entering ASL with track circuit.

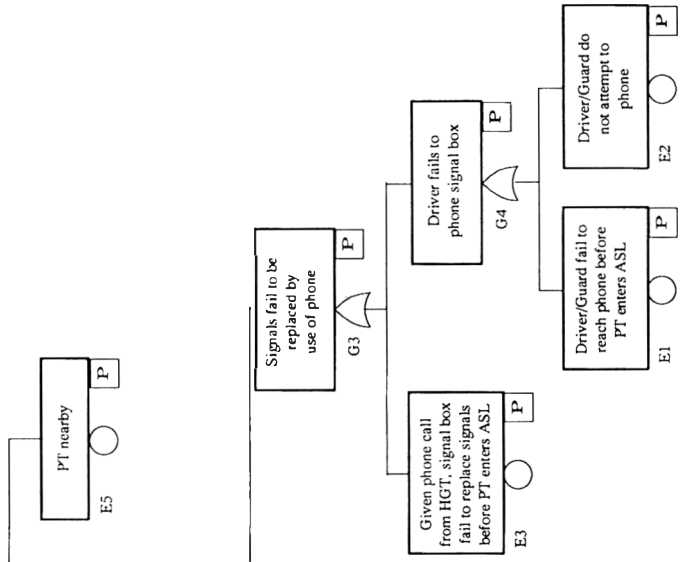
PT nearby
E5
P
Signals fail to be replaced by use of phone
G3
P
Given phone call from HGT, signal box fail to replace signals before PT enters ASL
E3
P
Driver fails to phone signal box
G4
P
Driver/Guard fail to reach phone before PT enters ASL
E1
P
Driver/Guard do not attempt to phone
E2
P

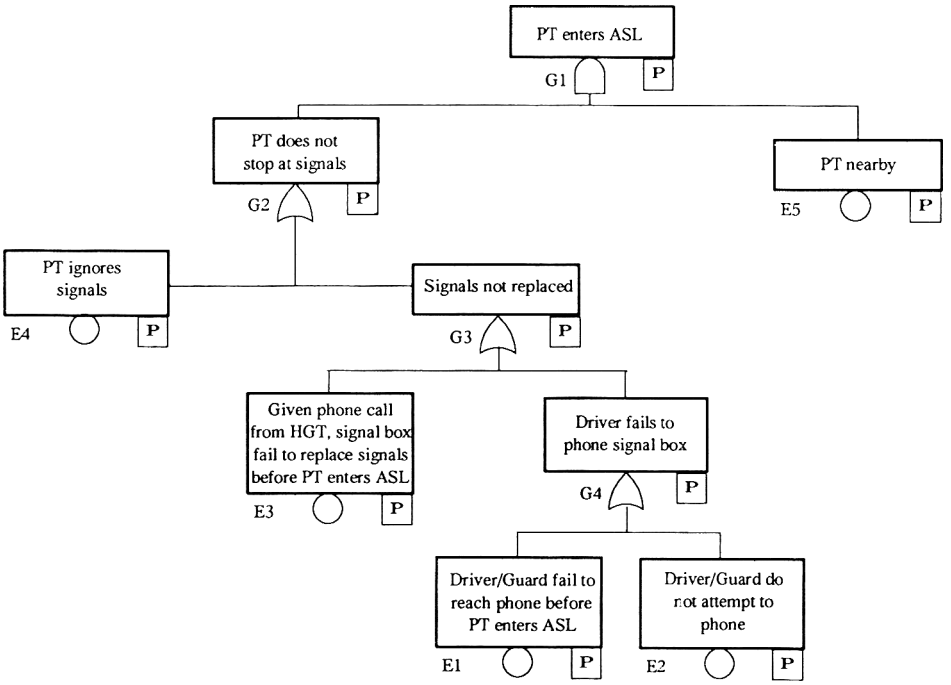

Fig. 12. Fault tree for PT entering ASL without track circuit.

where L_H is the hazard length and L_T the length of the train, and $X_A \leq 1$.

The number of carriages affected (integer) will be given by:

$$N_{CA} = \text{INT}(N_C X_A + 0.5) \tag{14}$$

where N_C is the number of carriages on the train. Using a uniform density (Q_P) of passengers per carriage, for a given level of harm x, the number of people experiencing that level of harm or more will be:

$$N_x = Q_P\{\text{INT}(N_C X_X + 0.5)\} \tag{15}$$

Then, if three hazard ranges of LD_{10}, LD_{50}, and LD_{90} are used, the number of fatalities for event E in weather j is given by:

$$N_{E.j} = 0.95N_{Ej.\,90} + 0.7(N_{Ej.\,50} - N_{Ej.\,90}) + 0.3(N_{Ej.\,10} - N_{Ej.\,50}) \tag{16}$$

For Case 2, the proportion of the train affected will be:

$$X_A = W_H / L_T \tag{17}$$

where W_H is the width of the hazard zone and the number of passenger fatalities is given by the expression (16) above.

For Cases 3 and 4, the passenger train is actually involved in the incident and that incident is severe enough to lead to puncture of a tank. We would

therefore expect the passenger carriages to be very close to or alongside the release. Given the local effect of the train carriages on the dispersion of dense gases, these cases can be treated as for Case 1 by ignoring any tendency for the gas to drift across the rails under the influence of the wind.

The 'obedient train' cases, Cases 6 and 7, can be treated as Cases 1 and 2 but with the 200 yard 'overlap' length subtracted from the hazard range or width, respectively. The frequency of affecting an obedient train with the wind blowing along the tracks (Case 6) is given by:

$$F_{CL} = \frac{F_1 P_1 P_3 (1 - G2) E_5 L_H}{2(L_L + 2L_T)} \tag{18}$$

where L_L is the length of the ASL. Similarly, for obedient trains when the wind blows along the tracks:

$$F_{OP} = \frac{F_1 P_1 (1 - P_3)(1 - G2) E_5 (W_H/2)}{2(L_L + 2L_T)} \tag{19}$$

The frequency of N or more fatalities — Flammable materials

Because of the very small hazard range, the interaction of passenger trains with flammable liquid spills and fires is only likely to lead to a small number of fatalities. This study therefore concentrated on liquefied flammable gases, notably LPG, which have significantly greater hazard ranges. The treatment for toxic gases given above can be extended by the exclusion of some events on the basis of low hazard or low frequency, and by the inclusion of additional events. Excluded are:

- flash fires caused by equipment leaks;
- VCEs in the case of 'non-obedient' trains as the interaction probability is small;
- VCEs in the case of 'obedient' trains as the interaction probability is very low;
- BLEVEs for 'non-obedient', 'passing' trains as the interaction probability is very low.

The cases for LPG interactions are:

Case 1 – PT drives into the flammable cloud, the wind is along the track. Ignition causes a flash fire

Case 2 – PT drives into the flammable cloud, the wind is across the track. Ignition causes a flash fire

Case 3 – PT collides with a derailed HG train and punctures a tank. Ignition of the resulting cloud causes a flash fire

Case 3a – PT collides with a derailed HG train and punctures a tank. Ignition causes a fireball of the tank contents

Case 4 – PT collides with a HG train and, as a consequence of the collision, a tank is punctured. Ignition of the resulting cloud causes a flash fire

Case 4a – PT collides with a HG train and, as a consequence of the collision, a tank is punctured. Ignition causes a fireball of the tank contents

TABLE A1

Ignition probabilities used in PASSTRAM

Event	Probability
Immediate ignition	0.3
Delayed ignition	0.5
Fireball	0.3
BLEVE after flash-fire	0.1

Obedient long – The PT is stopped at signals but is affected by a flash fire caused by a LPG release nearby, the wind is along the tracks
Obedient long, a – The PT is stopped at signals. After being affected by a flash fire caused by a LPG release nearby, it is subsequently affected by a BLEVE. The wind is along the tracks
Obedient perp – The PT is stopped at signals but is affected by a flash fire caused by a LPG release nearby, the wind is across the tracks
Obedient perp, a – The PT is stopped at signals. After being affected by a flash fire caused by a LPG release nearby, it is subsequently affected by a BLEVE. The wind is across the tracks.

Domino events, where fires spread between tank cars leading to several flash fires/BLEVEs, will not extend overall hazard ranges and will only increase slightly the interaction frequencies. For these reasons, they were not considered further.

For flammable events, rail passengers can be considered to be 'indoors' in terms of impact and we have adopted the same assumptions as with 'off-rail' populations; that is:

- 50% of rail passengers within a flash fire (LFL) or fireball radius will die;
- outside the flammable cloud (LFL), rail passengers survive.

Given the special circumstances of the PT/HGT interaction, the ignition probabilities used for the main analysis were judged inappropriate. In this case the ones listed in Table A1 were used.

Event frequencies and the corresponding numbers of passenger fatalities can be calculated in the same manner as for toxic events as described above.

Journal of Hazardous Materials, 33 (1993) 261–273
Elsevier Science Publishers B.V., Amsterdam

Relief vent sizing and location for long tubular reactors

M.A. Grolmes[a] and M.H. Yue[b]

[a]*Fauske & Associates, Inc., 16W070 West 83rd Street, Burr Ridge, IL 60521 (USA)*
[b]*Merck & Company, Inc., 126 East Lincoln Highway, Rahway, NJ 07065 (USA)*

Abstract

The DIERS (Design Institute for Emergency Relief Systems) methodology for emergency relief evaluation is recognized as a state-of-the-art procedure for reacting systems operated in batch or semi-batch mode process vessels. By comparison, the evaluation of emergency relief requirements for tubular reactors has received little consideration. This paper addresses the questions of location and size requirements for long tubular reactors. Much of the DIERS methodology is applicable in principle, and this paper suggests where certain key details may be modified for tubular reactor considerations. This paper presents emergency relief evaluation procedures for both tempered and pure gassy reacting systems and provides example illustrations of each case.

1. Introduction

Tubular reactors (sometimes referred to as plug flow reactors) are geometrically quite different from batch reactors. For the purpose of this paper we will consider a typical tubular reactor as a continuous flow reactor system made up of a relatively small diameter pipe but having a very long length-to-diameter ratio (L/D), perhaps ranging from several hundred to several thousand. Such reactors are rarely straight, and often consist of a sequence of straight segments and reversing "hair-pin" turns enclosed in heat exchange or temperature control shells.

Upset conditions which lead to requirements for pressure relief may include any of the following considerations:

(a) Loss of flow and temperature control
(b) Reagent feed error
(c) External fire
(d) Other site specific considerations

Correspondence to: M.A. Grolmes, Fauske & Associates, Inc., 16W070 West 83rd Street, Burr Ridge, IL 60521 (USA).

0304-3894/93/$06.00

As is often the case for a batch reactor process, the necessary information required to characterize the run-away reaction for emergency relief evaluation will require empirical bench-scale calorimetry tests. This essential part of the DIERS methodology has been adequately described in References [1–5] for example, and is equally applicable to tubular reactors. Benchscale test data should establish whether the reacting system under consideration is tempered (reaction rate may be limited by evaporation of volatile reagents) or generates non-condensable gas (gassy). In either case, the test data for the specific chemical system should provide the relevant reaction rate data required for vent sizing analysis.

This background information is an essential and well-established part of the DIERS methodology and will be assumed as prerequisite for consideration of tubular reactors. However, use of this data for vent size evaluation has emphasized batch reactors and the purpose at hand is to illustrate how the same methods may be adapted to long tubular reactor devices.

2. Features of tubular reactors

There are several features of tubular reactors that are important to recognize at the outset. The device shown in Fig. 1, which is only one example of the concept, serves to illustrate several features. Relative to batch reactors, the in-reactor inventory is usually quite small. Depending on specific material of construction, the pressure rating is usually quite high owing to the usually small diameter. If this is indeed the case, then relative to a batch reactor, the thermal inertia or so-called phi factor may be significant in slowing the rate of a postulated run-away reaction. This point will be addressed later in the paper.

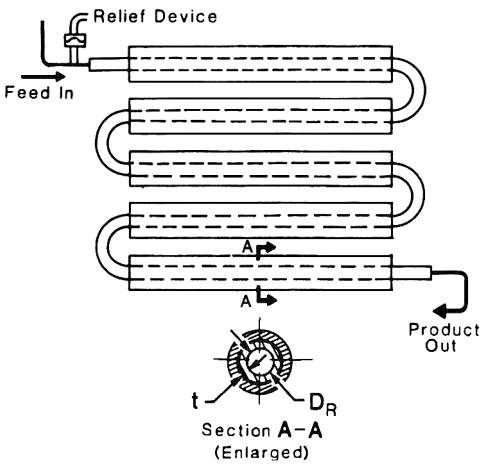

Fig. 1. Illustration of a long tubular reactor.

In spite of the long length of the reactor, locations for emergency relief may be limited due to concentric heat exchange equipment. Therefore, one essential question regarding pressure relief for tubular reactors is the maximum length of reactor which can be protected by a single pressure relief device, when the relief vent area is limited by the cross-section area of the reactor itself.

The last significant characteristic of tubular reactors which will be mentioned here is that the relief vent flow rate will be significantly affected by length of the reactor. Fortunately, prior analysis of the two-phase discharge of long pipes may be utilized to enable the batch reactor vent sizing evaluation models to be adapted to tubular reactors.

3. Discharge rates in long tubes

The two-phase discharge of non-reacting flashing liquids was evaluated in Ref. [6] by means of a detailed numerical model which considered sensitivity to flow regime assumptions as well as numerical nodalization of the pipe line. Pipe lengths of several kilometers were considered. This analysis set the stage for a one-step analytical approximation developed in Ref. [7]. Grolmes and Fauske [7] showed how the long-pipe two-phase discharge coefficient models established in Ref. [8] could be utilized to provide good agreement with detailed numerical models. These methods are adopted here.

A discharge coefficient, or flow reduction factor F, may be defined as

$$F = G/G_{max} \tag{1}$$

where G is the actual discharge mass flux and G_{max} is the two-phase discharge mass flux for an ideal no-loss geometry. For flashing liquids characteristic of tempered reacting systems, G_{max} may be approximated by [9]:

$$G_{max} = \frac{\lambda}{v_{fg}} \frac{1}{\sqrt{CT}} \tag{2a}$$

or the equivalent form when the Clausius–Clapeyron equation holds,

$$G_{max} = \frac{dP}{dT}\sqrt{\frac{T}{C}}. \tag{2b}$$

For non-flashing, two-phase discharge of a gassy system, the more rigorous formulation for G_{max}, found in Ref. [10], may be approximated by

$$G_{max} = \sqrt{P_0(1-\alpha)\rho_f}\,\frac{\left[\frac{2}{\alpha}\left\{\left(\frac{1-\alpha}{\alpha}\right)(1-\eta) - \ln\eta\right\}\right]^{1/2}}{1/\eta + (1-\alpha)/\alpha} \tag{3}$$

where

$$\eta = \left[2.016 + \left[(1-\alpha)/2\alpha\right]^{0.7}\right]^{-0.714}. \tag{4}$$

The terms in eqs. (2) and (3) are defined as follows: λ is the latent heat of vaporization, v_{fg} is the difference between vapor specific volume v_g and liquid specific volume v_f, C is the liquid heat capacity, T is the absolute temperature, dP/dT is the slope of the vapor pressure–temperature relation, P_0 is the source pressure, ρ_f is the liquid density, α is the gas volume fraction, and η is the choking pressure ratio (see Ref. [10]).

If the ambient pressure ratio, defined as $\eta_{amb} = P_{amb}/P_0$, is greater than η defined by eq. (4), for gassy systems, G_{max} may be represented by the incompressible form

$$G_{max} = \sqrt{2(1-\alpha)\rho_f(P_0 - P_{amb})}. \tag{5}$$

Grolmes and Fauske [7] showed that the discharge coefficient for flashing flow in long horizontal tubes in the subsonic region could be represented by

$$F = \frac{127}{98} \frac{\omega^{1/2}(1+\omega)^{-1/3}}{\sqrt{N}} \tag{6}$$

where

$$\omega = P_0 \rho_f / G_{max}^2 \quad \text{(eq. 2)}. \tag{7}$$

In eq. (6), the friction length parameter N is defined

$$N = 4f(L/D)_{equivalent} \tag{8}$$

and for two-phase turbulent flow a constant value of

$$f = 0.005$$

is often assumed for the friction factor.

For a non-flashing two-phase gassy system at void fractions α, approaching zero, the incompressible form of the discharge coefficient F is given by

$$F = (1+N)^{-1/2} \tag{9}$$

where N has the same meaning as defined by eq. (8) above.

Figure 2 shows the above relations for flashing and non-flashing discharge flows in the long L/D range. As a further simplification, one can represent an arbitrary flashing system whose ω value lies in the range of $10 < \omega < 30$ and for $L/D > 1000$, by the relation

$$F = 2N^{-1/2}. \tag{10}$$

Equations (10) and (6) are also compared in Fig. 2.

Equations (9) and (10) provide two convenient representations for the vent flow discharge coefficient for systems of interest. Note that for batch type process vessels, the effective discharge coefficient is rarely less than 0.5. However, for long tubular reactors, the effective relief discharge coefficient might well be less than 0.1.

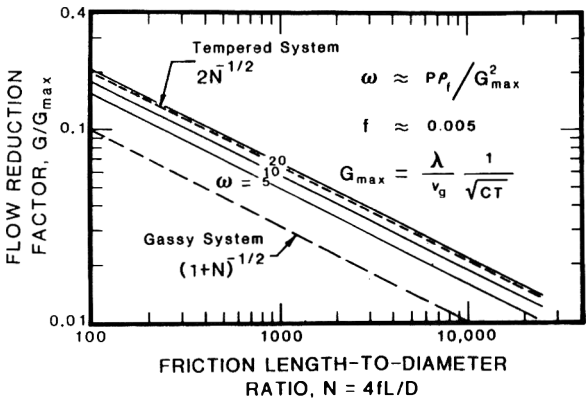

Fig. 2. Flow reduction factor for large friction length-to-diameter ratios representing subsonic discharge of saturated liquid flashing flow, and non-flashing gassy systems. Solid lines represent eq. (6) for flashing systems. Dashed lines represent approximations given by eqs. (9) and (10).

4. Adaptation of DIERS vent sizing relations to the problem of tubular reactors

The analysis presented here takes the approach that defining the maximum length of tubular reactor, which can be relieved by a vent area equal to the reactor flow area, is equivalent to the normal vent size evaluation for a batch reactor. We consider here both tempered as well as pure gassy systems.

It should be noted at the outset that in adapting analytic methods developed for batch reactors to tubular reactors, an implicit assumption of uniformity regarding temperature, concentration and/or extent of reaction within the tubular reactor that in most cases is far from reality. It is also true that, in most cases, the results of the proposed analysis will be more conservative due to real non-uniformities. For example, consider a flow cessation in a tubular reactor with a corresponding run-away reaction. The hottest zone which may be of considerably less extent than the total reactor will determine the system pressure and pressure relief activation. The expansion or relief of this zone will lead to pressure mitigation more quickly than if the total length of the tubular reactor were at uniform conditions. None-the-less, it is felt that the net conservative features of the proposed methods are justifiable in view of the essential absence of reported performance experience on emergency relief of tubular reactors.

4.1 Tempered systems

For tempered systems we cite the well established model of Leung [11], as the reference formulation. We choose to represent Leung's formulation in the following way:

$$A = \beta^* A_0 \tag{11}$$

where A is a required vent area and A_0 is a reference vent area based on reacting system characteristics and β^* is a dimensionless term which collects all parameters important to the allowance for pressure increase after relief activation as:

$$\beta^* = \left[\frac{T^{\bullet}_{set} + T^{\bullet}_{max}}{2T^{\bullet}_{set}}\right]\left[1 + \left(\frac{\rho_f C(T_{max} - T_{set})}{T_{set}(dP/dT)}\right)^{1/2}\right]^{-2}. \tag{12}$$

In eq. (12) the new terms are: T_{set} and T_{max}, which refer to the system temperature corresponding to the relief set pressure and to the maximum pressure to be allowed after relief activation, respectively; $T^{\bullet}_{set}$ and $T^{\bullet}_{max}$, which refer to the rate of temperature change (non-vented basis) at the same pressure conditions.

In eq. (11), the reference area A_0 is defined as

$$A_0 = \frac{M\rho_f (C/T_{set})^{3/2} T^{\bullet}_{set}}{F(dP/dT)^2} \tag{13}$$

where M is the tubular reactor inventory defined as

$$M = \rho_f L_R A_R \tag{14}$$

and A_R is the cross section area of the tubular reactors.

The flashing discharge mass flux of eq. (2b) has already been incorporated into eq. (13). Now, if one sets the vent area A in eq. (11) equal to the reactor area, A_R, then on combining (14), (13) and (11), one finds a relation for the maximum reactor length L_0 which can be vented by a single device which is given in dimensionless form as

$$\frac{L_0}{D_R} = \frac{F(dP/dT)^2}{\beta^* D_R \rho_f^2 (C/T_{set})^{3/2} T^{\bullet}_{set}}. \tag{15}$$

Equation (15) can be cast in more convenient form by considering the following additional details. First, recall F will be given by eq. (10) and N can be related to L_0 by the expanded form below.

$$F = \frac{2}{\sqrt{\Sigma K_i + 4f L_0/D_R}}. \tag{16}$$

The loss coefficients K_i may represent any relevant fitting factor. For example, one may encounter a 180° pipe bend which may be represented by 50 equivalent length-to-diameter ratios. On this basis the K factor for a 180° bend would be $4 \times 0.005 \times 50 = 1.0$.

A second detail applicable to eq. (15) is to note that most vapor pressure–temperature relations, including mixtures, can be represented over some suitable temperature range by a two-parameter Antoine equation of the form

$$P = \exp(a + b/T) \tag{17}$$

where T is the absolute temperature and a and b are the parameters that fit eq. (17) to specific data. The term exp(a) will have pressure units and the term b will have units, K.

With the above, the slope of the vapor pressure–temperature equation can be represented as

$$\frac{dP}{dT}=\frac{-bP}{T^2} \tag{18}$$

and with eqs. (16) and (18) we can represent (15) in the form

$$\frac{L_0}{D_R}=\frac{\dfrac{2}{\sqrt{\Sigma K_i+4fL_0/D_R}}\dfrac{P_{set}^2 b^2}{D_R T_{set}^4}\left(\dfrac{T_{set}}{C}\right)^{3/2}}{\beta^* \rho_f^2 T_{set}^{\bullet}}. \tag{19}$$

In the implementation of eq. (19) the important related terms of T_{set} and $T_{set}^{\bullet}$ will be obtained from empirical test data in the same manner as for batch reactor applications. Examples will be illustrated later in the paper.

If the actual reactor length L_R is less than the length L_0 defined in eq. (19), then a relief vent size less than the reactor cross section area would be adequate. The previous relations may be manipulated to show that to a first order the relative relief vent area is given by

$$\frac{A}{A_R}=\frac{L_R}{L_0}. \tag{20}$$

The above relation is conservative, and could be further refined by the consideration that the internal flow resistance factor should also be reduced by the ratio $(A/A_R)^2$ which leads to an iteration solution requirement.

4.2 Gassy systems

Gassy systems may be treated in a similar manner. The reference vent sizing approach using the DIERS methodology for gassy system in batch reactors is to balance the volumetric discharge rate Q_d, where

$$Q_d=\frac{FGA}{(1-\alpha)\rho_f} \tag{21}$$

with the volumetric gas generation rate, Q_g, given by

$$Q_g=\frac{M}{M_t}\frac{V_t}{P_m}P_{max}^{\bullet}, \tag{22}$$

The required vent area for a batch reactor is given by the combination of (21) and (22) as

$$A=\frac{(1-\alpha)\rho_f M V_t P_{max}^{\bullet}}{FGM_t P_m}, \tag{23}$$

The new terms introduced in the above relations are found in the Q_g term which contains information based on empirical test data (cf. [12]): M_t is the test sample mass, V_t is the free volume in the test equipment, $P^{\bullet}_{max}$ is the maximum pressure rise rate in the test volume V_t, and P_m is the maximum pressure allowed during relief activation.

We assume that the tubular reactor inventory $M = \rho A_R L_R$ and that G is given by eq. (5) for non-flashing flow. The discharge coefficient F is represented by eq. (9) in the modified form $F = (1 + \Sigma K_i + 4fL/D_R)^{-1/2}$. We further assume the initial void fraction $\alpha = 0$.

With the above one finds the maximum length for a single relief device of area A_R given by

$$\frac{L_0}{D_R} = \frac{M_t}{\rho_f^2 V_t P^{\bullet}_{max}} \frac{P_m}{D_R} \left(\frac{2\rho_f (P_m - P_{amb})}{1 + \Sigma K_i + 4f L_0/D_R} \right)^{1/2}. \tag{24}$$

In the same manner as pointed out for tempered systems, if the actual reactor length L_R is less than L_0, then the relative reduction in vent area is given to a first order by

$$\frac{A}{A_R} = \frac{L_R}{L_0}.$$

Other comments relative to required correction to the internal friction resistance as noted previously also apply here.

The maximum length for a single relief device for a gassy system, as defined by eq. (24), should be conservative relative to other possible evaluations for certain scenarios. For example, we note the possibility that a flow blockage with continued reaction for a gassy system can lead to early relief activation, and therefore allow time for venting the reactor inventory prior to reaching the maximum reaction rate assumed in eq. (24). However, completion of an empty time evaluation will typically require more test information than needed for eq. (24).

5. Illustrative examples

The following examples will illustrate use of the previous tubular reactor evaluation models.

5.1 Tempered system case

We will set up a basis for evaluation of a tempered system as if certain information were available from test data.

5.2 Maximum reaction temperature and phi-factor

It is assumed that an estimate of the heat of reaction can be obtained directly from appropriate calorimetry data in which the reaction temperature increase

is measured,

$$\delta = \frac{\phi M_w C \Delta T}{x} \tag{25}$$

where δ is the heat of reaction [J/mol]; ϕ is the test cell thermal inertia, where it is assumed that $\phi = 1.08$; M_w is the molecular weight of the reactant, where it is assumed that $M_w = 120$ g/mol; C is the liquid heat capacity, where it is assumed that $C = 2.1$ J/g °C; ΔT is the measured temperature rise, where it is assumed that $\Delta T = 310$ °C; and x is the reactant weight fraction, where it is assumed that $x = 0.5$.

With the above assumed values, one finds

$$\delta = \frac{1.08 \times 120 \times 2.1 \times 310}{0.5} = 169 \times 10^3 \text{ J/mol.}$$

However, with a known heat of reaction, inversion of eq. (25) allows one to estimate the expected reaction temperature rise for other conditions in which x, or ϕ, may be different from test values. For example, in the ideal limit of $\phi = 1.0$, eq. (25) would define the adiabatic reaction temperature increase.

The value of $\phi = 1.08$ is typical of a good reaction calorimeter. The working definition of the ϕ factor is

$$\phi = 1 + \frac{(MC)_{\text{test cell}}}{(MC)_{\text{test sample}}}. \tag{26}$$

A good approximation of eq. (26) for a steel wall vessel and an organic sample is

$$\phi \approx 1 + 10t/D$$

where t and D are the vessel wall thickness and diameter respectively. A typical value for a 1 inch schedule 40 pipe, tubular reactor ($t = 0.133$ inch, $D = 1.049$ inch) would be $\phi = 2.27$. With the previously estimated heat of reaction, $\delta = 169 \times 10^3$ J/mol and other property values previously assumed, eq. (25) inverted for reaction temperature rise for various cited values of the ϕ factor are:

ϕ	ΔT
1.0	335 °C
1.08	310 °C
2.27	148 °C

5.3 Reaction kinetics and P–T relation

The reaction self-heat rate would normally be obtained from calorimetry test data. However, to provide an illustrative example the following expression for

reaction self-heat rate is based on assumed kinetics rate constant parameters:

$$\frac{dT}{d\phi} = (T_m - T)u \exp[-w/(T+273.15)] \tag{27}$$

where $dT/d\phi$ is the reaction self-heat rate (°C/min); T_m is the maximum reaction temperature (°C); T is the instantaneous reaction temperature (°C); u is the pre-exponential rate constant parameter, here assumed to be $u = 7.266 \times 10^7$ min^{-1}; and w is the activation energy parameter, here assumed to be $w = 9148$ K.

The kinetics parameters, u and w, represent a hypothetical reaction having an onset temperature of ≈ 76 °C where the self-heat rate will approximately double with every 10 °C temperature increase. A hypothetical pressure temperature relation given by

$$P(\text{psia}) = 5.9 \times 10^5 \exp[-4167.5/(T+273.15)] \tag{28}$$

will have a normal boiling point temperature of 120 °C.

Figure 3 shows the self-heat rate ($dT/d\phi$) for three cases along with the pressure temperature relation. The three reaction cases correspond to ϕ factors of 1.0, 1.08 and 2.27 with the corresponding values of T_{max} relative to 76 °C as also indicated in Fig. 3.

Note the profound effect of the assumed ϕ factor for the 1 inch schedule 40 pipe ($\phi = 2.27$). In fact, Fig. 3 suggests that if the relief set pressure or reactor design pressure is greater than 150 psia, the reaction path defined by case 3 could perhaps be contained without pressure relief. Also note that the differences in self-heat rate between the adiabatic case, $\phi = 1.0$ and the hypothetical calorimeter case, $\phi = 1.08$, are small. With respect to case 3 in Fig. 3,

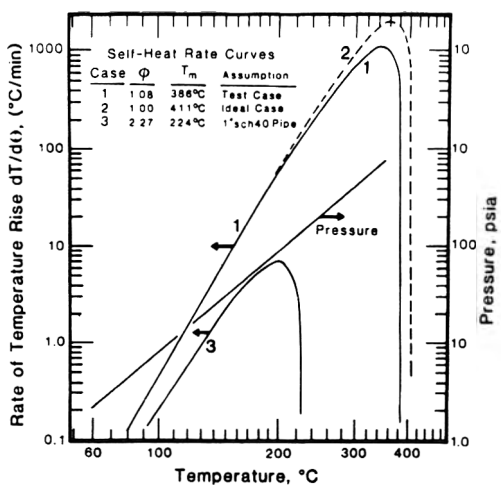

Fig. 3. Self-heat rate(s) and pressure–temperature relations for tempered system example problem.

any similarly large ϕ factor can often result in a significant reduction in pressure relief requirement. However, each case should be examined carefully since the effect of the heavy containment wall is always overstated in the static lumped heat capacity model considered here. The effect of the wall will also be less for flowing systems. However, the potential benefits may justify a more detailed thermal evaluation. These considerations having been noted, the calorimetry test case, $\phi = 1.08$ and $T_m = 386\,^\circ\mathrm{C}$, will be used for the example evaluation.

5.4 Evaluation case

Consider the following evaluation case: $P_{set} = 150$ psig or 164.7 psia ($1.136 \times 10^6\ \mathrm{N/m^2}$), $P_{max} = 197.6$ psia (20% overpressure) ($1.363 \times 10^6\ \mathrm{N/m^2}$), $T_{set} = 236\,^\circ\mathrm{C}$ (509 K), $T^{\bullet}_{set} = 171.6\,^\circ\mathrm{C/min}$ (2.86 °C/s), $T_{max} = 248\,^\circ\mathrm{C}$ (521 K), and $T^{\bullet}_{max} = 237\,^\circ\mathrm{C/min}$ (4 °C/s). In addition, we assume that $\rho_f = 900\ \mathrm{kg/m^3}$, $C = 2100\ \mathrm{J/kg}$, $D_R = 2.54 \times 10^{-2}$ m (1 inch) and $\Sigma K_i + 4f L_0/D_R = 0.025\, L_0/D_R$.

Using eqs. (15) through (19) and the above parameter list leads to

$$\left(\frac{L_0}{D_R}\right)^{3/2} = \frac{12.65 \times (1.136 \times 10^6)^2 (4167.5)^2 (509/2100)^{3/2}}{2.54 \times 10^{-2}\, 509^4 \beta^* 900^2\, 171.6/60}.$$

The term β^* must be evaluated using eq. (12). If one evaluates the term

$$\frac{dP}{dT} = \frac{bP}{T^2} = \frac{4167.5 \times 1.1356 \times 10^6}{509^2} = 18267\ \mathrm{N/m^2\,K}$$

then one finds, using the previous parameters,

$$\beta^* = \frac{(171.6 + 236.9)}{2 \times 171.6}\left[1 + \left(\frac{900 \times 2100 (247.7 - 236)}{509\, 18267}\right)^{1/2}\right]^{-2}$$

or

$$\beta^* = 0.184.$$

Therefore, completing the evaluation, one finds

$$\left(\frac{L_0}{D_R}\right)^{3/2} = 46429 \qquad \text{or} \qquad \frac{L_0}{D_R} = 1282.$$

For a 1 inch (2.54 cm) diameter reactor, $L \approx 32.5$ m.

5.5 Gassy systems

An example illustration of the use of eq. (24) for gassy systems can be presented on the basis of the following assumed property, test data, and case specific data:

Case specific: $P_m = 400$ psia or 27.6×10^5 Pa

$P_{amb} = 14.7$ psia or 1.0×10^5 Pa

$D_R = 1$ inch or 2.54×10^{-2} m

$\rho_f = 900\ \mathrm{kg/m^3}$

Test data: $M_t = 0.01\,\text{kg}$

$V_t = 0.4 \times 10^{-3}\,\text{m}^3$

$P^{\bullet}_{max} = 400\,\text{psi/min}$ or $6.67\,\text{psi/s}$

Assumption: $1 + \Sigma K_i + 4f\,L/D \approx 0.025\,L_0/D$

With the above, one can evaluate eq. (24) to find

$$\left(\frac{L_0}{D_R}\right)^{3/2} = \frac{0.01 \times 400 \times (2 \times 900 \times 26.6 \times 10^5)^{1/2}}{900^2 \times 0.4 \times 10^{-3} \times 6.67 \times 2.54 \times 10^{-2} \times 0.025^{1/2}} = 31890$$

or

$L_0/D_R = 999$ or $L_0 = 25.4\,\text{m}$.

6. Concluding remarks

We have shown how the conventional vent sizing relations for batch reactors, as often used in implementation of the DIERS methodology, can be adapted to long tubular reactors. In specific instances, a tubular reactor may have a significant thermal inertia effect which can further mitigate the severity of a run-away reaction. This should be evaluated carefully since there may also be cases where the thermal inertia effect is less significant. For long reactors, it is likely in most cases that a non-reclosable relief device will be preferred. One implication of the relatively large friction effect on the discharge flow rate may be the inability to satisfy the requirements of reclosable safety relief valves for minimum upstream pressure drop.

The evaluations presented here indicate a maximum length which can be protected by a single relief device without indicating an explicit preference for location. However, as a practical matter, preference should be given to a relief device location nearest the presumed location of the mixture that is farthest removed from completion of the run-away reaction scenario. This may be, in most cases, at the inlet of the reactor where feed reagents are introduced. In circumstances where the normal product represents a potentially unstable hazard, the exit location may be preferred.

Highly viscous systems may also generate special requirements. While the methods presented here are generally applicable, use of turbulent flow, constant friction factor is not recommended for laminar flow discharge.

Finally, the important aspects of the DIERS methodology requiring system characterization for run-away reaction scenarios through empirical test data are equally important for tubular reactor consideration.

References

1 H.G. Fisher, DIERS Research program on emergency relief systems, Chem. Eng. Prog., 81(8) (1985) 33–36.
2 H.G. Fisher, An overview of emergency relief system design practice, Plant/Operations Prog. 10(1) (1991) 1–12.
3 J.C. Leung and H.K. Fauske, Runaway system characterization and vent sizing based on DIERS methodology, Plant/Operations Prog., 6(2) (1987) 77–83.
4 J.C. Leung, H.K. Fauske and H.K. Fisher, Thermal runaway reactions in a low thermal inertia apparatus, Thermochimica Acta, 104 (1986) 13–19.
5 J.E. Huff, Frontiers in pressure-relief system design, Chem. Eng. Prog., 84(9) (1984) 44–51.
6 M.A. Grolmes, J.C. Leung and H.K. Fauske, Transient two-phase discharge of flashing liquid following a break in a long transmission pipe line, In: T.N. Veziraĝlu and A.E. Bergles (Eds.), Multi-Phase Flow and Heat Transfer III. Part A Fundamentals, Proc. 3rd Multi-Phase Flow and Heat Transfer Symp. Workshop, Miami Beach, FL, April 18–20, 1983, Elsevier, Amsterdam, 1984, pp. 567–574.
7 M.A. Grolmes and H.K. Fauske, Vapor cloud formation and dispersion following break in very long transmission pipeline, Paper presented at AIChE Spring National Meeting, April 2–6, 1989, Houston, TX.
8 J.C. Leung and M.A. Grolmes, The discharge of two-phase flashing flow in a horizontal duct, AIChE J., 33(3) (1987) 524–527, also errata, 34(6) (1988) 1030.
9 H.K. Fauske, Emergency relief system (ERS) design, Chem. Eng. Prog., 81(8) (1985) 53–56.
10 J.C. Leung and M. Epstein, A Generalized Correlation for Two Phase Non-Flashing Choked Flow, ASME J. Heat Transfer, 112 (1990) 528–530.
11 J.C. Leung, Simplified vent sizing equations for emergency relief requirements in reactors and storage vessels, AIChE J., 32(10) (1986) 1743–1745.
12 M.A. Grolmes, J.C. Leung and H.K. Fauske, Reactive systems vent sizing evaluation, In: Proc. Int. Symp. on Runaway Reactions, Cambridge, MA, March 7–9, 1989, AIChE Publication ISBN 0-8169-0460-X, New York, 1989.

Journal of Hazardous Materials, 33 (1993) 275–293
Elsevier Science Publishers B.V., Amsterdam

Dispersion and deposition of smoke plumes generated in massive fires

Ahmed F. Ghoniem[a], Xiaoming Zhang[a], Omar Knio[a], Howard R. Baum[b] and Renald G. Rehm[b]

[a]*Massachusetts Institute of Technology, Cambridge, MA 02139 (USA)*
[b]*National Institute of Standards and Technology, Gaithersburg, MD 20899 (USA)*

Abstract

Massive fires resulting from the uncontrolled burning of crude oil from spills or industrial accidents produce large smoke-laden buoyant plumes which rise in the wind direction before they equilibrate within a stably stratified atmosphere. Beyond this point, the plume material cools by entrainment and the plume becomes negatively buoyant due to the heavy smoke loading. The trajectory of the descending plume, which determines the ground distribution of smoke, is the subject of this paper. A computational model for the simulation of large-scale smoke plumes resulting from such fires is developed and applied to investigate the effects of the plume initial properties on its trajectory and smoke deposition patterns. Attention is focused on the descent and dispersion of wind-driven plumes in a homogeneous atmosphere, and the smoke deposition on flat terrain. Results show that the plume dynamics in the cross-wind direction are dominated by two buoyantly generated, coherent, streamwise vortices which distort the plume cross section into a kidney-shaped structure. The strength of the two vortices and their separation increase as the plume falls. The plume width grows under the action of these vortices at a rate which increases as the plume settles on the ground, leading to a smoke footprint which does not resemble the prediction of Gaussian dispersion models. The effects of the injection altitude and the initial shape of the plume cross section on the transport and dispersion of the negatively buoyant smoke plume are investigated. Plumes falling from higher elevations disperse more in the vertical direction while those falling from lower elevations disperse further in the horizontal cross-wind direction. Plumes with circular cross-sections reach the ground faster and disperse horizontally further than plumes with elliptical cross-sections with the minor axes in the vertical direction. Vertical plume dispersion is weakly dependent on the shape of its initial cross-section.

1. Introduction

Wind-driven buoyant plumes are responsible for the long-range dispersion of smoke and chemicals emitted from massive fires resulting from oil spills, uncontrolled oil-well fires, and large-scale industrial accidents [1–4]. The

Correspondence to: Ahmed F. Ghoniem, Massachusetts Institute of Technology, 77 Massachusetts Avenue, Room 3-342, Cambridge, MA 02139 (USA). Phone: (617)253-2295, Fax: (617)253-5981, Email address: ghoniem@eddy.mit.edu.

0304-3894/93/$06.00

environmental impact of the fire, which becomes a factor in whether the fire should be fought or left to burn, is determined by the plume trajectory. While the horizontal motion of the plume is governed by the prevailing wind, its vertical motion is determined by buoyancy and is a function of the initial density distribution within the plume cross-section and atmospheric stratification. Typically, the density of the plume* is determined by the temperature and the smoke concentration of the fire plume. Both vary during the plume rise due to entrainment and mixing with the surrounding air. At a certain height, the plume becomes buoyantly stable [5–7] and as it cools further, it starts to fall due to the smoke concentration. Plumes generated by oil fires are of particular interest due to their high smoke loading (10–15 percent of the original fuel burned). The large smoke particulate matter increases the environmental hazard and complicates the analysis, since the smoke cannot be treated as a passive convected scalar. The purpose of this work is to develop a computational model to simulate the buoyant plume dynamics.

Currently available plume models can be divided into two categories [8–12], scale, or integral models; and numerical, or field models. In the former category, dimensional arguments and/or integral conservation expressions are used to derive relations among characteristic, global parameters, such as the maximum plume rise, as a function of the source and ambient conditions. These relationships contain constants, e.g. entrainment rates, which are determined using scaled experiments. In most cases, the plume concentration distribution is assumed to be Gaussian in the plane normal to the plume axis [6, 10]. This simplification limits the applicability of integral models since, as shown below, the underlying assumptions may not hold in many relevant cases. On the other hand, numerical models offer the possibility of more detailed and accurate predictions of the plume dynamics. Typically, these models rely on the numerical integration of the averaged conservation equations, supplemented with turbulence-closure schemes, to describe the field in detail. The application of these models has been limited by the uncertainty associated with the validity of turbulence models in buoyant flows, and the high computational expense associated with using fixed-grid integration schemes.

In this work, a comprehensive numerical model of smoke dispersion and deposition is developed as an effective alternative to both approaches. The model does not rely on experimentally-fitted constants or closure models, and is endowed with efficiency by relying on grid-free, Lagrangian numerical methods to integrate the equations of motion. In this formulation, Lagrangian elements are naturally convected and redistributed in regions of high strain, thereby adapting to severe and rapid changes in the plume structure [13–17]. Far-field and normal boundary conditions are easily applied by using the appropriate form of the Greens function used to represent the velocity induced

* The plume is defined as the mixture of fine combustion products, including smoke particulates, and air entrained and mixed with these products during plume rise.

by a given Lagrangian element. The capability of the model is illustrated by computing the dispersion of a wind-transported dense plume in a uniform atmosphere and its deposition on a flat terrain.

The quantity that is of direct environmental impact is the downwind "footprint" of the smoke plume as a function of fire strength, smoke loading, and wind pattern. This quantity is directly related to the trajectory of the descending plume, a problem which has so far received less attention than rising thermal plumes. Attention is therefore focused on negatively buoyant, descending smoke plumes and their interaction with a flat ground. Much, although not all, of the information required to assess the environmental hazard of the smoke generated from large fires can be obtained from this analysis of the descending smoke plume. We consider cases in which the plume self-induced turbulence far exceed atmospheric turbulence and show that the former plays an important role in determining the plume trajectory and the distribution of smoke within its cross section. We also show that this distribution differs greatly from the conventionally assumed Gaussian due to the formation of strong streamwise vorticity.

The paper is organized as follows. In Section 2, we describe the formulation of the model including the major assumptions used and the non-dimensionalization procedure. The numerical scheme is briefly summarized in Section 3. Detail of the latter can be found in the open literature. In Section 4, results pertaining to the shape of the plume, its trajectory and the smoke distribution are shown and analyzed. The effects of the initial height and shape of the plume are also discussed. Finally, conclusions are presented in Section 5.

2. Formulation of the problem

We consider the evolution of an isothermal smoke plume initially at the thermally stabilized height HT. The plume is characterized by the (excess) particulate mass flux

$$\dot{m}_p = \int \rho_p^* U \, dA,$$

the integration is over the plume cross-wind section, where ρ_p^* is the density of the particulate phase, with the total density $\rho^* = \rho_0^* + \rho_p^*$, and ρ_0^* is the ambient density. The initial plume cross section is taken to be an elliptical cross section of semi-major (horizontal) axis R_y and semi-minor (vertical) axis R_z. The major direction of motion is the horizontal x-direction, with a uniform ambient wind velocity U. The geometry is illustrated in Fig. 1. The specification of initial altitude and shape of the plume cross section is obtained from a plume rise analysis which will be described elsewhere.

The present analysis is based on the following assumptions:

(i) the large-scale plume motion of interest here can be regarded as steady;
(ii) molecular diffusion of mass and momentum are negligible compared with vorticity-induced entrainment;

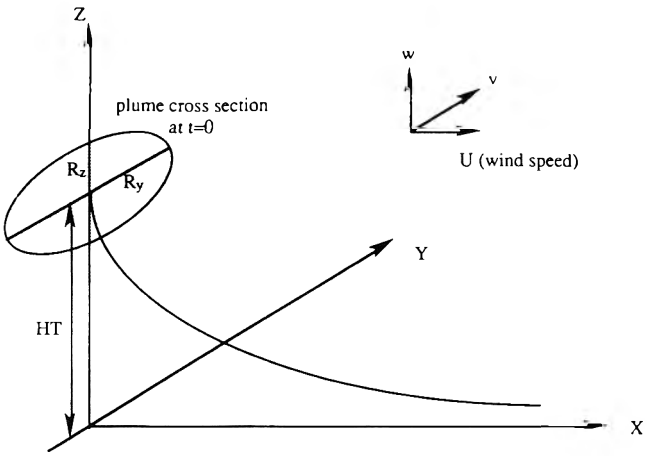

Fig. 1. A schematic representation of the initial plume cross-section and height, its trajectory in the ind direction, the coordinate system and the velocity components.

(iii) the ambient-wind speed U is uniform and much larger than plume-induced velocity components (u, v, w) in the (x, y, z) coordinate directions;
(iv) the smoke particulate can be treated as a continuum fluid;
(v) the stratification and turbulence in the atmosphere can be neglected.

The first four assumptions are quite reasonable and widely adopted in most plume modeling. The last assumption is used as a first-order model for atmospheric conditions. It will be systematically relaxed in future work.

Given the above assumptions, the plume evolution can be described in a transverse (y^*, z^*) plane perpendicular to the ambient wind direction. We introduce dimensionless transverse coordinates, (y, z), and streamwise coordinate, t, as follows:

$$(y, z) = (y^*, z^*)/R_z$$

$$t = \frac{x^*/U}{R_z/V} = \frac{x^*}{U}\sqrt{\frac{\varepsilon g}{R_z}} \tag{1}$$

where $V = \sqrt{\varepsilon R_z g}$, $\varepsilon = \dot{m}_p/\rho_0^* U R_z^2 \ll 1$, and g is the acceleration of gravity. The dependent variables are the transverse velocity components, (v^*, w^*), the perturbation pressure relative to its ambient hydrostatic value, p^*, and the particulate density ρ_p^*. They are made dimensionless as follows:

$$(v, w) = (v^*, w^*)/V$$

$$p = \frac{UR_z}{\dot{m}_p g} p^* \tag{2}$$

$$\rho = \frac{UR_z^2}{\dot{m}_p}\rho_p^* = \frac{\rho_p^*}{\varepsilon\rho_0^*}$$

The conservation of mass, particulates and momentum in the transverse plane then take the form:

$$\frac{\partial v}{\partial y}+\frac{\partial w}{\partial z}=0$$

$$\frac{\partial \rho}{\partial t}+v\frac{\partial \rho}{\partial y}+w\frac{\partial \rho}{\partial z}=0$$

$$(1+\varepsilon\rho)\left(\frac{\partial v}{\partial t}+v\frac{\partial v}{\partial y}+w\frac{\partial v}{\partial z}\right)+\frac{\partial p}{\partial y}=0 \tag{3}$$

$$(1+\varepsilon\rho)\left(\frac{\partial w}{\partial t}+v\frac{\partial w}{\partial y}+w\frac{\partial w}{\partial z}\right)+\rho+\frac{\partial p}{\partial z}=0$$

The quantity ε is a measure of the particulate-to-ambient-air density ratio, proportional to ρ_p^*/ρ_0^*, if ρ_p^* is uniformly distributed over the plume cross-section. This ratio is quite small, typically O(0.01), making the Boussinesq approximation valid in most practical cases. Invoking this approximation, the problem then contains only two non-dimensional parameters, the plume initial stabilization height HT/R_z, and the initial plume aspect ratio $AR=R_y/R_z$. Initially, the particulate density profile within the ellipse must be specified, together with the transverse components of the induced velocity field. In what follows, the initial smoke density is assumed constant, and the transverse velocity components are zero. The velocity components must vanish as $(y, z) \to \infty$, and the normal component of the velocity $w=0$ at the ground $z=0$. For later use in connection with the vortex method, we note that eq. (3) leads to the following evolution equations for the streamwise component of vorticity ω.

$$\frac{\partial \omega}{\partial t}+v\frac{\partial \omega}{\partial y}+w\frac{\partial \omega}{\partial z}+\frac{1}{(1+\varepsilon\rho)^2}\frac{\partial \rho}{\partial y}-\frac{\varepsilon}{(1+\varepsilon\rho)^2}\left[\frac{\partial \rho}{\partial y}\frac{\partial p}{\partial z}-\frac{\partial \rho}{\partial z}\frac{\partial p}{\partial y}\right]=0 \tag{4}$$

where the vorticity is defined as follows:

$$\omega=\frac{\partial w}{\partial y}-\frac{\partial v}{\partial z}$$

The non-Boussinesq terms in the equation are retained mainly for use in future work directed at the near-source plume-rise problem. They play no role in the present problem. Using the vorticity transport equation, the mathematical formulation of the problem is completed by invoking the pressure gradient from the momentum equations,

$$\frac{\partial p}{\partial y}=-(1+\varepsilon\rho)\frac{\mathrm{d}v}{\mathrm{d}t},$$

and,

$$\frac{\partial p}{\partial z}=-\rho-(1+\varepsilon\rho)\frac{\mathrm{d}w}{\mathrm{d}t} \tag{5}$$

and satisfying the conservation of species and incompressibility condition, respectively:

$$\frac{d\rho}{dt} = 0$$

and

$$\frac{\partial v}{\partial y} + \frac{\partial w}{\partial z} = 0 \tag{6}$$

3. Numerical scheme

The vortex element method is used to integrate the vorticity transport equation, eq. (4). The method is based on the discretization of the support of vorticity into vortex elements, and the transport of these elements along particle trajectories. The vorticity of an element is radially distributed in a small neighborhood of its center according to Gaussian core function with a characteristic radius, δ. The velocity field is computed by discrete convolution over the fields of the vortex elements using the desingularized Biot–Savart law. Details of the method, as applied to the plume problem, are described in Refs. [14] and [17]. Vorticity source terms appearing in eq. (4) are evaluated using the transport element method. Similar to the vortex method, the latter relies on the discretization of the density gradient into a finite number of Lagrangian transport elements which move with the local velocity. The density gradient changes with the stretching and tilting of material lines, while the density is obtained by direct summation over the field of transport elements. Details of this method, which has also been applied in combustion problems [15, 16], are given in Ref. [14].

Normal boundary conditions at the ground, $z = 0$, are satisfied by accounting for the image system of the vortex/transport elements. We discretize the zone of finite density gradient between the plume and the surrounding using two layers of elements. Both the vortex and transport element methods invoke a redistribution scheme which introduces new elements, as necessary, to maintain the spatial resolution of the computations. This results in an efficient and adaptive solution scheme which captures severe and rapid distortions of the flow map while concentrating the computational effort in zones of finite vorticity and density gradient. The accuracy of this scheme and of the associated plume predictions have been extensively investigated [14, 17].

4. Results

The global structure of descending plumes and of their vorticity field are discussed first for a plume with $HT/R_z = 5$, $AR = 3$ *and* $\rho = 0.106$. The results are

illustrated by plotting, in Figs. 2 and 3, respectively. three-dimensional surfaces of constant smoke concentration and streamwise vorticity. Both figures were obtained by assembling the instantaneous, or local constant smoke density or vorticity contours into a three-dimensional plot, using the computational t-coordinate as a physical x-coordinate. Note that some inevitable numerical diffusion creeps into the plotting procedure, which employs interpolation formulae to find the functional values of smoke concentration and vorticity at the corner of a uniform mesh, that leads to the break-off of some of the plume material into separate blobs. These three-dimensional plots are meant to delineate what a laboratory experiment of a descending plume would show. The results indicate that the initial elliptical plume cross-section is rapidly reshaped into a kidney shaped object and that close to the ground, the smoke distribution is far from the commonly assumed Gaussian.

From extensive computations, and as shown in Figs. 2–4, we find that the large-scale features of the dispersion and deposition of dense plumes can be described in terms of four distinct stages which separate the initial fall and the onset of smoke settlement on the ground. The dynamical processes which distinguish each of these stages are interpreted in terms of the correspondence between the plume structure and the vorticity field, as summarized below. The purpose of devising this way of describing the numerical results is to facilitate

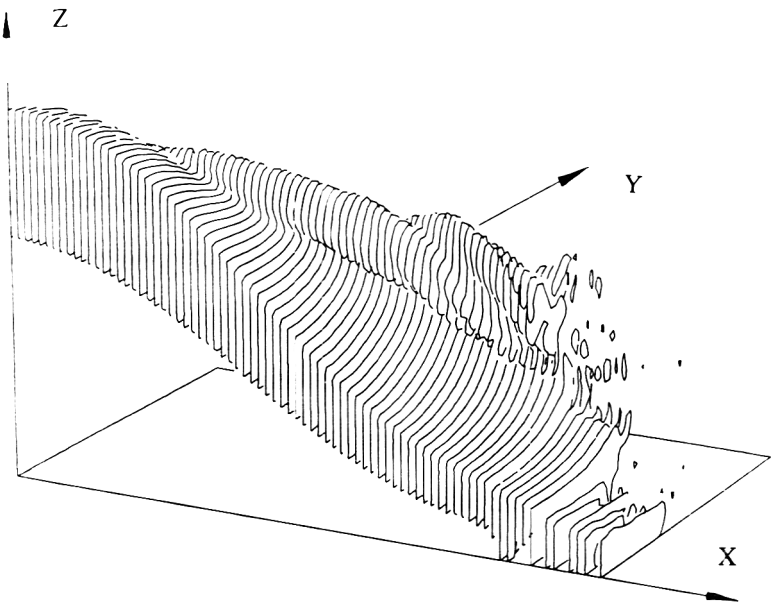

Fig. 2. A three-dimensional perspective plot depicting a surface of constant smoke concentration. $\rho=0.03$. generated for a case with $HT=5R_z$. $R_y=3R_z$, and $\rho=0.106$. Due to symmetry with respect to the x z plane. contours lying in the $y<0$ region have not been reproduced. The location of the observer is the same as that in Fig. 1.

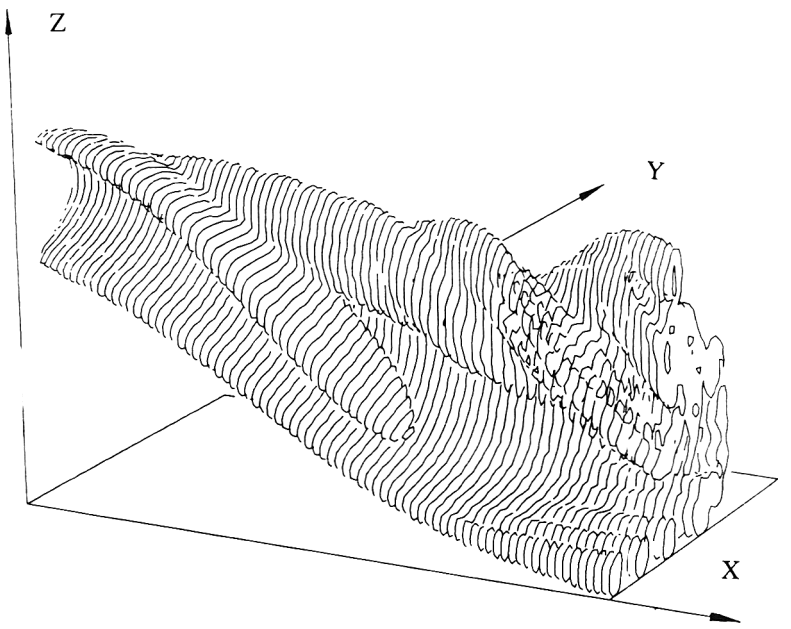

Fig. 3. A three-dimensional perspective plot of streamwise vorticity, $\omega = 0.2$, for the same plume shown in Fig. 2.

their use in formulating future integral models of plume motion. The plume descent starts with an initial acceleration stage, during which the deformation of the plume cross-section is very small and vorticity is generated along the plume air interface. During the second stage, the streamwise vorticity on each side of the plume centerline intensifies and rolls into a large-scale eddy thus generating a counter-rotating vortex structure ($x = 6$–12, in Fig. 4). The induced motion of this vortex pair deforms the plume's smoke distribution into a kidney-shaped cross-section. The structure of the plume at large elevation is in qualitative agreement with the experimental measurements of Hewett et al. [5] who observed a similar kidney-shaped cross-sections downwind the plume source.

With further intensification of the streamwise vorticity under the action of baroclinic torques, small-scale roll-up occurs ($x = 18$–24, in Fig. 4). This third stage is characterized by the generation of streamwise vorticity of opposite signs on both sides of the symmetry plane, and by the increasing complexity of the smoke distribution. Vorticity generation and roll-up transforms some of the plume's potential energy into kinetic energy which is distributed between the plume and its surrounding. The rotational velocity field induced by the vorticity of the plume sets up an entrainment field towards the plume cross-section. Most entrained fluid is engulfed by the large-scale eddy roll-up, while the secondary small eddies induce smaller entrainment currents. The continuous roll-up of the vorticity layer forming on the boundary of the plume cross-section,

which is responsible for maintaining the entrainment towards the plume center, is due to the familiar Kelvin–Helmholtz instability of vorticity layers.

As the smoke approaches the ground, a fourth, ground-settlement stage is observed ($x=24$–30, in Fig. 4). The dynamics of the flow in this stage is increasingly influenced by the proximity to the ground. The associated deceleration field leads to fast and tight widening of the plume structure and its cross-wind straining into two large blobs of smoke connected by a thin crescent. This mechanism is similar to the straining of thermals colliding with walls placed perpendicular to their direction of motion, observed and clearly recorded in laboratory experiments [18, 19]. (Note that mathematically, the behaviour of the plume cross-section in the wind direction is exactly the same as that of a thermal in time.) These experiments show the formation of similar large-scale features and their subsequent separation into two lumps of the thermal fluid as they collide with the wall. The further away from the wall/ground the release point of the thermal/plume is, the more concentrated its material becomes in the two large structures. The early formation of the large-scale features is also depicted by the numerical results of Meng and Thomson [20], who computed the motion of thermals.

One of the important implications of this side roll-up process is the resulting smoke deposition patterns. Clearly, the smoke distribution along the cross section close to the ground is not uniform and may not necessarily possess a maximum at the center $y=0$. This is contrary to classical plume dispersion models which assume that the smoke distribution is Gaussian both in y- and z-directions, and that the smoke ground imprint follows Gaussian function centered at the x-axis of the plume. We note that this departure from a Gaussian distribution is solely due to the plume self-generated vorticity, or turbulence which render the dynamics field surrounding the plume cross-section highly non-uniform.

4.1 The entrainment field

Since most plume models rely on certain assumptions regarding the entrainment field and estimates of the entrainment velocity established by the plume, we examine here, using the numerical simulation results, the form and strength of this field. Besides the formulation of plume models, the entrainment field is used in other applications where the "fire-induced wind" may be important in determining the impact of the fire events on the local environment. Figure 4 shows a superposition of the plume cross-sections and the velocity field in its surrounding for the case shown in Fig. 2. The velocity vectors in the plane of the plume cross-section are displayed as short lines starting from a set of equally distributed mesh points. As indicated above, the roll-up of the vorticity generated along the boundary between the plume material and the surrounding establishes two strong coherent vortices at the far ends of the horizontally expanding plume cross-section. The figure indicates that the field of the large eddy resembles that of a Rankine vortex in which the maximum velocity is reached close to but not at the center of the

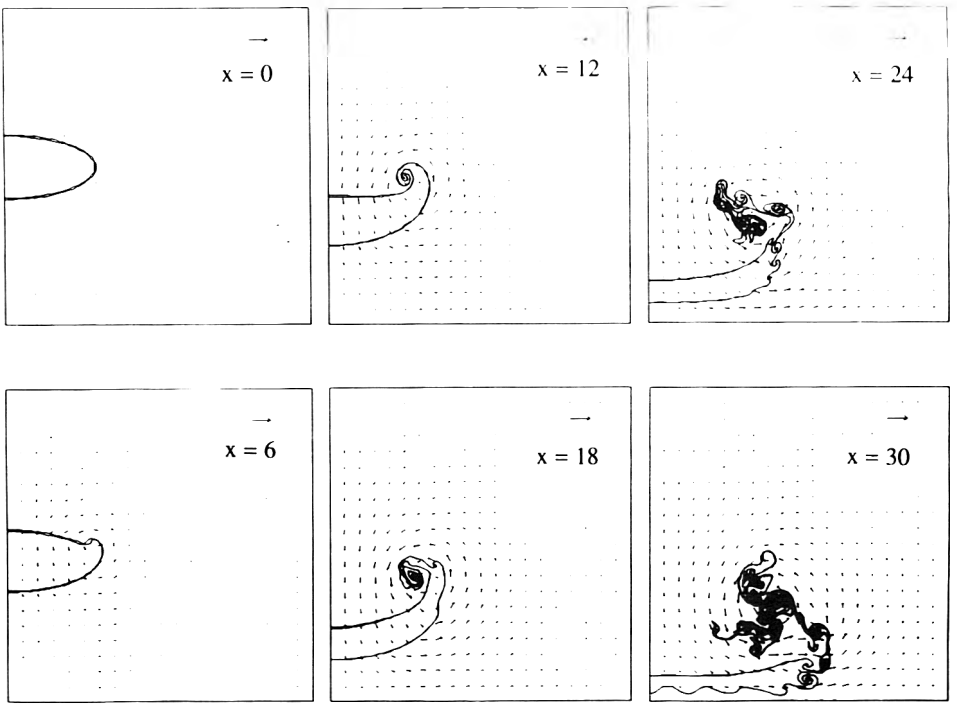

Fig. 4. A superposition of the boundary between the plume and the surrounding, and the velocity induced by the plume motion. The characteristic velocity of the gravity induced flow is shown by the horizontal arrow on the top right-hand corner. The velocity field is shown by a vector whose length is proportional to the velocity, starting from the point where the velocity is computed.

eddy. The maximum entrainment velocity, which as shown in the figure is of the order of magnitude of V, occurs close to the center of the large eddy and stays around the same value for the majority of the plume's journey.

Two interesting observations can be made using these results: The centers of the large eddies stay farther away from the ground than the rest of the plume cross section even as part of the plume material settles on the ground. This means that the turbulent field produced by the plume is not likely to be dissipated quickly as the plume approaches the ground and, at least for some time following the settlement, some circular wind motion will be felt close to the area of plume touch-down. The second observation concerns the waves developing on the lower side of the plume as it touches the ground. The evolution of these waves lead to the formation of small scale eddies which induce their own wind close to the ground, augmenting that induced by the primary large eddies.

4.2 Mechanism of vorticity generation

Detailed flow computations reveal that most of the vorticity generation occurs close to the interface between the plume and the air where density

gradients are high. A short distance away from this interface, the density is uniform, vorticity is zero and the motion is essentially irrotational. A schematic interpretation of the generation and behavior of the streamwise vortices is shown in Fig. 5, where we have invoked the Boussinesq approximation. With $\varepsilon = 0$, the vorticity generation term in the transport equation is proportional to the horizontal density gradient. For a plume with an elliptical initial cross-section, vorticity of opposite signs form on the sides of the plume centerline due to the opposite horizontal density gradients, Fig. 5a, with its maximum absolute value at the far ends. This vorticity layer rolls up to form two large-scale counter-rotating streamwise vortices, so that two additional areas with opposite horizontal density gradients are established on both sides of the plume-air interface, Fig. 5b. Thus, at later stages, vorticity with opposite signs forms on either side of the symmetry plane. The evolution of the vorticity field indicates that a simplified overall plume model which describes the interaction of the plume with its surrounding and its settlement on the ground can be constructed by assuming that the plume dynamics are driven by a kidney-shaped vortex with a time-dependent circulation and width. Values of circulation and distance between the two vortices will be given later.

Extensive numerical experiments have been conducted to investigate the dependence of the results on the initial conditions and plume configurations, the only two parameters left in the problem specification. The dynamics of falling plumes and details of the expected smoke-deposition process are further examined in the following sections. In particular, the effects of initial plume height and shape are discussed in detail. The dependence of the plume width on these two parameters is of special interest since it determines the area contaminated by the plume material. The strength of the plume induced vortex pair is also important since it governs the motion induced by the plume.

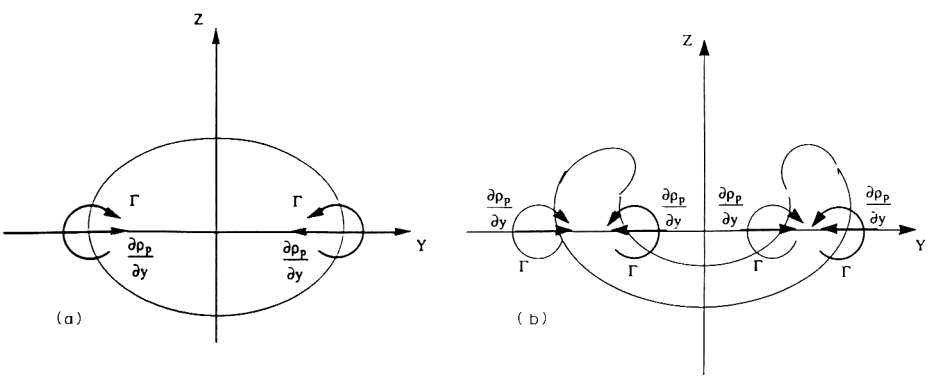

Fig. 5. Schematic illustrations showing (a) the mechanism of baroclinic vorticity generation, and (b) the roll-up of the streamwise vortices and the resulting deformation of the plume cross-section.

4.3 Effect of the initial plume height

Results depicting the plume cross-sections along its trajectory, shown in Fig. 6 for $HT/R_z = 3$ and 30, keeping all other parameters the same, suggest that plumes released from a height close to the ground produce a ground smoke distribution with higher concentration on the sides than at the center. We also find that higher initial elevations lead to more uniform ground-smoke distribution. Moreover, the vertical dispersion is larger for plumes released from higher elevations, while the opposite is true for horizontal plume dispersion. These assertions are illustrated in Figs. 7 and 8 which, respectively, show the

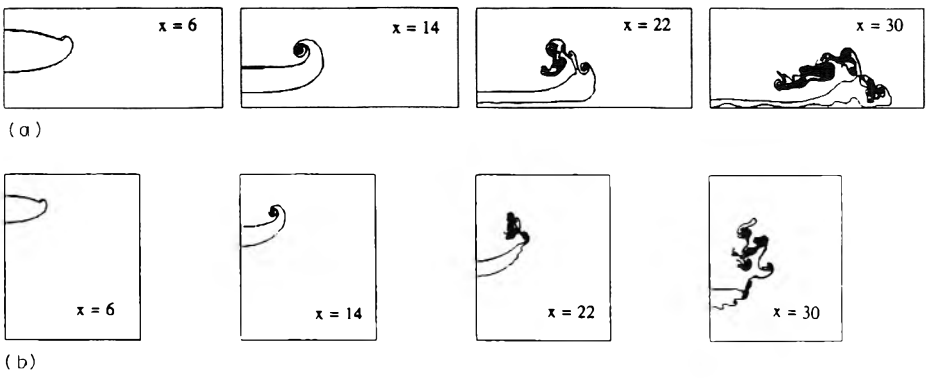

Fig. 6. The plume cross-section at different downwind stations for the case with: (a) $HT/R_z = 3$, and (b) $HT/R_z = 30$. Both cases start with same cross-section and same smoke distribution.

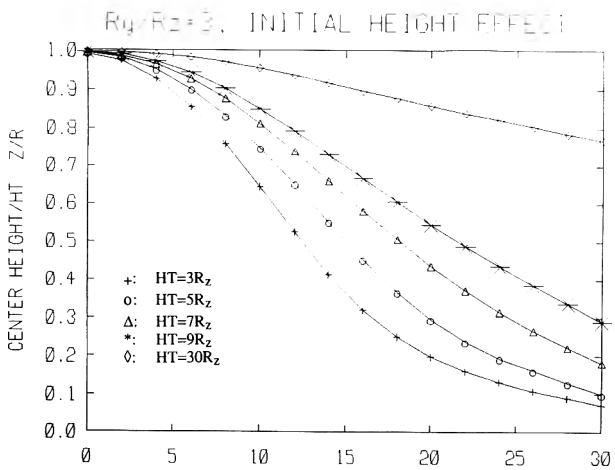

Fig. 7. Streamwise evolution of the height of smoke plumes with $R_y = 3R_z$, and $\rho = 0.106$. Curves are generated for initial heights $HT = 3R_z(+)$, $5R_z$ (○), $7R_z$ (Δ), $9R_z$ (*), and $30R_z$ (◇).

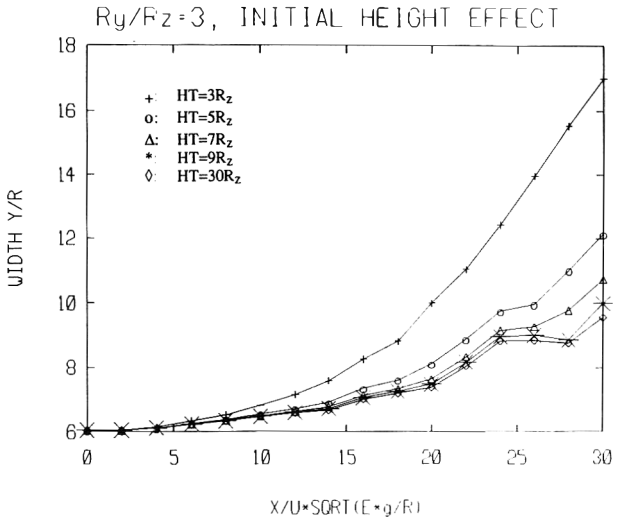

Fig. 8. Streamwise evolution of the width of the smoke plume in Fig. 7. Symbols as in Fig. 7.

trajectories of descending plumes with initial heights in the range $3R_z \leqslant HT \leqslant 30R_z$ and the corresponding horizontal dispersion, defined as the horizontal spread of the plume cross-section.

The plume descent occurs such that most of the horizontal dispersion develops at later stages, when the plume motion is strongly affected by the presence of the ground. When the plume falls from high altitude, its width exhibits an oscillatory behavior. This is due to the intermittent roll-up of large eddies which entrain plume fluid towards their centers as they propagate in the cross-wind direction away from the symmetry plane.

The motion of these large eddies and the generation of smaller scale vortices generate entrainment currents which accompany the horizontal and vertical plume dispersion. The evolution of these currents is measured in terms of the total peripheral length of the interface separating the plume from ambient air at a given cross-section. During the initial acceleration stage, there is little entrainment as the plume suffers a mild deformation. The entrainment rate is higher following large-eddy roll-up which causes the engulfment of a large amount of ambient fluid, and increases further during the later stages when small-scale vortices, generated along the plume surface, induce local entrainment fluxes.

The plume deformation was also correlated with the large-scale features of the baroclinic generation of streamwise vorticity. The latter are determined by the total positive circulation, total negative circulation, and the sum of the two, all computed on one side of the symmetry plane ($y > 0$). While the positive circulation, which constitutes most of the vorticity in this region, grows steadily during the early stages, the negative vorticity increases only after large scale roll-up has occurred. Thus, during the first and second stages,

the vorticity field can be modeled as a pair of counter-rotating vortices whose strength increases under the action of the gravitational field. However, at later stages, the single large eddy on each side of the plume should be replaced by a counter-rotating vortex pair, in order to model the generation of both signs of vorticity, and the associated small-scale roll-up and enhanced entrainment rates.

4.4 Effect of initial plume shape

The effect of the initial plume shape on the descent and dispersion processes is now examined. We simulated the motion of plumes with the same cross-sectional area but with different aspect ratios, $AR=1$, 3, 6. In all cases, the initial height $HT=5R$, R being the square root of the initial plume cross-sectional area. Figure 9 shows a comparison between the shape of the plume cross-sections at three cross-sections for $AR=1$ and 6. Figures 10 and 11 show the heights and widths for all three cases, plotted against the downwind coordinate, t, which is defined as the normalized distance travelled from the initial source location.

Examination of these results indicates that different initial cross-sections produce different plume trajectories. This dependency is explained by noting that the rate of vorticity generation, which governs the strength and shape of the large-scale vortices, is strongly dependent on the curvature of the plume boundary. Plumes with small AR, i.e. rounded cross-sections, get more distorted, reach the ground earlier, and disperse horizontally faster than plumes with flatter cross-sections. However, in all cases, the plume tends to break-up into two parts symmetrical about $y=0$. For $AR=1$, this observation is confirmed by experimental results [18, 19]. Moreover, the shape of the initial plume cross-section appears to have a weak effect on the rate of vertical dispersion.

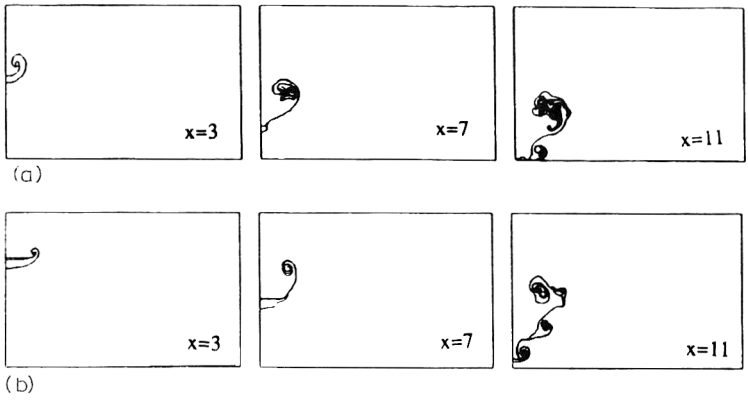

Fig. 9. The plume cross-section at different downwind stations for plumes with: (a) $AR = 1$ and (b) $AR = 6$. Both cases have the same initial height and smoke density distribution within the plume cross-section.

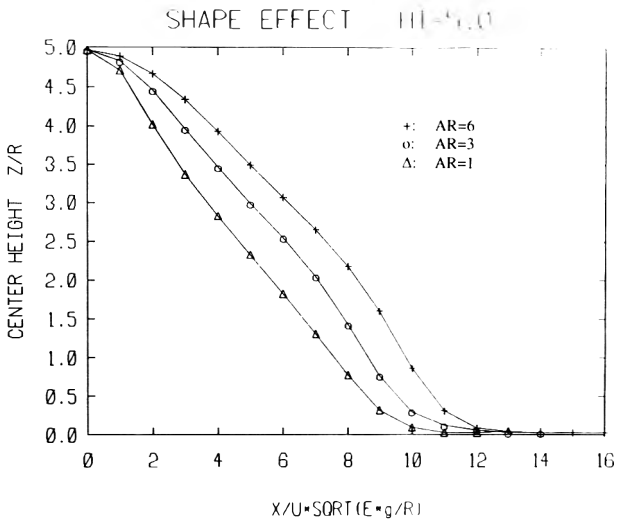

Fig. 10. The streamwise evolution of the height of smoke plumes with $\rho = 1$, $HT = 5R$ and same initial cross-sectional area. Curves are generated for aspect ratios of initial plume sections of $AR = 6$ (+), 3 (○), and 1 (Δ).

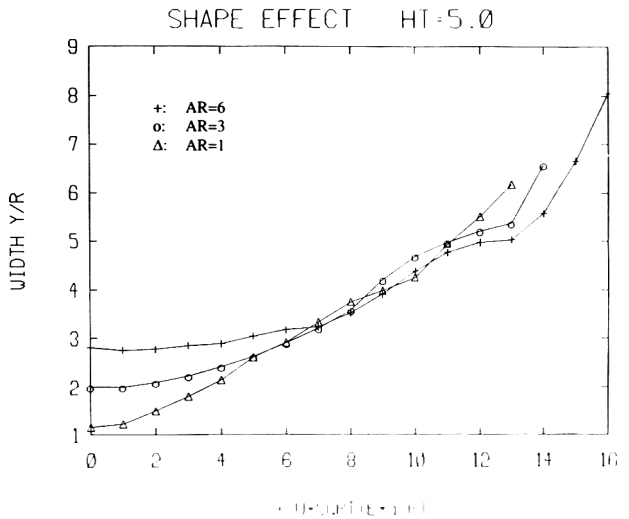

Fig. 11. Streamwise evolution of the width of the plumes in Fig. 10. Symbols as in Fig. 10.

4.5 *Global structure parameters*

Results presented here, which are supported by other results reported in the literature, show that the motion of the plume, when atmospheric turbulence is weak, is strongly governed by two large streamwise eddies which form due to the roll-up of the vorticity generated along the plume interface. This vortex pair is responsible for the conversion of some of the plume potential energy

into kinetic energy, especially in the plane of its cross section. As we have seen, this kinetic energy is shared by the plume material and the surroundings, and is the source of the strong flow established by the plume motion and the associated entrainment. Thus, it is of interest to characterize this vortex pair by the smallest number of parameters and to study the dependence of these parameters on the initial plume conditions. These characteristic plume parameters could then be used in future plume studies.

A vortex pair can be described by the distance between the centers of the two vortices and the strength of each vortex. The first quantity is proportional to the plume width shown in Figs. 8 and 11. Figure 12 shows the total circulation of each of the vortices for the two cases shown in Figs. 6 and 9, i.e. for different initial plume height and cross section. As expected, vorticity generation, and thus enhancement of the eddies, is fastest during the early stages and is diminished quickly as the plume settles on the ground. The relationship between the acceleration of the plume cross-section, its proximity to the ground and the circulation within its cross-section is shown clearly in Fig. 12b where for a circular plume, which falls the fastest, the circulation rises at the highest slope. Later, and as the plume approaches the ground, the circulation of a circular plume reaches an asymptotic value earlier than any other plume.

5. Conclusions

A novel computational model for the simulation of buoyant plumes has been presented. The model was applied to study the plume dynamics, the dispersion and deposition of its material in a homogeneous atmosphere. and their dependence on the plume initial conditions. Results show that:

(1) Starting from a symmetrical elliptical distribution, the cross-section of descending smoke is deformed into a kidney-shaped structure due to the formation of a counter-rotating streamwise vortex pair. These vortices cause the large-scale engulfment of ambient air towards their centers. At later stages, small-scale vortices develop and enhance entrainment currents.

(2) As the plume approaches the ground, the large-scale eddies acquire a strong cross-wind convective motion away from the symmetry plane. This leads to horizontal dispersion of the smoke plume and results in the deformation of its cross-section into two large lumps separated by a thinning crescent. Accordingly, the ground smoke deposition is lower along the symmetry plane than at neighboring cross-wind locations.

(3) Plume trajectories and dispersion rates are strongly dependent on the initial plume height and shape. The corresponding variations are correlated with streamwise vorticity patterns, whose generation depends on the curvature of the plume interface and on the gravitational acceleration field.

(4) Plumes falling from a higher elevation disperse more in the vertical direction while those falling from a lower elevation disperse more in the horizontal direction.

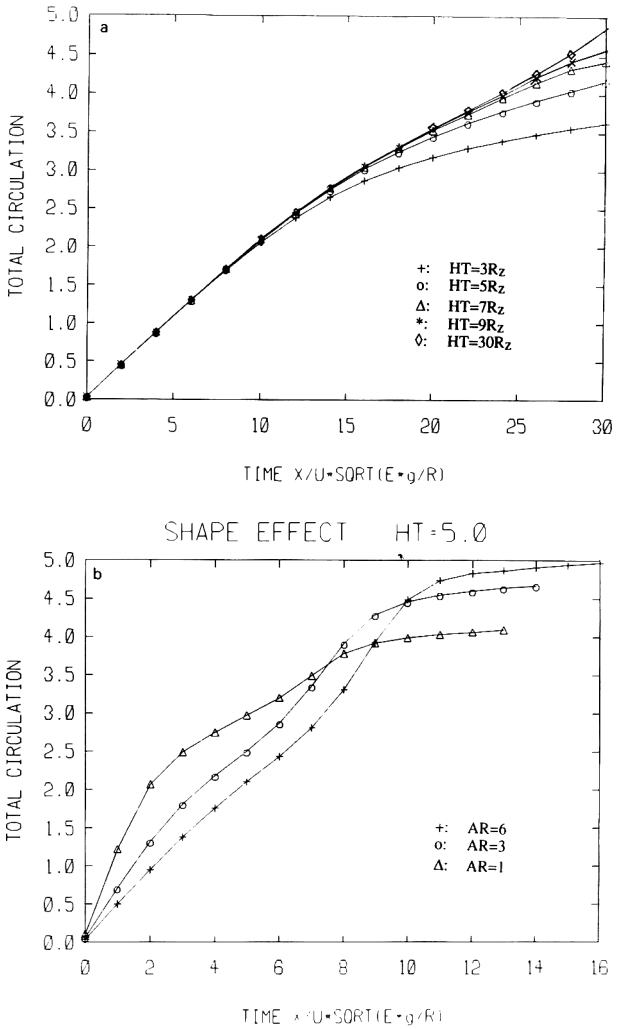

Fig. 12. Variation of the total circulation of each large coherent vortex in the plume cross-section with downwind distance. Shown is the circulation of the right-hand side of the plume for (a) the cases shown in Fig. 7, and (b) the cases shown in Fig. 10.

(5) Plumes with a more rounded cross-section reach the ground faster and disperse horizontally further than plumes with a flatter cross section. The shape of the cross-section has a weak effect on the rate of vertical dispersion.

(6) The strong deformation of the plume cross-section, which leads to a substantial departure of the plume material ground imprint from a Gaussian, is due to the buoyancy generated turbulence within the plume.

Acknowledgement

This work has been jointly supported by the Mineral Management Services of the Department of the Interior and the Building and Fire Research Laboratory of the National Institute of Standards and Technology. We wish to acknowledge Dr. D. Evans of NIST for his review of the paper. The computer, support has partially been provided by the Illinois National Center for Supercomputer Applications.

Nomenclature

AR	$=R_y/R_z$, plume aspect ratio
g	gravitational acceleration
HT	initial height of the plume center
$\dot{m}_p$	$=\int \rho_p^*(y, z) U \mathrm{d}A$, excess mass flux of the plume
p	dimensional perturbation pressure
R	square root of the plume cross sectional area
R_y	major (horizontal) axis of the elliptical plume cross section
R_z	minor (vertical) axis of the elliptical plume cross section
u, v, w	perturbation velocity components in x, y, z direction, respectively
U	uniform wind speed
V	$=\sqrt{\varepsilon R_z g}$, velocity scale of the perturbation velocity
x	horizontal wind direction
y	horizontal direction normal to the wind
z	vertical direction
t	nondimensional form of x^*

Greek

δ	core radius of the vortex and transport element
ε	$=\dot{m}_p/\rho_0^* U R_z^2$, plume mass flux ratio
ρ^*	$=\rho_0^* + \rho_p^*$, total dimensional plume density
ρ_0^*	uniform background air density
ρ_p^*	excess particulate density due to the presence of the smoke
ρ	non-dimensional particulate density
ω	vorticity in the wind direction

Superscript

*	dimensional quantity

References

1 D. Evans, H. Baum, B. McCaffrey, G. Mulholland, M. Harkleroad and W. Manders, Combustion of Oil on Water, Report NBSIR 86-3420, NBS, Gaithersburg, MD, 1986, issued November 1987.

2 D. Evans, G. Mulholland, D. Gross, H. Baum and K. Saito, Environmental Effects of Oil Spill Combustion, Report NISTIR 88-3822, NIST, Gaithersburg, MD, 1987, issued September 1988.
3 D. Evans, G. Mulholland, D. Gross, H. Baum and K. Saito, Generation and dispersal of smoke from oil spill combustion, Proc. of the 1989 Oil Spill Conf. (API/EPA/USCG), February 13–16, 1989, San Antonio, TX.
4 D. Evans, H. Baum, G. Mulholland, N. Bryner and G. Forney, Smoke Plumes from Crude Oil Burns, NISTIR Report, NIST, Gaithersburg, MD, 1992.
5 T.A. Hewett, J.A. Fay and D.P. Hoult, Atmos. Environ., 5 (1971) 767.
6 J.A. Fay, Annu. Rev. Fluid Mech., 5 (1973) 151.
7 W. Rodi (Ed), Turbulent Buoyant Jets and Plumes, Pergamon Press, Oxford, 1982.
8 A. Venkatram and J.C. Wyngaard (Eds), Lectures on Air Pollution Modeling, American Meteorological Society, Boston, MA, 1988.
9 A. Askari, S.J. Bullman, M. Fairweather and F. Swaffield, Combust. Sci. Technol., 73 (1990) 463.
10 J. Seinfeld, Atmospheric Chemistry and Physics of Air Pollution, Wiley, 1986.
11 J.S. Puttock (Ed), Stably Stratified Flow and Dense Gas Dispersion, Clarendon Press, Oxford, 1988.
12 R.E. Britter, Annu. Rev. Fluid Mech., 21 (1989) 317.
13 A.F. Ghoniem, G. Heidarinejad and A. Krishnan, J. Comput. Phys., 79 (1988) 135.
14 A. Krishnan and A.F. Ghoniem, J. Comput. Phys., 99(1) (1992) 1.
15 A.F. Ghoniem, O.M. Knio and A. Krishnan, 23rd Symp. (Int.) on Combustion, The Combustion Institute, London, 1990, p. 699.
16 A.F. Ghoniem and A. Krishnan, 22nd Symp. (Int.) on Combustion, The Combustion Institute, London, 1988, p. 665.
17 A.F. Ghoniem, X. Zhang and O.M. Knio, First Annual Report on Development of a Computational Model for Smoke Plume Dispersion and Deposition, NIST, Gaithersburg, MD 20899, 1992.
18 G. Tsang, Atmos. Environ. 5, 445 (1971).
19 S.J. Barker and S.C. Crow, J. Fluid Mech., 82 (1977) 659.
20 J.C.S. Meng and J.A.L. Thomson, J. Fluid Mech., 84 (1978) 433.

Journal of Hazardous Materials, 33 (1993) 295–305
Elsevier Science Publishers B.V., Amsterdam

Fluid discharge resulting from puncture of spherical process vessels

Peter W. Hart and Jude T. Sommerfeld

School of Chemical Engineering, Georgia Institute of Technology, Atlanta, GA 30332 (USA)

Abstract

Risk analysis associated with incidents of puncture or rupture of process vessels generally requires estimation of actual or average fluid discharge rates resulting from such an incident. Most formulas developed to date for fluid discharge rates from vessels generally assume that the flow opening is located at the bottom of the vessel; this is undoubtedly due to the previously predominant interest in computing time requirements for gravity drainage of process or storage vessels. An accidental puncture, however, such as resulting from a moving vehicle, can occur at almost any elevation. Hence, from a risk analysis point of view, it would be useful to have formulas which would estimate fluid discharge amounts and rates from a flow opening at any arbitrary elevation. In this article, the differential and algebraic equations governing liquid discharge from an opening at any point on the surface of a spherical vessel are solved. This solution is then generalized in terms of dimensionless efflux times, liquid volumes and average release rates as functions of dimensionless elevations.

1. Introduction

The general subject of fluid flow rates from vessels, either storage or process, has posed numerous problems of engineering interest for many years now — to both practicing engineers concerned with production, inventory, safety and other aspects as well as to engineering professors as a source of practical mathematical material. Thus, papers [1–3] dealing with liquid efflux rates from some of the simpler and more common vessel shapes (e.g., vertical circular cylinders) date back to as early as 1949. These early efforts considered drainage through either a hole (e.g., orifice) or through a piping system, and for the most part addressed gravity flow only, ignoring any pressure head in the vessel. An exception here is the early work of Burgreen [3], as well as the much more recent work of Woodward and Mudan [4].

Correspondence to: Dr. J.T. Sommerfeld, School of Chemical Engineering, Georgia Institute of Technology, Atlanta, GA 30332 (USA)

0304-3894/93/$06.00

Significant interest developed in this subject of tank drainage — perhaps at least partially from safety considerations — during the 1980s. Numerous articles appeared during this decade, many of them treating vessel shapes of more complex geometry, wherein the cross-sectional area formed by the liquid surface varies with the elevation of the latter. In one of the earlier such articles [5], formulas were summarized to compute the time requirements to empty vessels of four different shapes: vertical cylinder, cone, horizontal cylinder (with flat ends), and sphere. These expressions were all developed for drainage through a hole or orifice located at the bottom of the vessel. Later articles gave similar formulas for draining elliptical vessel heads often present at the bottom of vertical cylinders [6], elliptical saturator troughs (horizontal elliptical cylinders with flat ends) [7] such as employed in the textile finishing industry, and horizontal cylinders with elliptical dished heads or ends [8]. Some of these formulas are beginning to find their way into recent textbooks [9] on process safety.

Also in recent years the more complicated problem of vessel drainage through a piping system, originating at the bottom of the vessel, has been studied in considerable detail. Thus, one of the earlier articles [10] on this subject pertains to the simplest case of draining a vertical cylindrical tank (and hence of constant cross-sectional area) through such a piping system. Later works gave analogous formulas for draining spherical vessels [11], conical tanks [12] and horizontal cylinders [13], all through a piping system. Analytical solutions were obtained in all of these cases, although the mathematical expressions in the latter case include elliptic functions. A summary [14] of formulas to compute efflux times for drainage, either through a bottom drain hole or through a piping system originating at the vessel bottom, for about a dozen different vessel shapes was recently prepared.

As indicated above, however, all of these cited works have been concerned with fluid discharge rates from the bottom of a vessel, such as in a drainage situation. Some years ago there was an article [15], in which an approximate method for estimating fluid level changes in vertical cylindrical tanks with a multiplicity of outlets (or leaks), of various sizes and at different elevations, was presented. Because of increasing concerns about safety and loss prevention, there exists today a need for accurate formulas to compute fluid discharge and vessel emptying rates for an opening of a given size and at an arbitrary elevation. Such a need may arise, for example, in analyzing an accident scenario resulting from a moving vehicle, e.g., a forklift truck, being driven into the side of a vessel and creating an aperture for fluid discharge at some elevation. Thus, in this article the material and mechanical energy balance equations describing liquid efflux from a spherical tank under the influence of gravity are derived and solved. The solution is then generalized in terms of dimensionless variables, i.e., normalized efflux times, liquid volumes and average release rates as functions of dimensionless elevations.

2. Balance equations

The dynamic material balance for the liquid in the tank in this relatively simple case merely reduces to the rate of accumulation being equal to the negative of the output rate:

$$\frac{dV}{dt} = -q \tag{1}$$

or, more specifically:

$$A\frac{dh}{dt} = -A_0 v_2 \tag{2}$$

For the simpler geometric vessel configurations, e.g., vertical cylinders, the cross-sectional area (A) of the liquid surface in the vessel is a constant quantity and not a function of the variable liquid level (h). This results in a very tractable, non-linear differential equation.

The orifice equation is generally used to represent fluid discharge rates through openings in vessels, irrespective of their size, shape or location. Thus, the effluent liquid velocity (v_2) is represented by the following equation:

$$v_2 = C_0\sqrt{2g(h-h_0)} \tag{3}$$

where C_0 is known as the orifice discharge coefficient; it generally is a function of the fluid velocity (as incorporated in a Reynolds number) and the downstream (orifice)/upstream diameter ratio, although a constant value (between 0.60 and 1.0) is typically assumed for a given application. As indicated in Fig. 1, h_0 is the vertical elevation of the hole above the bottom of the sphere, and h is the variable elevation of the liquid level in the vessel. Equation (3), which derives from the Bernoulli equation, essentially equates the potential energy of the liquid head in the tank, represented by $(h-h_0)$, with the kinetic energy of the outflowing liquid, with any friction losses accounted for by C_0.

3. Mathematical solution

Insertion of eq. (3) into eq. (2) and rearrangement then leads to the following general expression to be integrated:

$$t = \frac{1}{C_0 A_0\sqrt{2g}}\int_{h_0}^{h_1}\frac{A}{\sqrt{h-h_0}}\,dh \tag{4}$$

in order to determine the time (t) required for the liquid level to fall from its initial elevation of h_1 to the elevation of the discharge hole h_0. The area (A) formed by the liquid level in this case of a spherical vessel is given by $\pi C^2/4$, where C is the length of the chord formed by the liquid level. It can simply be shown with the aid of the Pythagorean Theorem that this latter quantity is

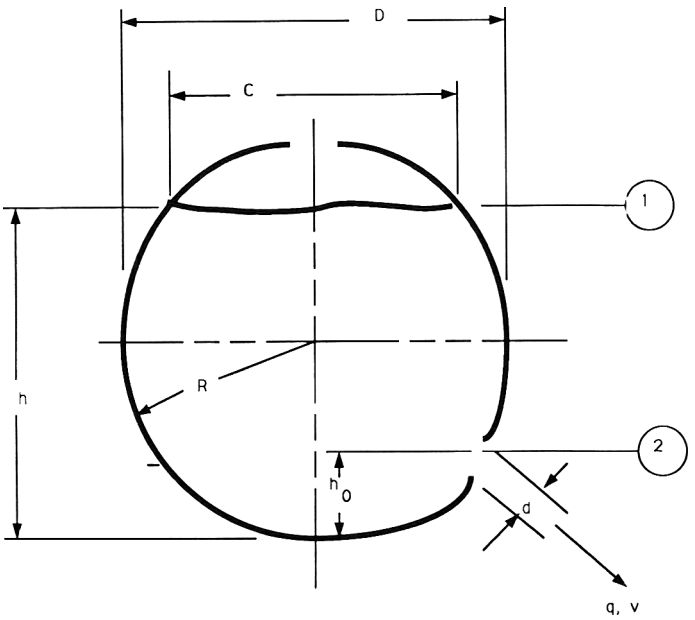

Fig. 1. Sketch of a spherical vessel with a puncture hole in its side and resulting liquid drainage.

given by $2(hD-h^2)^{1/2}$. Equation (4) then becomes:

$$t=\frac{\pi}{C_0A_0\sqrt{2g}}\int_{h_0}^{h_1}\frac{hD-h^2}{\sqrt{h-h_0}}\,dh \tag{5}$$

as the specific expression to be integrated.

The integration of eq. (5) can be found in most tables of integrals. In this particular case the lower limit of h_0 (corresponding to the elevation of the hole and thus the end of the discharge process) vanishes, and there results:

$$t=\frac{2\pi}{15C_0A_0\sqrt{2g}}\left[5Dh_1+10Dh_0-3h_1^2-4h_1h_0-8h_0^2\right]\sqrt{h_1-h_0} \tag{6}$$

When $h_0=0$, as in conventional drainage from a hole or orifice in the bottom of a spherical tank, eq. (6) becomes:

$$t=\frac{\sqrt{2}\pi}{3C_0A_0\sqrt{g}}\left[\left(D-\frac{3h_1}{5}\right)h_1^{3/2}\right] \tag{7}$$

which is the same expression as presented by Foster [5] in his summary article.

4. Generalization of solution

In order to impart greater generality and usefulness to eq. (6) above, let us convert that equation to dimensionless form by the introduction of several dimensionless variables. Specifically, let us define two dimensionless elevations, one corresponding to the initial liquid level in the spherical vessel:

$$x_1 \equiv h_1/D \tag{8}$$

and the other representing the elevation of the discharge hole:

$$x_2 \equiv h_0/D \tag{9}$$

It is necessary to define two more dimensionless quantities. The first of these is the dimensionless size of the flow opening, represented as follows:

$$x_3 \equiv d_o/D \tag{10}$$

and the other is a dimensionless time, given by the following expression:

$$Y \equiv \sqrt{\frac{2g}{D}}t \tag{11}$$

After insertion of the dimensionless quantities from eqs. (8)–(11) into eq. (6), the latter equation can be written in the following form:

$$Y = \frac{8}{15C_0x_3^2}\left[5x_1 + 10x_2 - 3x_1^2 - 4x_1x_2 - 8x_2^2\right]\sqrt{x_1 - x_2} \tag{12}$$

There are four independent parameters appearing in eq. (12) — x_1, x_2, x_3 and C_0, in addition to the dimensionless dependent variable of the time (Y) required for vessel drainage. A commonly assumed value for the orifice discharge coefficient (C_0) is 0.60. Thus, for a given dimensionless opening size (x_3), one can construct a graph which is based upon eq. (12) and which depicts the behavior of the time required for complete drainage of the vessel from an initial dimensionless liquid level of x_1 down to the dimensionless elevation of the opening. Figure 2 represents such a graph for fixed values of $C_0 = 0.60$ and $x_3 = 0.005$; the latter value might correspond, for example, to a hole 5 cm in diameter in the side of a spherical vessel with a diameter of 10 m. This graph shows how the time required for tank drainage increases with the amount of liquid contained in the tank (as measured by x_1), as well as with increased elevation of the drainage hole (x_2); this latter effect undoubtedly results from the reduced hydrostatic head as x_2 increases. The crossover in the curves for the higher values of x_2 (> 0.30) is interesting.

The actual amount of fluid released to the environment is generally of considerable interest in any accident scenario. Again because of the more

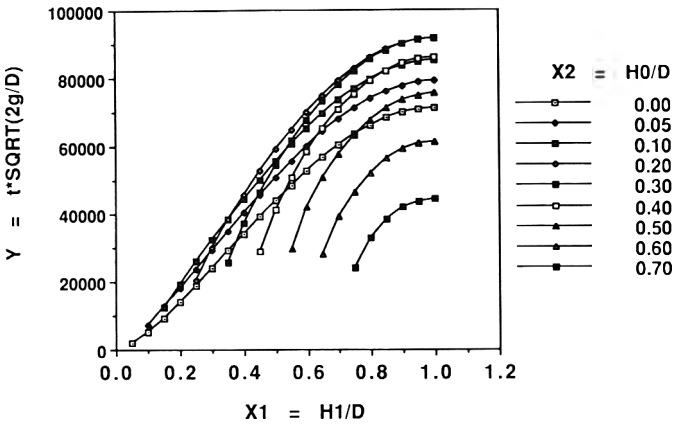

Fig. 2. Dimensionless time (Y) for complete drainage of a spherical vessel as a function of dimensionless initial liquid elevation (x_1) and elevation (x_2) of the drainage hole. $x_3 = 0.005$; $C_3 = 0.60$.

complex geometry of spheres, the calculation of such amounts is somewhat more complicated than for vessels of constant cross-sectional areas, such as vertical circular cylinders. None the less, formulas do exist for calculating the volume of spherical segments. Thus, the volume (V) of a segment h units high of a sphere with a diameter of D is:

$$V = \frac{\pi h^2}{6}[3D - 2h] \tag{13}$$

Recognizing that the complete volume (V_s) of a sphere of diameter D is given by $V_s = \pi D^3/6$, the segmental volume from eq. (13) can be normalized to the complete sphere volume to yield a dimensionless segmental volume:

$$\frac{V}{V_s} = x^2[3 - 2x] \tag{14}$$

where $x = h/D$ and corresponds to any liquid elevation.

The total amount of fluid released in a given incident will then be the difference in volumes corresponding to the initial spherical segment and that corresponding to the final spherical segment at the elevation of the discharge hole. Denoting this fluid volume, dimensionless and normalized to V_s, by U, we have:

$$U = x_1^2[3 - 2x_1] - x_2^2[3 - 2x_2] \tag{15}$$

Figure 3 then shows how this dimensionless volume U varies with the two dimensionless elevations — x_1 and x_2. Not surprisingly, U increases monotonically with increasing x_1 and decreases monotonically with increasing x_2,

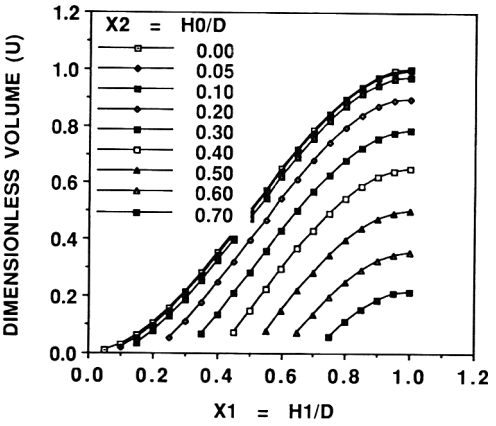

Fig. 3. Dimensionless volume (U) of liquid stored in a spherical vessel between some dimensionless initial liquid elevation (x_1) and elevation (x_2) of a drainage hole.

and with the greatest slopes occurring near the middle bulge ($x_1 = 0.5$) of the spherical vessel.

The curves of Fig. 3 are based solely upon the static geometric calculations of eqs. (13)–(15), and are thus valid for any spherical vessel. That is, the volume of a spherical segment with two horizontal bases at arbitrary elevations can be readily computed from these equations. Flow dynamics add another dimension to the problem. Consider the related task of determining the time required for the spherical vessel to drain from some initial liquid level elevation of h_1 down to some intermediate level of h_i through an opening of diameter d located at a lower elevation of h_2. In this case the volume drained will still be given by eqs. (13)–(15), evaluated for x_1 and $x_i = h_i/D$; but determination of the time requirement here necessitates two evaluations of drainage times from eq. (6):

$$t(h_1 \rightarrow h_i) = t(h_1 \rightarrow h_0) - t(h_i \rightarrow h_0) \tag{16}$$

Alternately, the above calculations can be done in dimensionless form via two applications of eq. (12).

Some representative volumetric rate of fluid discharge from the vessel is often needed in the analysis of puncture accident scenarios. According to Woodward and Mudan [4], a reasonable such rate to use is roughly midway between the initial and average discharge rates. The initial rate is readily obtained from eqs. (1)–(3), with h set equal to h_1. Evaluation of the average rate, however, requires integration of the differential balance equations, as performed in this article. Specifically, this average rate is given by the total volume of liquid contained in the spherical segment (between h_1 and h_0) of interest divided by the time required to drain this liquid through the puncture hole. In dimensionless form, this average rate can be expressed as follows:

$$W = U/Y \tag{17}$$

A plot of W versus x_1 for various values of x_2 ($<x_1$) is shown as Fig. 4; this figure, like Fig. 2, is for values of $C_0 = 0.60$ and $x_3 = 0.005$. Figure 4 is somewhat similar to Fig. 3 for the dimensionless volume U, in that the average dimensionless discharge rate (W) generally increases with increasing x_1 and decreases with increasing x_2.

5. Example calculations

Let us illustrate the calculation procedure outlined above with the following example. We consider a spherical storage vessel, vented to the atmosphere, with a diameter of 10 m and initially filled with a corrosive solution to a depth of 7 m. A forklift truck is accidentally driven into this vessel, creating a puncture hole of about 5 cm in diameter 2 m above the vessel bottom. Assuming uncontrolled release of fluid from this vessel down to the puncture location, it is desired to determine how much fluid is released over what period of time, and hence the average discharge rate. A constant orifice discharge coefficient of $C_0 = 0.60$ is to be used for these calculations.

The dimensionless elevations are readily computed as $x_1 = 0.70$ and $x_2 = 0.20$. Similarly, the dimensionless orifice size (x_3) is found to be 0.005. For this particular configuration, the factor of $8/(15C_0x_3^2)$ is then computed as 35,556. Inserting these various values into eq. (12), we find a dimensionless drainage time of $Y = 79{,}200$. With $g = 9.807$ m/s^2 and $D = 10$ m, this dimensionless drainage time translates to a value of 56,550 s. Similarly, from eq. (15) the total dimensionless volume (U) of fluid drained over this time interval is 0.680 (of the complete volume of a sphere with a diameter of 10 m). Thus, this dimensionless volume corresponds to a fluid volume of 356 m^3. Lastly, the dimensionless

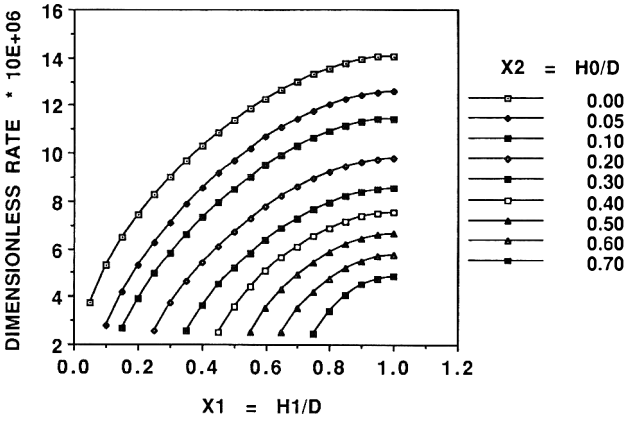

Fig. 4. Dimensionless average rate ($W = U/Y$) of discharge from a spherical vessel as a function of dimensionless initial liquid elevation (x_1) and elevation (x_2) of the drainage hole. $x_3 = 0.005$; $C_0 = 0.60$.

average draining rate from eq. (17) is 8.59×10^{-6}, while the actual average draining rate is $(356\,m^3/56{,}550\,s) = 0.00629\,m^3/s = 22.7\,m^3/h$. This latter quantity compares with an initial discharge rate, as evaluated from eqs. (1)–(3) with $h = 7.0$ m, of $42.0\,m^3/h$. The middle value between these two discharge rates is then about $32.3\,m^3/h$.

6. Discussion

While the mathematical analysis and derivation presented above are rigorous, several of the assumptions made in the early formulation of this problem of drainage from a ruptured sphere may be questioned. Thus, the selection of a given value for the orifice discharge coefficient (C_0) and the assumption of a constant value for this coefficient merit some attention. As can be found in any standard text on the unit operations of chemical engineering [16], this discharge coefficient varies with the Reynolds number for the fluid stream flowing through the opening as well as with the orifice diameter/upstream diameter ratio. It is well known [16] that 0.61 is a reasonably constant value for the discharge coefficient of a sharp-edged orifice when the Reynolds number through the orifice exceeds 30,000, irrespective of the ratio of the diameters. If the orifice is not sharp-edged but rounded at the upstream face (highly unlikely in the event of a puncture hole), the discharge coefficient has a value varying from 0.70 to 0.88. Given that any aperture accidentally created in the side of a process vessel is likely to be highly jagged in nature, a value of 0.61 for C_0 would appear to be a high-side estimate. The value of 30,000 is not a terribly large value for the Reynolds number, and hence the assumption of a constant value for C_0 should be valid for the vast majority of all fluids with viscosities close to water; certainly, exceptions here might include ethylene glycol and kerosene. Also, there might be deviations in the value of C_0 as the drainage of fluid neared its termination, but such deviations would impact upon only a small fraction of the total amount of fluid discharged.

One method of addressing the problem of a variable value of C_0 would be to break up the problem into several segments for values of the liquid elevation (h), and to employ different values of the discharge coefficient for these various segments. This approach would then require successive application of eqs. (6) and (16) to these segments, for h_1, h_2, h_3 . . . Admittedly, this procedure could shortly become very cumbersome, and one might be better advised to employ some computerized numerical integration scheme to solve the original differential equation.

Secondly, estimation of the actual flow area (A_0) associated with a puncture hole could prove somewhat difficult. One method for estimating such a puncture area might derive from mechanical calculations involving the vessel shell thickness and mass and velocity of the moving object, among other variables. If puncture by a forklift truck is indeed the concern, some estimate of the opening might be made from the cross-sectional area of a truck prong. In any event,

there is no requirement in this analysis that the puncture hole indeed be circular, as eq. (10) might suggest. Given an estimate of the flow area (A_0), an equivalent diameter (d_0) for the discharge opening can always be readily computed if dimensionless charts are to be used.

Lastly, there is the question of an internally pressurized fluid, which this article does not specifically address. In the simpler case wherein this internal pressure is constant, such as resulting from a tank pressure controller or the vapor phase over a volatile liquid, this constant tank pressure head may simply be added to the hydrostatic liquid head, $2g(h-h_0)$, in eq. (3); Woodward and Mudan [4] employed this procedure to develop equations for calculating liquid and gas discharge rates through holes in the bottom of process vessels of different shapes. If this tank pressure head decreases as the vessel drains (as in the case of an unvented vessel), however, the governing differential equation in all but the simplest geometric configurations (vertical cylindrical) becomes quite cumbersome.

7. Conclusions

The engineering equations describing fluid discharge from a hole of arbitrary size and at any location on a spherical vessel can be readily solved; the vessel can be of any diameter and initially filled to an arbitrary liquid level.

The mathematical solution obtained to these equations can be generalized in terms of dimensionless variables. This solution can be useful in risk analyses of scenarios associated with accidental puncture of spherical storage or process vessels, such as might result from impaction by a moving vehicle, e.g., a forklift truck. Specifically, this solution allows computation of the amount of fluid discharged to the environment, duration of such fluid discharge and average discharge rate over this time period.

Nomenclature

A cross-sectional area of the liquid surface in the vessel at any time, m^2
A_0 cross-sectional area of the hole for liquid flow out of the vessel, m^2
C length of chord formed by liquid level in vessel, m
C_0 orifice discharge coefficient
D diameter of spherical vessel, m
d diameter of the hole for liquid flow out of the vessel, m
g acceleration due to gravity, m/s^2
h elevation of liquid level in vessel at any time, m
h_i intermediate elevation of liquid level in vessel, m
h_0 elevation of hole above the bottom of the spherical vessel, m
h_1 elevation of initial ($t=0$) liquid level in vessel, m
q liquid volumetric flow rate out of the vessel, m^3/s

R radius of spherical vessel, m
t time, s
U dimensionless volume of liquid initially contained in vessel
V liquid volume in the vessel, m^3
v_2 linear velocity of liquid out of the vessel, m/s
W dimensionless average rate of vessel drainage ($=U/Y$)
x dimensionless elevation of liquid level ($=h/D$)
x_i dimensionless elevation of intermediate liquid level ($=h_i/D$)
x_1 diensionless elevation of initial liquid level ($=h_1/D$)
x_2 dimensionless elevation of hole in vessel ($=h_0/D$)
x_3 dimensionless inside diameter of hole in vessel ($=d/D$)
Y dimensionless time for complete drainage of vessel ($=t(2g/D)^{1/2}$)
π number pi (3.14159 . . . .)

References

1 J.F. Heiss and J. Coull, Nomographs speed flow calculation, Chem. Eng., 56 (1949) 104–107.
2 W.A. Rostafinski, Graphs find vessel drain time, Pet. Refiner, 39 (1960) 213–216.
3 D. Burgreen, Development of flow in tank draining, J. Hydraulics Div., Proc. Am. Soc. Civ. Eng., HY 3 (1960) 13–28.
4 J.L. Woodward and K.S. Mudan, Liquid and gas discharge rates through holes in process vessels, J. Loss Prev. Proc. Ind., 4 (1990) 161 165.
5 T.C. Foster, Time required to empty a vessel, Chem. Eng., 88 (1981) 105.
6 F.H. Koehler, Draining elliptical vessel heads, Chem. Eng., 91 (1984) 90–92.
7 J.T. Sommerfeld, Inventory and drainage of saturator troughs, Am. Dyestuff Rep. 79 (1990) 44–49.
8 J.T. Sommerfeld, Tank draining revisited, Chem. Eng., 97 (1990) 171–172.
9 D.A. Crowl and J.F. Louvar, Chemical Process Safety: Fundamentals with Applications, Prentice-Hall, Englewood Cliffs, NJ, 1990, 426 pp.
10 N.J. Loiacono, Time to drain a tank with piping, Chem. Eng., 94 (1987) 164–166.
11 J.A. Schwarzhoff and J.T. Sommerfeld, How fast do spheres drain?, Chem. Eng., 95 (1988) 158–160.
12 J.T. Sommerfeld, Drainage of conical tanks with piping, Chem. Eng. Educ., 24 (1990) 145–147.
13 J.T. Sommerfeld and M.P. Stallybrass, Elliptic integral solutions for drainage of horizontal cylindrical vessels with piping friction, Ind. Eng. Chem. Res, 31 (1992) 743–745.
14 K.K. Papas and J.T. Sommerfeld, Comparisons of tank drainage times: Orifice drains versus piping, Paper presented at the AIChE Summer Natl. Meeting, Pittsburgh, PA, August, 1991, 21 pp.
15 H.H. Elder and J.T. Sommerfeld, Rapid estimation of tank leakage rates, Chem. Proc. (London), 20 (1974) 15–16.
16 G.G. Brown, A.S. Foust, D.L. Katz, R. Schneidewind, R.R. White, W.P. Wood, G.M. Brown, L.E. Brownell, J.J. Martin, G.B. Williams, J.T. Banchero and J.L. York, Unit Operations, Wiley, New York, 1950, 611 pp.

Journal of Hazardous Materials, 33 (1993) 307–318
Elsevier Science Publishers B.V., Amsterdam

Expansion zone modeling of two-phase and gas discharges

John L. Woodward

DNV Technica Inc., 355 East Campus View Boulevard, Columbus, OH 43235 (USA)

Abstract

An expansion zone model couples a discharge rate model with a high momentum jet dispersion model for sonic or choked flow. Conventional expansion zone modeling, as based on an overall force balance, predicts large increases in the expansion zone diameter and only moderate increases in the expansion zone velocity at a range of low superheat. Alternately, it is shown that any analytic solution for a discharge model can be used also as an expansion zone model. In particular, the homogeneous equilibrium model (HEM) for two-phase discharge and the model for isentropic discharge of an ideal gas are used to exemplify expansion zone modeling. The new approach predicts, in contrast to the conventional approach, large increases in velocity and only moderate increases in expansion zone diameter. Experimental data are needed to decide which model is more nearly correct.

1. Introduction

An expansion zone model couples the predictions of a discharge rate model and a jet dispersion model as depicted in Fig. 1. Accidental leaks from a vessel or pipe often occur from a noncircular source such as a loose flange; but are usually modeled as a discharge from a round orifice or pipe of equivalent discharge area. Such a discharge develops a converging zone and an expansion zone.

Discharge modeling concentrates on the converging zone, since the mass discharge rate is determined by the mass flux at the choke point, G_2, and the discharge coefficient, C_D, in addition to the discharge area, A_1. Air entrainment is usually assumed negligible in both the converging and expansion zones and is treated by the jet dispersion model. The inputs needed by the jet dispersion model are provided by the expansion zone model. These include the velocities of the vapor and liquid, jet diameter, vapor quality, temperature, and density or mass discharge rate. The velocity is important in establishing the mean drop size by the mechanism of aerodynamic breakup.

Correspondence to: John L. Woodward DNV Technica Inc., 355 East Campus View Boulevard, Columbus, OH 43235 (USA) Fax: (614) 848-3955.

0304-3894/93/$06.00

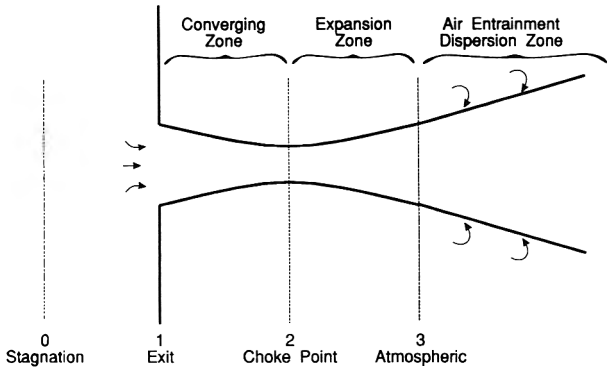

Fig. 1. Definition of terms for high-momentum jet discharge from an orifice.

Moodie and Ewan [1] explored the expansion zone and provided a model for gas jets and some data for two-phase jets. Their gas jet model made use of an empirical centerline momentum model attributed to Kleinstein [2]. An empirical approach was advocated to account for the temperature change across the shock wave which develops at the choke point as flow becomes sonic.

In practice, the expansion zone model predictions are an integral part of subsequent dispersion modeling which are tuned to match available experimental data. Thus, whenever changes are made to the expansion zone model, the dispersion model must be retuned to fit the data. The approach recommended here assumes negligible temperature change across the shock wave. The validity of this assumption is considered hereafter, but, in any event, a change in this assumption would likely be "washed out" by subsequent retuning of the dispersion model.

2. Converging, expanding flow

As illustrated in Fig. 1, contraction occurs as the fluid accelerates upon leaving an orifice or entering a nozzle as pressure drops from the stagnation pressure, P_0, to the choked pressure, P_2. The area at the choke point, A_2, is given by

$$A_2 = C_D A_1 \tag{1}$$

where A_1 is the discharge area and C_D is the discharge coefficient have a value typically in the range

$$0.5 < C_D < 1.0$$

Bragg [3] showed that C_D can be calculated considering the acceleration from P_0 to P_1 once P_2 is known. For subcooled liquids, $C_D = 0.61$, but for saturated liquids and gases, $C_D \rightarrow 1.0$ using Bragg's formulas.

As the pressure in the discharging jet further decreases from P_2 to P_3, where P_3 is usually the atmospheric pressure, P_a, the jet expands. Churchill [4] points out that for compressible flow contraction is characteristic of accelerating subsonic flow (Mach Number <1) and expansion is characteristic of accelerating supersonic flow (Mach Number >1). In addition, flashing liquids expand because the flashing decreases the two-phase density. Two-phase density is very sensitive to the vapor quality, x, in the range $0<x<0.01$.

3. Conventional model based on force balance

A commonly cited expansion zone model, used for example by Fauske and Epstein [5] is attributed to Dryden et al. [6]. This model is derived from an overall force balance, including the annular area A_3-A_1 as follows.

$$wu_1-wu_3+P_1A_1+P_3(A_3-A_1)-P_3A_3=0$$

which, since

$$w=G_1A_1=G_3A_3 \tag{2}$$

reduces to

$$u_3=u_1+\frac{P_1-P_3}{G_1} \tag{3}$$

where

$$G_1=C_DG_2$$

The expansion zone area is

$$A_3=\frac{wv_3}{u_3} \tag{4}$$

where v_3 is given by eq. (12).

4. Expansion zone model for ideal gas discharge

The well-known solution for the discharge of an ideal gas can be used to illustrate how to obtain an alternative expansion zone model. For isentropic expansion of an ideal gas the specific volume and temperature at the end of the expansion zone are given by [7]

$$\frac{v_0}{v_3}=\left(\frac{T_3}{T_0}\right)^{1/(k-1)}=\eta_a^{1/k} \tag{5}$$

With this equation of state, the momentum balance is integrated in standard texts (for example Churchill [8]) to give

$$G^{*2} = \left(\frac{2k}{k-1}\right)\eta^{2/k}\left(1-\eta^{(k-1)/k}\right) \tag{6}$$

where η is the dimensionless pressure ratio and G^* is the dimensionless mass flux. Equation (6) applies for subsonic flow when $\eta = \eta_a > \eta_c$ where

$$\eta_c = \left[\frac{2}{k+1}\right]^{k/(k-1)} \tag{7}$$

and for $\eta = \eta_a < \eta_c$, the flow is choked (sonic) and

$$G_c^* = k\left[\frac{2}{k+1}\right]^{(k+1)/(k-1)} \tag{8}$$

Figure 2 plots eqs. (6) and (8) using the following dimensionless variables

$$\rho^* = \frac{1}{2}\left(\frac{\rho}{\rho_c}\right) = \frac{1}{2}\left(\frac{\eta}{\eta_c}\right)^{1/k} \tag{9a}$$

$$u^* = \frac{1}{2}\left(\frac{u}{u_c}\right) = \frac{1}{2}\frac{G^*}{G_c^*(\rho/\rho_c)} = \frac{1}{2}\frac{G^*}{G_c^*}\left(\frac{\eta_c}{\eta}\right)^{1/k} \tag{9b}$$

$$A_3 = A_2\frac{G_c^*}{G^*(\eta)} \tag{9c}$$

The parameter value of $k = 1.2$ is used in Fig. 2 for which $\eta_c = 0.5645$. We use $A_2 = 0.75$ in Fig. 2 simply for clarity of plotting. Figure 2 shows G^*, u^* and A at

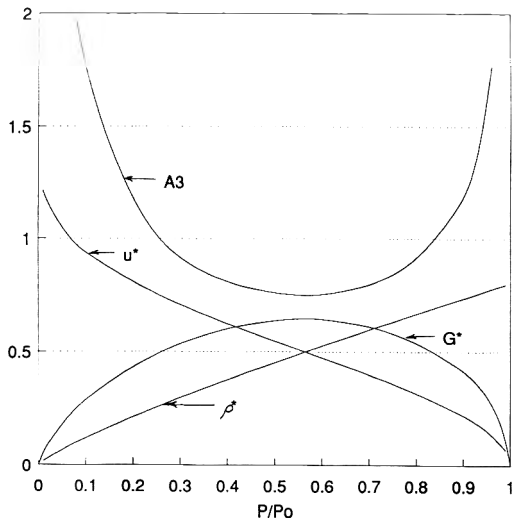

Fig. 2. Adiabatic gas discharge profiles ($k = 1.2$).

any value of $\eta = P/P_0$. In particular, at $\eta_c = P_c/P_0$, the choked conditions are reached and A is at a minimum value, A_2.

At values of $\eta_a = P_a/P_0$, the expansion zone conditions are reached, assuming only that the solutions given by eq. (9) apply across a shock wave which could develop at the throat. Figure 2 shows the expansion zone area increasing as the mirror image to the decreasing G^* function. The expansion zone velocity, expressed as $u^*(\eta_a)$ increases by as much as a factor of two over the velocity at the choke point if η_a is as low as 0.06.

5. Expansion zone modeling for two-phase discharge

The approach just illustrated is a general one, and can be readily applied to any analytic solution for the discharge of a compressible fluid. A number of such solutions have been developed and expressed as $G^*(\eta)$, each with the characteristic that the $G^*(\eta)$ function is zero at the extremes $\eta = 0$ and 1, and so reaches a maximum at an intermediate point η_c giving the choked flux $G_c^*(\eta_c)$. Any such solution can be evaluated at $\eta = \eta_a$ to give $G_{amb}(\eta_a) = G_3$ which, by the definition $G_3 = u_3/v_3$ gives the expansion zone velocity

$$u_3 = v_3 G_3(\eta_a) = G^*(\eta_a)(P_0\rho_0)^{-1/2} v_3 \tag{11}$$

where

$$v_3 = [xv_G + (1-x)v_L]_3 \tag{12}$$

Mass continuity gives the expansion zone area, A_3

$$w = C_D A_1 G_C = A_3 G_{amb}$$

or

$$A_3 = C_D A_1 \frac{G_C^*(\eta_C)}{G_3^*(\eta_a)} = \frac{\pi}{4} D_3^2 \tag{13}$$

For equilibrium models of flashing liquids, vapor quality is given by an isentropic flash, assuming vapor–liquid equilibrium

$$x_3 = \frac{S_{LO} - S_{L3}}{S_{GL}} \tag{14}$$

However, it is well established that equilibrium is not established for orifice discharge, or for short nozzles or pipes (Henry [9], Morris [10], Hardekopf and Mewes [11], and Fauske [12]). For this reason, it is more appropriate to apply a nonequilibrium model, such as that suggested by Henry and Fauske [13]. They postulate that the nonequilibrium vapor quality is related to the equilibrium vapor quality by

$$x_3 = N x_{e3}$$

where Fauske in [DIERS, 14] recommends

$$N=\begin{cases} x_{e3}/0.14 & x_{e3}\le 0.14 \\ 1.0 & x_{e3}>0.14 \end{cases}$$

as an empirical correlation which matches predictions to observed data.

The temperature in this case is the liquid saturation temperature, $T_S(P_a)$. If $\eta_s<\eta_a$, $x_3=0$, and there is no expansion in the expansion zone. If this case $G^*_{amb}=G^*_C$ and eq. (13) reduces to

$$A_3=A_2=C_D A_1 \tag{15}$$

for highly subcooled, nonflashing liquid flow.

5.1 Application with HEM

As an example, the above solutions are illustrated for the homogeneous equilibrium model (HEM) for flashing and subcooled liquid flow by Leung [14] and Leung and Grolmes [15].

The HEM assumes nonslip flow, $u_G=u_L$, and thermodynamic equilibrium along the flow path. Other assumptions are $x=x_0=$constant (frozen flow), isothermal flow, $v_G\gg v_L$, $H_{LG}=H_{LGO}$, $C_{PL}=C_{PLO}$, and that v_{GLO} can replace $v_{GL}(P)$. In spite of these quite restrictive assumptions, the HEM has gained wide acceptance as an adequate approximation, for example by AIChE's DIERS (Design Institute of Emergency Relief Systems) [16–18]. It is known to provide a lower bounding approximation [19] for orifice (nonequilibrium) flow, and an adequate model for nozzle or pipe (equilibrium) flow.

The HEM integrates the pressure derivative of eq. (12) from P_0 to P to define a correlating parameter ω given by

$$\omega=\frac{x_0 v_{GO}}{v_0}+\frac{T_0 P_0 C_{PLO}}{v_0}\left[\frac{v_{GLO}}{H_{GLO}}\right]^2 \tag{16}$$

The first term is α_0 the initial void fraction. The two-phase specific volume is related to ω by

$$\frac{v}{v_0}=\frac{\omega}{\eta}+(1-\omega)$$

For frictionless nozzle or orifice flow, the momentum balance is integrated to give

$$G^*=\frac{\left[2\left((1-\eta_s)+\omega\eta_s\ln\frac{\eta_s}{\eta}+(1-\omega)(\eta_s-\eta)\right)\right]^{1/2}}{\omega\frac{\eta_s}{\eta}+(1-\omega)} \tag{17}$$

The critical mass flux is found by setting $dG^*/d\eta=0$ to give the following transcendental equation which gives the critical pressure ratio, η_C implicitly

$$\frac{(\omega-1)^2}{2\omega\eta_S}\eta^2-2(\omega-1)\eta+\left(\frac{3}{2}\omega\eta_S-1\right)-\omega\eta_S\ln\frac{\eta_S}{\eta}=0 \tag{18}$$

Once η_C is found as a root of eq. (18), G_C^* is given by

$$G_C^* = \eta_C / \omega^{1/2} \tag{19}$$

Equation (18) applies when flashing occurs before or at the choke point. If flashing occurs after the choke point, it affects the expansion zone, but not the discharge rate. In this case the discharge rate is given by the liquid-phase Bernoulli equation. Leung [15] found that a criterion for determining whether flashing occurs before or after the choke point is

If

$$\eta_S < \frac{2\omega_s}{1+2\omega_s} \tag{20}$$

then flashing occurs in the expansion zone, and mass flux is given by the Bernoulli equation

$$G_C^* = [2(1-\eta_C)]^{1/2} \tag{21a}$$

with

$$\eta_C = \max(\eta_S, \eta_a) \tag{21b}$$

Otherwise, η_C is given by eq. (18) and G_C^* by eq. (19).

6. Comparison of models

Typical predictions of the alternative models are given for a flashing liquid in Figs. 3–5 for the new model (eqs. 11–15, with the HEM, eqs. 17–21) and in Fig. 6 for the conventional model (eqs. 3 and 4). These depict constant pressure discharge of propane from 8 atm tank pressure with one meter of liquid head through a 50 mm orifice. For subcooled tank temperatures ($T < 231$ K) the expansion zone area in either case is given by eq. (15). The models differ most for temperatures just above the normal boiling point. In this region, the conventional model predicts a large increase in diameter and, consequently, a mild increase in velocity. In contrast, the new model predicts a moderate increase in diameter, since the ratio G_2/G_3 is near unity in the low subcooled region. Correspondingly, the new model predicts a large increase in velocity.

This behavior occurs because the two-phase density drops rapidly with slight increases in vapor quality as shown in Fig. 4. For the conventional model A_3 is linear in specific volume, v_3, whereas for the new model, u_3 is linear in v_3. Thus, using the nonequilibrium vapor quality reduces the predicted A_3 in Fig. 6 and the predicted u_3 in Fig. 3.

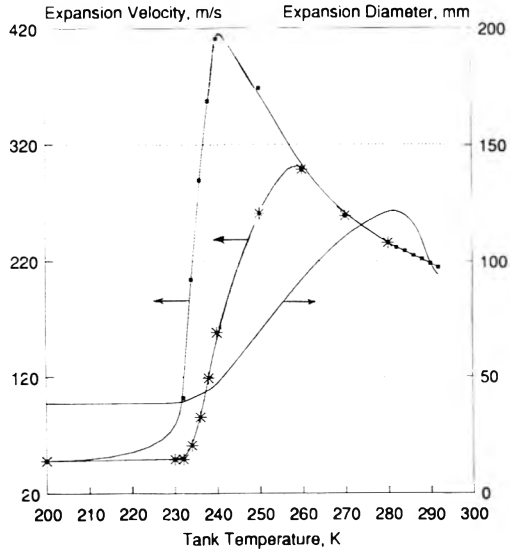

Fig. 3. Expansion velocity and diameter as a function of tank temperature. (■) Equilibrium velocity, (*) nonequilibrium velocity, and (—) expansion diameter. (propane, 1 m head, 50 mm hole.)

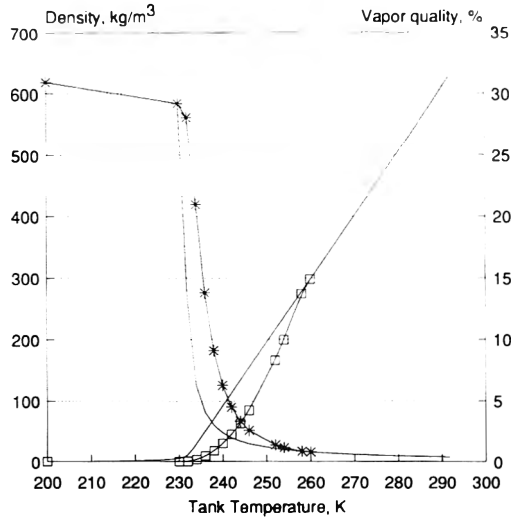

Fig. 4. Expansion zone model for propane gas, 1 m head, 50 mm orifice with constant pressure discharge. Equilibrium values are indicated by solid lines, nonequilibrium values by the symboled lines.

For the new model, further increases in temperature move G^*_{amb} farther down the curve from G^*_2, so the expansion zone diameter increases, which tends to decrease the expansion zone velocity. For temperatures above about 270 K, the vapor pressure curve increases rapidly, so $1-\eta_s$ which equals $1-\eta_c$ in eq. (21a) decreases rapidly with temperature. The consequent decrease in G^*_2 with temperature is partly compensated by an increase in the discharge coefficient, C_D, also shown in Fig. 5. The rapid decrease in G^*_2 for temperatures above about 270 K causes the expansion zone diameter to peak and then decrease (see Fig. 3 and 4). Flashing at or before the choke point occurs for temperatures above about 289 K in this case.

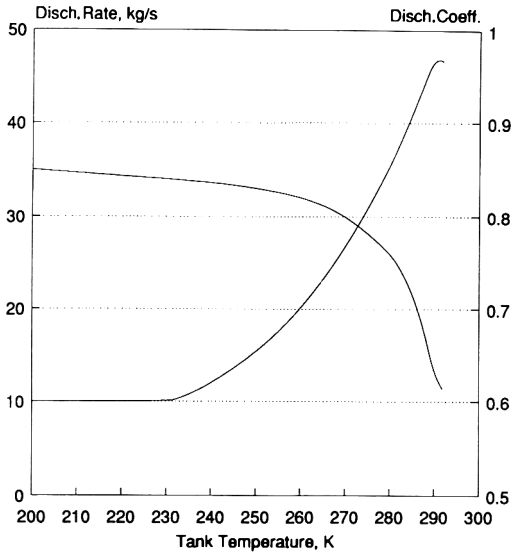

Fig. 5. Discharge rate predictions for constant pressure discharge (propane, 1 m head. 50 mm hole).

6.1 Estimation of shock wave

The error in ignoring shock wave effects can be estimated, using the following formulas for the pressure, density, and temperature ratio across a shock wave given by Nettleton [20]

$$\frac{P'_3}{P_2} = \frac{2\gamma M_S^2 - (\gamma - 1)}{\gamma + 1} \tag{22a}$$

$$\frac{\rho'_3}{\rho_2} = \frac{(\gamma + 1) M_S^2}{(\gamma - 1) M_S^2 + 2} \tag{22b}$$

$$\frac{T'_3}{T_2} = \frac{\left[\gamma M_S^2 - \frac{(\gamma - 1)}{2}\right]\left[\frac{(\gamma - 1)}{2} M_S^2 + 1\right]}{\left(\frac{\gamma + 1}{2}\right) M_S^2} \tag{22c}$$

where $M_S = u_3/a$ is the Mach number, and $a^2 = \gamma R T_s / M_C$ the sonic speed.

Figure 7 plots the pressure and temperature ratios given by eqs. (22a) and (22c) against tank temperature. The largest temperature ratio is 1.15, so the error in ignoring this temperature change is at most 15%. The presence of a shock wave produces a discontinuous decrease in pressure of

$$P'_3 = \max \begin{cases} P_2/(P'_3/P_2) \\ P_a \end{cases}$$

which shortens the length of the expansion zone, but does not, per se, invalidate the assumptions inherent in applying eqs. (11)–(15).

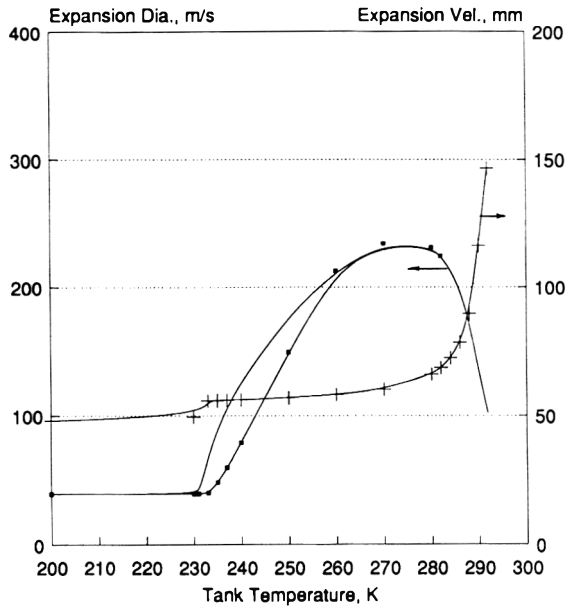

Fig. 6. Conventional expansion zone model for constant pressure discharge (propane, 1 m head, 50 mm hole). (■) Nonequilibrium expansion diameter, (—) equilibrium expansion diameter, and (+) expansion velocity.

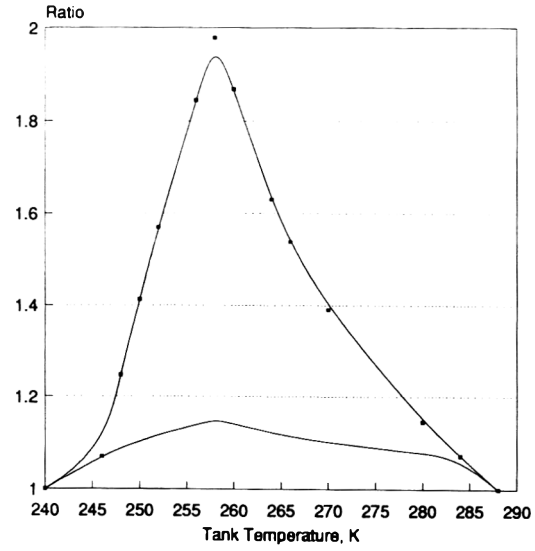

Fig. 7. Temperature and pressure change across shock wave. (■) P_3'/P_2, and (—) T_3'/T_2 (propane, 1 m head, 50 mm hole).

7. Conclusions

Two alternative models for the expansion zone velocity and diameter give predictions which agree for subcooled liquids, but differ substantially for gases and flashing liquids. For flashing liquids, both models are sensitive to the two-phase specific volume, v_3. Area, A_3, is linear in v_3 for the conventional model, wheras velocity, u_3, is linear in v_3 for the new model. Both model predictions seem more reasonable when the assumption is made that the equilibrium vapor quality, x_{3e}, is achieved only at high degrees of superheat. Experimental data are needed to decide which model is more nearly correct. Fortunately, though, the influence of the expansion zone model predictions upon subsequent dispersion modeling is usually absorbed in tuning the dispersion model. If the expansion zone model is changed, the jet dispersion model tuning should be checked and adjusted as needed.

8. Nomenclature

a	speed of sound, $m\,s^{-1}$
C_D	discharge coefficient, (−)
C_p	heat capacity at constant pressure, $J\,kg^{-1}\,K^{-1}$
C_v	heat capacity at constant volume, $J\,kg^{-1}\,K^{-1}$
G	mass flux, $kg\,m^{-2}\,s^{-1}$
G^*	$G/(P_0\rho_0)^{1/2}$, dimensionless mass flux
H_{GL}	heat of vaporization, $(H_G - H_L)$ sat, $J\,kg^{-1}$
k	value equal to or below C_p/C_v
M_s	Mach number of expansion zone velocity
P	pressure, Pa
S	entropy, $J\,kg^{-1}\,K^{-1}$
S_{GL}	$S_G - S_L$, $J\,kg^{-1}\,K^{-1}$
T	temperature, K
u	velocity, $m\,s^{-1}$
v	specific gravity, $m^3\,kg^{-1}$
v_{GL}	$v_G - v_L$
w	mass discharge rate, $kg\,s^{-1}$
x	vapor quality, kg vapor/kg mixture
Greek	
ρ	density, kg/m^3
η	P/P_0
ω	parameter defined by eq. (7)

Subscripts

a	ambient
c	choke point, "critical" flow or Plane 2
G	vapor

L	liquid
0	stagnation conditions
s	saturation
0, 1, 2, 3	planes defined by Fig. 1

References

1 K. Moody and B.C.R. Ewan, Jets discharging to atmosphere, J. Loss Prev. Process Ind., 3 (1990) 68–76.
2 G.D. Kleinstein, Mixing in turbulent axially symmetric free jets, J. Spacecraft, 1(4) (1964) 403–408.
3 S.L. Bragg, Effect of compressibility on the discharge coefficient of orifices and convergent nozzles, J. Mech. Eng. Sci. 2 (1960) 35–44.
4 S.W. Churchill, Compressible flows, In: N.P. Cheremisinoff and R. Gupta (Eds.), Handbook of Fluids in Motion, Ann Arbor Science, Ann Arbor, MI, 1983, Chapter 8.
5 H.K. Fauske and M. Epstein, Source term considerations in connection with chemical accidents and vapour cloud modelling, J. Loss Prev. Process Ind., 1 (1988) 75–83.
6 H.L. Dryden, F.D. Murnaghan and H. Bateman, In: Hydrodynamics, Dover Publications, New York, 1936, p. 540.
7 R.E. Balzhiser and M.R. Samuels, Engineering Thermodynamics, Prentice Hall, Englewood Cliffs, NJ, 1977.
8 S.W. Churchill, The Practical Use of Theory in Fluid Flow, Book I, Inertial Flows, Etaner Press, Thornton, PA, 1980.
9 R.E. Henry, The two-phase critical discharge of initially saturated or subcooled liquid, Nuclear Sci. Eng., 41 (1970) 336–342.
10 S.D. Morris, Choking conditions for flashing one-component flows in nozzles and valves — A simple estimation method, I. Chem. E. Symp. Series No. 110, 1988, pp. 281–299.
11 F. Hardekopf and D. Mewes, The pressure ratio of critical two-phase flows, Chem. Eng. Technol., 12 (1989) 89–96.
12 H.K. Fauske, The Discharge of Saturated Water Through Tubes, Chem. Eng. Prog. Symp. Series, 61 (1965) 210–216.
13 R.E. Henry and H.K. Fauske, The two-phase critical flow of one-component mixtures in nozzles, orifices, and short tubes, Trans. Am. Soc. Mech. Eng. J. Heat Transfer, 93(5) (1971) 179–187.
14 J.C. Leung, A generalized correlation for one-component homogeneous equilibrium flashing choked flow, AIChE J., 32(10) (1986) 1743–1745.
15 J.C. Leung and M.A. Grolmes, A generalized correlation for flashing choked flow of initially subcooled liquid, AIChE J., 34(4) (1988) 688–691.
16 Design Institute of Emergency Relief Systems (DIERS) Report, Emergency Relief Systems for Runaway Chemical Reactions and Storage Vessels: A Summary of Multi-Phase Flow Methods, AIChE Pub. 132, FAI/83-27, October, 1983.
17 J.E. Huff, Multi-phase flashing flow in pressure relief systems, Plant/Operations Prog., 4(4) (1985) 191–199.
18 H.G. Fisher, An overview of emergency relief system design practice, Plant/Operations Prog., 10(1) (1991) 1–12.
19 S.M. Sami and T. Duong, A transient model for predicting nonhomogeneous non-equilibrium, critical, two-phase flows, Nuclear Technol. 83 (1989) 98–108.
20 M.A. Nettleton, Gaseous Detonations, Chapman and Hall, New York, 1987, p. 21.

ACTIVE LIBRARY® ON CORROSION

Elsevier Science Publishers B.V., the world's largest scientific publisher, and the National Association of Corrosion Engineers (NACE), the world's largest publisher of corrosion technology, are proud to announce the Active Library® on Corrosion, a novel hypertext/CD-ROM product, edited by Professor Walter Bogaerts and Dr. Klaas Agema (MTM Department, Leuven University, Belgium). The Active Library® on Corrosion has been developed by Elsevier as part of one of the projects of ESPRIT, the European Strategic Programme for Research and Development in Information Technology.

PRODUCT DESCRIPTION

The Active Library® on Corrosion (ALC) presents a vast amount of practical corrosion information, consisting of text and graphics (including hundreds of full-color photographs), which you can access through hypertext linking. In addition, the ALC contains several numerical and textual databases.

The ALC allows you (1) to make annotations to information screens via the sticky note editor, (2) to select screen sequences for storage in document trails which can be retrieved afterwards, and (3) to print the documents selected by you.

AUDIENCE

The Active Library® on Corrosion is aimed primarily at the individual corrosion engineer, but will also prove to be an indispensible educational tool for courses on corrosion, as well as an invaluable reference for scientific and technical personnel who deal with any corrosion topic.

The unique user interface and functions of the ALC will also be of great interest to students and researchers in the fields of hypertext, media technology and information retrieval.

CONTENTS

The Active Library® on Corrosion presents a comprehensive collection of corrosion information, divided over the following library sections:

1. **Reference Cube**
2. **Case Histories**
3. **Corrosion Control**
4. **Books** (full text of 4 books on corrosion control)
5. **Quick Reference**
6. **Databases**
7. **Glossary and Help information**

ELSEVIER
SCIENCE PUBLISHERS

SYSTEM REQUIREMENTS

For system requirements, a full colour brochure is available on request.

Listprice

1992 ISBN 0-444-89607-4
US$ 1250.00 / Dfl. 2250.00
(NACE individual members: US$ 1000.00 when ordered directly from NACE)

For further information in North America and for NACE members please contact
NACE
Attn. Marketing Department
P.O. Box 218340
Houston, TX 77218-8340, USA
Tel: (713) 492 0535
Fax: (713) 492 8254

In all other cases
ELSEVIER SCIENCE PUBLISHERS
Attn. Ms Carla G.C. Stokman
P.O. Box 330
1000 AH Amsterdam
The Netherlands
Tel: (+31-20) 5862 821
Fax: (+31-20) 5862 845

Distribution

The Active Library® on Corrosion is published by Elsevier in conjunction with NACE. NACE will sell and distribute the ALC to its members and in the North American market (USA and Canada). Elsevier will sell and distribute the ALC in the rest of the world.

Process Technology Proceedings Volume 10

Computer-Oriented Process Engineering

Proceedings of COPE-91, Barcelona, Spain, October 14-16, 1991

edited by **L. Puigjaner** *and* **A. Espuña**, *Department of Chemical Engineering, Universitat Politècnica de Catalunya, Barcelona, Spain*

The proceedings of COPE-91 represent the continuing effort of both the scientific and industrial community to make known what is new in research and development in the increasingly important inter-disciplinary field of computers in chemical engineering.

The symposium focussed on the following topics:

- Artificial Intelligence in Chemical Engineering
- Computer Integrated Process Engineering
- Reliability and Risk Assessment
- Process Design under Uncertainty
- Education and Training in Computer Applications

The theoretical and practical aspects of the use of computers in chemical engineering covered in this book should find wide use in libraries and research facilities, and should have a direct impact in the chemical industry, particularly in production automation, utility networks and computer integrated process engineering.

Contents:

1991 x + 450 pages
Price: US $ 166.50 / Dfl. 325.00
ISBN 0-444-88786-5

Elsevier Science Publishers
P.O. Box 211, 1000 AE Amsterdam, The Netherlands
P.O. Box 882, Madison Square Station, New York, NY 10159, USA

SUBMISSION OF PAPERS

Submission of a manuscript implies that it is not under consideration for publication elsewhere and further that, with the exception of review papers, original work not previously published is being presented.

Papers should be submitted to Dr. G.F. Bennett, Department of Chemical Engineering, University of Toledo, 2801 W. Bancroft Street, Toledo, OH 43606, U.S.A. or Dr. R.E. Britter, Department of Engineering, University of Cambridge, Cambridge CB2 1PZ, Great Britain. Authors in the Far East should submit papers to Dr. T. Yoshida, Chemical Engineering Laboratory, Department of Mechanical Engineering, Faculty of Engineering, Hosei University, 7-2 Kajino-cho 3-chome, Koganei-shi, Tokyo 184, Japan.

MANUSCRIPT PREPARATION

Three copies of the manuscript should be submitted in double-spaced typing on pages of uniform size with a wide margin on the left. The top copy should bear the name and the full postal address of the person to whom the proofs are to be sent. A summary of 100–200 words is required.

References should be numbered consecutively throughout the text and collected together in a reference list at the end of the paper. Journal titles should be abbreviated. The abbreviated title should be followed by the volume number, year (in parentheses), and page number.

ILLUSTRATIONS

Line drawings should be in a form suitable for reproduction, drawn in Indian ink on drawing paper. They should preferably all require the same degree of reduction, and should be submitted on paper of the same size as, or smaller than, the main text, to prevent damage in transit. Photographs should be submitted as clear black-and-white prints on glossy paper. Each illustration must be clearly numbered. Colour illustrations can be reproduced at the author's expense.

Legends to the illustrations must be submitted in a separate list.

All tables and illustrations should be numbered consecutively and separately throughout the paper.

LANGUAGE

The principal language of the journal is English, but papers in French and German will be published.

PROOFS

Authors will receive page proofs, which they are requested to correct and return as soon as possible. No new material may be inserted in the text at the time of proofreading.

REPRINTS

A total of 50 reprints of each paper will be supplied free of charge to the principal author. Additional copies can be ordered at prices shown on the reprint order form which accompanies the proofs.

A pamphlet containing detailed instructions on the preparation of manuscripts for JOURNAL OF HAZARDOUS MATERIALS may be obtained from the publishers.

0304-3894/93/$06.00

This issue is printed on acid-free paper.

PRINTED IN THE NETHERLANDS

VOL. 33, NO. 2 FEBRUARY 1993

JOURNAL OF HAZARDOUS MATERIALS

CONTENTS

SUBSCRIPTION INFORMATION

1993 Subscription price: Dfl. 1400.00 plus Dfl. 132.00 (p.p.h.) = Dfl. 1532.00 (approx. US $850.00). This covers volumes 32–35. The Dutch guilder price is definitive. The U.S. dollar price is subject to exchange-rate fluctuations and is given only as a guide. Subscription orders can be entered only by calendar year (Jan.–Dec.) and should be sent to: Elsevier Science Publishers B.V., Journals Department, P.O. Box 211, 1000 AE Amsterdam, The Netherlands, Tel. (020) 5803642, Telex 18582 ESPA NL, Fax (020) 5803598, or to your usual subscription agent. Claims for missing issues will be honoured, free of charge, within six months after publication date of the issue. All back volumes are available. Our p.p.h. (postage, package and handling) charge includes surface delivery of all issues, except to the following countries where air delivery via S.A.L. (Surface Air Lifted) mail is ensured: Argentina, Australia, Brazil, Canada, Hong Kong, India, Israel, Japan, Malaysia, Mexico, New Zealand, Pakistan, P.R. China, Singapore, South Africa, South Korea, Taiwan, Thailand, and the U.S.A. For Japan, air delivery by S.A.L. requires 25% additional charge; for all other countries airmail and S.A.L. charges are available upon request. Customers in the U.S.A. and Canada wishing information on this and other Elsevier journals, please contact Journal Information Center, Elsevier Science Publishing Co., Inc., 655 Avenue of the Americas, New York, NY 10010, Tel. (212) 633-3750, Fax (212) 633-3764.

0304-3894(199302)33:2;1-Q